The Pennsylvania State University

The Graduate School

Program in Cellular and Molecular Biology

ENDOGENOUS OPIOIDS AND MULTIPLE SCLEROSIS

A Dissertation in

Cellular and Molecular Biology

by

Kristen Rahn

Submitted in Partial Fulfillment
of the Requirements
for the Degree of

Doctor of Philosophy

August 2009

The dissertation of Kristen Rahn was reviewed and approved* by the following:

Patricia J. McLaughlin
Professor of Neural and Behavioral Sciences
Dissertation Advisor
Chair of Committee

Peter A. Arnett
Associate Professor of Psychology

Robert H. Bonneau
Professor of Microbiology and Immunology

Richard B. Tenser
Professor of Neurology, and Microbiology and Immunology

Ian S. Zagon
Distinguished University Professor

Henry J. Donahue
Professor of Orthopaedics
Director of the Cell and Molecular Biology Graduate Program

*****Signatures are on file in the Graduate School

Abstract

Multiple sclerosis (MS) is an autoimmune disease that affects over 2 million people worldwide. There are Food and Drug Administration (FDA)-approved therapies for the disease, but none are effective enough to completely diminish the debilitating side effects associated with demyelination of the central nervous system. Opioids have been shown to regulate immune system function, but the role of opioids in MS has not been characterized.

The purpose of this research was to determine if manipulation of an endogenous opioid system affects the progression of MS using an *in vivo* experimental autoimmune encephalomyelitis (EAE) animal model. The endogenous opioid system was manipulated using an opioid receptor agonist ([Met^5]-enkephalin, Met-enk, opioid growth factor, OGF) or a high or low dose of an opioid receptor antagonist (naltrexone, NTX). Additional *in vitro* studies were conducted to determine if administration of exogenous OGF or NTX affects splenic-derived lymphocyte proliferation. OGF and NTX have been shown to decrease and increase the rate of cancer cell proliferation, respectively; the present studies focus on defining the unknown role of OGF and NTX in EAE progression. The *hypothesis* of this research was that endogenous opioid systems play a role in EAE pathogenesis. These experiments determined if disease course could be affected based on the availability and subsequent interactions of opioid peptide and receptors.

For the *in vivo* studies, EAE was induced in 7 - 8 week old female C57Bl/6 mice with a series of myelin oligodendrocyte glycoprotein (MOG) injections on Days 0, 3, and 6. Beginning with the first MOG injection, mice received a daily intraperitoneal injection of either phosphate-buffered saline (vehicle), a high dose of NTX to cause 24-hour opioid receptor blockade (HDN, 10mg/kg), a low dose of NTX to cause intermittent 4 - 6 hour opioid receptor blockade (LDN, 0.1mg/kg), or a high dose of opioid growth factor (OGF, 10mg/kg). Treatment was administered

at the same time each day. Behavioral symptoms were monitored daily and disease scores were assigned based on a 0 - 5 scale. A score of 0 was assigned to healthy animals free of EAE symptoms, and subsequent increasing scores correlated to increasing levels of disability. Animals were sacrificed 10, 20, 30, and 60 days post-EAE induction to monitor pre-clinical EAE, acute EAE, established EAE, and chronic EAE, respectively. Spinal cord demyelination was visualized with a luxol fast blue (LFB) stain, and additional spinal cord sections were stained with antibodies directed at astrocytes and damaged neurons to show changes in number or morphology of the cells.

In vitro studies were conducted to determine if OGF or NTX administration altered splenic-derived lymphocyte proliferation. First, the presence of both OGF and OGFr on splenic-derived mouse lymphocytes was confirmed with immunocytochemical analysis. Next, fresh lymphocytes were isolated from the spleens of normal mice, activated with phytohemagluttinin (PHA), treated in culture with OGF or NTX, and counted daily to measure proliferation over a 72 hour time period.

Results revealed that chronic LDN and OGF treatment decreased EAE disease severity, disease incidence, and disease index, and increased the average day of EAE disease onset compared to vehicle-treated mice. Continuous opioid receptor blockade with HDN had no effect on EAE disease onset or progression compared to vehicle treatment. Immunohistochemical analysis of astrocyte activation and neuronal damage showed that daily administration of LDN improved histological symptoms of EAE in comparison to vehicle treatment at 10, 20, and 30 days post-EAE induction. Similarly, daily injections of OGF decreased the level of astrocyte activation on Days 10, 20, 30, and 60 and the level of neuronal damage on Day 20 compared to vehicle-treated controls. Interestingly, mice given HDN had lower astrocyte counts on Days 30 and 60 and less neuronal damage on Day 30 compared to vehicle-treated mice. *In vitro* experiments demonstrated that OGF caused a decrease in lymphocyte proliferation compared to lymphocytes exposed to saline or NTX. It is possible that OGF is effective at treating EAE *in*

vivo due to a downregulation of immune system function due to an inhibition of lymphocyte proliferation. Similarly, intermittent opioid receptor blockade with LDN, which causes upregulation in the production of endogenous opioid peptide and receptor, could inhibit the hyperproliferative immune response in EAE. It is possible that LDN is beneficial *in* vivo because it causes an upregulation in opioid-opioid receptor interactions with subsequent decreased immune system function.

Collectively, these results indicate that intermittent opioid receptor blockade with LDN and administration of exogenous OGF can prevent or decrease the behavioral and histopathological signs of EAE. Although EAE is not a perfect model of MS, hallmarks of both diseases - inflammation, demyelination, and neurodegeneration - were decreased in EAE following LDN and OGF administration. Further studies should be conducted to determine the exact mechanism of action and efficacy in relapsing EAE models. However, these data robustly support the use of LDN and OGF for the clinical treatment of MS.

TABLE OF CONTENTS

Page

LIST OF FIGURES

LIST OF TABLES

Page

LIST OF ABBREVIATIONS

BBB	blood brain barrier
B-end	beta endorphin
CFA	complete Freund's adjuvant
CNS	central nervous system
Con A	concanavalin A
CSF	cerebrospinal fluid
δ	delta
DAB	diaminobenzidine
EAE	experimental autoimmune encephalomyelitis
EtOH	ethanol
FBS	fetal bovine serum
FDA	food and drug administration
GFAP	glial fibrillary acidic protein
HDN	high-dose naltrexone
HRP	horseradish peroxidase
IHC	immunohistochemistry
IL	interleukin
IMDM	Iscove's-Modified Dulbecco's Media
κ	kappa
kg	kilogram
LDN	low-dose naltrexone
Leu-enk	leucine enkephalin
LFB	luxol fast blue
LPS	lipopolysaccharide

M	molar
MBP	myelin basic protein
Met-enk	methionine enkephalin
mg	milligram
MHC	major histocompatibility complex
mL	milliliter
mm	millimeter
MOG	myelin oligodendrocyte glycoprotein
MRI	magnetic resonance imaging
MS	multiple sclerosis
NAL	naloxone
ng	nanogram
NGS	normal goat serum
NK cell	natural killer cell
NTX	naltrexone
OGF	opioid growth factor
OGFr	opioid growth factor receptor
PBS	phosphate buffered saline
PFC	plaque forming cell
PHA	phytohemagluttinin
PLP	proteolipid protein
PP-MS	primary progressive multiple sclerosis
PR-MS	progressive relapsing multiple sclerosis
RR-MS	relapsing-remitting multiple sclerosis
SP-MS	secondary progressive multiple sclerosis
TNF	tumor necrosis factor

μ	mu
μg	microgram
μL	microliter
μm	micrometer
VCAM	vascular cell adhesion molecule

ACKNOWLEDGEMENTS

My thesis committee played a fundamental role in the design and completion of this work. First and foremost, I would like to thank my thesis advisor, Dr. Patricia McLaughlin. Thank you for the countless hours of guidance and mentorship through the years. The lessons and skills you have taught me will be invaluable in my future endeavors, and I cannot thank you enough. Second, I would like to thank Dr. Ian Zagon. Your passion and excitement for science is truly inspiring, and you have taught me so much about research design and writing. To both Pat and Dr. Zagon, it has been my great pleasure to work in your laboratory, thank you so much for giving me this opportunity. Next, many thanks to Dr. Robert Bonneau for your leadership and supervision on the immunology component of this project, for allowing me to use your laboratory equipment to complete the work, and for taking the time to personally teach me so many novel techniques. To Dr. Peter Arnett, thank you for sharing your psychology expertise and for providing such valuable insight into the behavioral aspects of the project. Finally, thank you to Dr. Richard Tenser, your clinical expertise has been invaluable in keeping the translational goals of the project at the forefront of the research design. This project was truly a collaborative effort, and I thank you all for your ideas and guidance.

In addition to my committee members, I have received help and support from many others. Thank you to the past and present members of the Zagon/McLaughlin lab, including Matt Klocek, Chris Pothering, Renee Donahue, Anna Kober, Jessica Wentling, Cara Keiper, and Fan Cheng. Many thanks to the CMB graduate program staff, especially Lori Coover and Dr. Hank Donahue. I am grateful for the help I have received from Mike Elftman and Jennifer Mellinger from the Bonneau lab, Kathy Simon, Nate Scheaffer, Ray Scheetz, and Rich. I would also like to thank all of the friends I have made during my time here, especially Nikki Gudleski. Most importantly, I would like to thank my parents and my sisters for their love and support throughout the years.

CHAPTER 1: INTRODUCTION

1. Introduction

1.1. Multiple Sclerosis

1.1.1. Disease Introduction and Etiology

Multiple sclerosis (MS) is a an autoimmune disorder that affects over 400,000 people in the United States and approximately 2 million people throughout the world [1-3]. Approximately 1 in 400 people are diagnosed with MS, making it the most common neurological disorder in people under 40 years of age [4]. MS was first described by famed French neurologist Jean Charcot in 1868 as an accumulation of inflammatory cells in the white matter of the brain and spinal cord with irregular appearances of neurological dysfunction [5]. Since this initial discovery by Charcot, extensive studies on MS have revealed some aspects of disease pathogenesis and etiology. However, this debilitating disease is not completely understood and MS remains an incurable neurological disorder.

In MS, enzymatic digestion of the blood brain barrier leads to inflammation, demyelination, and axonal damage of the central nervous system (CNS) [6, 7]. The upregulation of immune cells and the production of myelin-specific antibodies at the site of active CNS lesions indicate that MS involves a dysregulation of the immune system [8]. The trigger of the autoimmune reaction in MS is unknown, and there are thought to be a wide variety of factors that contribute to disease pathogenesis, including hormones, genetics, and sunlight exposure. Similar to the affected population in other autoimmune diseases, twice as many women as men have MS [9]. Familial studies have demonstrated a potential genetic link contributing to MS [10, 11]. MS affects 0.2% of the general population, and this figure increases to 3-5% if a person has a first-degree relative who has been diagnosed with MS [10]. Genetics, and not familial environment, contribute to MS incidence, as adoptive studies have shown that a child adopted by a

parent with MS has the same likelihood of developing MS as anyone else in the general population (0.2%) [10]. An identical twin of a female with MS has a 170% increase in her likelihood of developing MS compared to a person in the general population [10]. However, concordance rates in identical twins are only 25%, so there must be other factors that contribute to susceptibility [12]. Genome-wide linkage studies in MS patients reveal a common occurrence of extended haplotypes on chromosome 6 that include the HLA-DRB1*1501 locus [11]. A 2009 study found a vitamin D response element in the promoter region for the HLA-DRB1, which was the first report to link genetic susceptibility to the environmental risk factor of insufficient vitamin D exposure [13]. Vitamin D has been implicated as a potential factor that contributes to development of MS, as countries farther from the equator have higher incidence of MS [13]. In an animal model of MS, vitamin D deficiency increases disease susceptibility and administration of vitamin D at the time of disease symptom onset prevented disease progression [14]. Exposure to infections may also affect the incidence of MS. As sanitation has improved and the rates of infections have dropped in Western countries, the incidence of MS has increased [15]. MS patients with parasite infections have a decreased relapse rate compared to uninfected MS patients [16]. It is likely that genetics, hormones, and the environment all contribute to the development of MS, and a combination of these factors could be responsible for the varying disease courses observed in the clinic.

Normal onset of MS occurs during adulthood, with only 5% of all MS cases diagnosed before the age of 18 [17]. Average age of disease inception ranges from 20-40 years of age [18]. Onset of MS during childhood produces a form of the disease that progresses slowly, but because onset is early patients reach a stage of irreversible disability earlier in life [19].

MS is an incurable disease. Due to the complex nature of MS, the degeneration of the myelin sheath surrounding neurons found anywhere in the brain or spinal cord can lead to a variety of symptoms ranging from bladder dysfunction to vision problems to paralysis [20]. There is also a seven-fold increase in the rate of epileptic seizures in MS patients compared to the general population [21]. The recent strides in MS research which have produced new therapies and treatments for the disease have lengthened the lifespan of an MS patient to that of a healthy person [22]. However, treatment is very expensive and quality of life is undoubtedly reduced, so more effective and inexpensive therapies need to be explored.

1.1.2. MS Pathogenesis

MS is considered a T cell-mediated autoimmune disease [23]. Inflammation is undoubtedly the first step in MS pathogenesis, and it is typically thought that inflammation leads to demyelination, which in turn exposes axons for neurodegeneration [24]. However, recent work has demonstrated that axonal damage might occur in some EAE models from “the inside out”, with neurodegeneration preceding demyelination [25, 26]. In the newer “inside-out” model, Wallerian degeneration and interruption of cross-talk between cells of the CNS are blamed for neurodegeneration-caused demyelination [25, 26]. It is possible that a combination of the two theories occurs in MS. Here the stages of MS will be addressed in the conventional order of inflammation, demyelination, and neurodegeneration.

1.1.2.1. Inflammation

Inflammation is required for the generation of an autoimmune reaction. The discovery of immunoglobulin in the cerebrospinal fluid (CSF) of MS patients in 1948 led to the idea that MS is an immune-mediated disease [27]. T cells specific for myelin antigens are present in both MS patients and healthy people, but in MS patients these

myelin-specific T cells become activated and mount an autoimmune reaction [28]. To enter and cause damage to the CNS, lymphocytes must cross the blood brain barrier (BBB). CXCR3 and CCR5, receptors on T lymphocytes, mediate the homing and trafficking of the T lymphocyte to the site of inflammation [29]. Alpha-4 integrins are adhesion molecules expressed on the surface of lymphocytes [30]. Alpha-4 beta-1 integrin, also known as very late activating antigen (VLA)-4, interacts with vascular cell adhesion molecule-1 (VCAM-1) to allow the "rolling" of the lymphocyte through the endothelial layers of the BBB and into the CNS [29]. Rolling is promoted by integrins, selectins, and carbohydrate interactions [29]. Increased permeability of the BBB also aids in lymphocyte entry into the CNS [24]. A recent study demonstrated that occludin dephosphorylation occurs just before the BBB becomes permeable and histological signs of disease are apparent [31]. Activated lymphocytes enter the CNS, but the exact pathway in MS that elicits CNS damage is unknown. It is thought that self or foreign peptide is taken up by an antigen presenting cell (APC), and the APC's major histocompatibility complex (MHC) Class I and II molecules can interact with and activate more $CD8^+$ and $CD4^+$ T cells [8]. Activation of T cells leads to the release of proinflammatory cytokines and the stimulation of other immune cells such as macrophages and B cells [8]. B cells produce antibodies specific for myelin peptide, more cytokines are released, and inflammation of the CNS continues [8]. In addition to the APCs of the immune system, CNS cells can also participate in T and B cell activation [8]. MHC Class I molecules are present in low numbers on cells of the CNS [32]. Viral infection can cause an upregulation of MHC Class I molecules on neurons, oligodendrocytes, microglia, and endothelia. MHC Class II molecules are found on microglia only [32]. The presence and upregulation of MHC production on neurons and oligodendrocytes suggest that these CNS cells can interact with T cells to directly

mediate damage in MS [32]. The presence of inflammation in the CNS is a hallmark of MS, and activation and deregulation of cells of the immune system and the CNS greatly increases inflammatory processes.

1.1.2.2. Demyelination

Following activation and entry of myelin-specific lymphocytes into the CNS, oligodendrocytes are damaged and demyelination occurs. Many different cells of the immune system contribute to the demyelinating process. Most immune cells are able to contribute to demyelination, but the process is most commonly mediated by antibody and complement. Antibody and complement are responsible for lesions in 40-50% of MS patients [33]. Complement is heavily concentrated in the demyelinated lesions in the brains of MS patients, in addition to the opsonins C3b and C3d that enhance the ability of macrophages and neutrophils to phagocytose disrupted myelin peptides [34-36]. In the brains of MS patients, B cells are more heavily concentrated in areas with acute demyelination compared to minimally demyelinated lesions [36]. Autoantibodies directed against peptides that make up the myelin sheath (myelin basic protein, proteolipid protein, cyclic nucleotide phosphodiesterase) are also heavily concentrated in lesioned areas in the brains of MS patients [36]. In addition to antibody and complement, $CD8^+$ T cells play an important role in the pathogenesis of MS. CD8+ T cells make up the largest percentage of lymphocytes in the MS brain [37]. All neuroectodermal cells in MS lesions express MHC class I molecules, making them a target for $CD8^+$ T cells [37]. In addition to their proinflammatory properties, $CD8^+$ T cells can also suppress the immune system and downregulate inflammation [33]. However, experiments with perforin, an important regulator of cytotoxic damage to immune cells, have made it clear that $CD8^+$ T cells at active MS lesions have a cytotoxic role and cause demyelination and axonal damage [38]. Bystander $CD4^+$ T cells do not contribute

to the demyelinating process, but once these $CD4^+$ T cells move into the CNS and become activated by myelin antigen they can directly mediate CNS demyelination [39].

After demyelination occurs, remyelination is possible and can prevent further CNS damage. The ratio of demyelination to remyelination determines if a patient will go on to develop secondary progressive MS (SP-MS) from relapse remitting MS (RR-MS) [33]. If remyelination occurs before axonal damage, irreversible physiological damage can be prevented. None of the FDA-approved therapies target oligodendrocytes to stimulate remyelination, but it is a very interesting possibility for future therapeutic intervention.

1.1.2.3. Neuronal Damage

In his 1868 paper describing MS, Charcot noticed the presence of neurodegeneration in demyelinated lesions [5]. As previously mentioned, it is unknown whether demyelination precedes or follows neurodegeneration in MS pathogenesis [25, 26], but there are many possible causes of neuronal damage [40]. Glutamate toxicity, direct antibody damage, proinflammatory cytokine damage, and T cell attack on the axons can all cause neurodegeneration [41]. Damage to neurons can occur in the early stages of MS, but clinical symptoms are not evident until a threshold level of damage has been reached [42]. If a mouse is given injections of a myelin peptide to induce EAE, up to 15% and 30% of axons can be damaged in the lumbar and cervical spinal cord sections, respectively, without the animal displaying behavioral symptoms of EAE [42]. In some patients neurodegeneration is visible in areas with normal appearing white matter and no inflammatory infiltrates [43], while damaged neurons in other patients are completely surrounded by inflammatory infiltrates [44, 45]. The first two stages of MS, inflammation and demyelination, are thought to be responsible for RR-MS, while the final

stage of neurodegeneration is what leads to the irreversible disabilities seen in SP-MS [42].

1.1.3. Clinical Subtypes of MS

MS progression varies between patients, and different disease courses are categorized as separate subtypes of MS. Approximately 80-85% of all MS patients are initially diagnosed with RR-MS [46-48]. RR-MS is characterized by short-term, acute exacerbations of disease symptoms followed by a full recovery [46-50]. After 10 years, about 40% of all RR-MS patients do not experience a full recovery between the relapses, developing SP-MS [46, 47, 49]. Because SP-MS involves both relapses and a steady disease progression, half of these MS patients require a walking aid [47, 48]. 10% of MS patients are initially diagnosed with the primary progressive form of MS (PP-MS), which involves a slow but steady increase in disease severity from the time of onset [48, 50, 51]. The remaining 5% of MS patients are originally diagnosed with progressive-relapsing MS (PR-MS) [48, 50]. PR-MS is similar to SP-MS in that acute exacerbations of MS symptoms occur, but in PR-MS a steady disease progression occurs from the time of disease onset [48, 52]. MS heterogeneity makes treatment especially difficult, and prognosis and treatment depend on disease course. RR-MS patients generally respond better to immunomodulatory therapies compared to those with PP-MS [46]. Post-mortem histological analysis of MS patients has shown that symptom presentation does not correlate with histological damage [46]. In addition to the differences in disease course, there are some differences in the affected populations and CNS pathogenesis of RR-MS and PP-MS. The average age of disease onset in RR-MS patients is 30 years, while the average PP-MS patient is diagnosed at 40 years of age [53]. Overall, MS affects approximately 2 women for every man, but in PP-MS the gender distribution is 1:1 [53]. Early spinal cord atrophy is common in PP-MS but

doesn't occur in RR-MS [53]. Gadolinium-enhancing lesions are prevalent in RR-MS but rare in PP-MS [53]. RR-MS patients generally respond to interferon or glatiramer acetate therapy, but PP-MS patients rarely respond to either treatment [53].

1.1.4. Diagnosis of MS

There are no specific biomarkers to test for that are uniformly present in the blood or CSF of MS patients, making definite diagnosis of MS very difficult [46]. Tools that are currently utilized to assist in MS diagnosis include magnetic resonance imaging (MRI), evoked potential tests, and spinal taps. MRIs can be used to observe both active and inactive lesions [54, 55]. While MRI is an unquestionably valuable tool for MS diagnosis, the test provides abnormal results (i.e. presence of a lesion) in only 90-95% of people with MS [54, 56], and lesions that resemble those in the brains of MS patients occur in the brains of healthy people as a natural part of the aging process [54]. Additionally, there is no correlation between the efficacy of a treatment in the clinic and the efficacy of a treatment as evidenced by MRI [55]. Evoked potential tests are useful to confirm neurological disability and demyelination, and studies that utilize evoked potential tests are generally able to correlate the test to clinical disability [56, 57]. However, evoked potential tests cannot detect subclinical lesions [57] and they give restricted information on the exact location of the lesion [56]. Spinal taps and protein electrophoresis of CSF demonstrate the presence of oligoclonal bands of gamma immunoglobulin in 90-95% of all MS patients [54, 58]. Oligoclonal immunoglobulin bands that are present in the CSF remain there for life [54], so false positive tests due to another autoimmune disease or dysregulation of the immune system are possible. While these tests are valuable, none are absolute predictors of MS and better markers should be explored.

In 2001, the McDonald Criteria was established by the International Panel for the Diagnosis of MS [59]. The purpose of the criteria was to serve as a tool for neurologists to more accurately and reliably diagnose MS. Based on these criteria, a patient has confirmed RR-MS if he or she has demonstrated dissemination of disease in both space and time, meaning he or she has had clinical episodes that last at least 24 hours but the episodes are separated by 30 days, and that he or she has distinct changes in lesions as evidenced by MRI or CSF analysis [59]. According to the McDonald Criteria, "An "attack" (exacerbation, relapse) refers to an episode of neurological disturbance of the kind seen in MS, when clinicopathological studies have established that the causative lesions are inflammatory and demyelinating in nature." [59] The time between episodes can range from weeks to decades [60]. The McDonald Criteria for PP-MS states that the patient must have disease progression for 1 year, and 2 of the 3 following evidences: 1. 9 MRI brain lesions or 4 brain lesions and abnormal visual evoked potential test; 2. 2 MRI spinal cord lesions; 3. CSF oligoclonal bands or increased IgG index [53].

While these criteria aid in diagnosis of the disease, there is still a significant amount of time that passes between the time the patient and physician suspect MS and the time a positive diagnosis is made. An easily testable marker or series of tests that could confirm a positive MS diagnosis would reduce this window, expedite the start of disease treatment, and potentially allow the clinician to choose which treatment regimen would best treat each patient on an individual basis. Additionally, it is speculated that MS initiation begins as early as 13-15 years of age, and diagnosing the disease in the beginning stages would improve both prognosis and likelihood of a given therapy to succeed at stopping disease progression. [61]

1.1.5. Current Treatments

The challenge of finding effective MS treatments has been made especially difficult due to the varying disease courses between patients. There are currently 6 FDA-approved drugs used to treat MS. The presence of inflammatory infiltrates in CNS lesions has led many investigators to target potential MS therapeutic interventions to the immune system [62]. Newly-diagnosed patients generally begin treatment with an immunosuppressive agent, and if there is no improvement in MS symptoms with immunosuppression a more aggressive therapy that may cause more serious side effects is warranted [62]. Each therapy decreases relapse rate by approximately 30% compared to placebo [63].

In 1993, Interferon (IFN)-beta-1b (Betaseron) became the first disease-modifying therapy to be approved by the FDA for the treatment of RR-MS [64]. IFN-beta-1b modulates the immune response in MS by downregulating the expression of the interleukin-2 (IL-2) receptor in NK cells, T cells, and B cells [2, 65]. By decreasing the amount of pro-inflammatory stimulation by IL-2, the production of the pro-inflammatory cytokine IFN-gamma (IFN-γ) by T cells and macrophages and the rate of T cell proliferation decrease [65]. IFN-beta-1b has also been shown to decrease production of the proinflammatory cytokine IFN-γ by $CD4^+$ $CD28^+$ T cells [66].

IFN-beta-1a (Avonex) was approved by the FDA in 1996 for the treatment of RR-MS [64]. The route of administration for Avonex is an intramuscular injection, and injections are given to patients weekly [64]. Another form of IFN-beta-1a (Rebif), different from Avonex in the frequency and route of administration, was approved for MS treatment in Europe and Canada in 1998 and in the United States in 2002 [64]. Rebif is given to patients in a subcutaneous injection 3 times per week [64]. IFN-beta-1a therapies are thought to work by stimulating an upregulation in interleukin-10 (IL-10)

production [2]. IL-10 is an anti-inflammatory cytokine expressed in monocytes, Th2 cells, and mast cells [67]. An animal study highlighted the importance of IL-10 in MS prevention, as IL-10 knockout animals had significantly decreased thresholds for disease induction [68].

Glatiramer acetate (Copaxone®) is an FDA-approved treatment for RR-MS that is given to patients via a daily subcutaneous injection [64]. It is a polypeptide made up of four amino acids that stimulates T cells at the CNS lesion site to develop into anti-inflammatory T cells [2, 69, 70]. Because the drug is made up of amino acids found in myelin, it is also hypothesized that this immunomodulatory therapy acts as a decoy by competing with CNS peptides for antigen presentation [2, 69, 70].

Mitoxantrone (Novantrone) is an immunosuppressant MS therapy that works by inhibiting T cell, B cell, and macrophage activation and proliferation [2, 69]. The complete mechanism of action is unknown, but because it is a type 2 topoisomerase inhibitor there are potential toxicities associated with taking the drug; it is recommended that therapy lasts a maximum of two to three years [2]. Mitoxantrone has successfully decreased disease symptoms in EAE models. When administered at the time of disease induction [71] or at the time of disease onset [72], and during a remission in a relapsing EAE model [72], the drug was successful at decreasing disease symptoms or preventing relapses. In human clinical trials, mitoxantrone reduced RR-MS relapse rate and decreased the percentage of patients with an EDSS above 5 from 70.8% to 41.7% after one year of treatment [73]. Mitoxantrone is the first and only drug to be approved for the treatment of PP-MS, SP-MS, and worsening RR-MS [74].

Natalizumab (Tysabri®) is a monoclonal antibody directed against the alpha4-integrin chain of the VLA-4 found on the surface of lymphocytes, which binds to the brain endothelium VCAM-1 to mediate passage through the BBB and into the CNS [2, 69, 75,

76]. The drug is given by an intravenous infusion once per month, and it works by inhibiting passage of lymphocytes into the CNS [64]. In the phase III AFFRIM (Natalizumab Safety and Efficacy in Relapsing Remitting Multiple Sclerosis) clinical trials, Natalizumab decreased relapse rate by 68% and decreased the number of gadolinium enhancing lesions by 92% after one year of treatment [77]. Natalizumab was the most successful treatment for MS, but the drug was removed from the market in 2005 due to 3 reported cases of progressive multifocal leukoencephalopathy [64, 76, 78]. The drug was re-introduced to the market in 2006 with a "black-box warning" and mandatory participation of prescribing clinics in the TOUCH program, which educates on the drug and requires regular reports on patient responses [61]. While precautions have been taken with the re-introduction of Natalizumab, 5 patients have been diagnosed with PML since it has been back on the market in 2006 [76].

A potential way to increase the efficacy of the FDA-approved therapies for MS is to administer them in combination with one another. The SENTINEL (Safety and Efficacy of Natalizumab in Combination with IFN-Beta-1a in Patients with Relapsing Remitting Multiple Sclerosis) clinical study published in 2006 demonstrated that combination therapy of Natalizumab with IFN-beta-1a led to a decrease in the probability of patient disease progression to 23%, compared to those patients receiving placebo with IFN-beta-1a who had a 29% chance of disease progression [79]. RR-MS patients benefit from initial treatment with mitoxantrone followed by glatiramer acetate, as these patients experienced a decrease in the number of gadolinium-enhancing MRI lesions and a decrease in the frequency of adverse events compared to those patients given glatiramer acetate alone [80, 81]. The recently published GLANCE (Glatiramer Acetate and Natalizumab Combination Evaluation) study testing the safety and efficacy of Natalizumab with glatiramer acetate showed that Natalizumab plus glatiramer acetate

decreased the number of new lesions formed per year in RR-MS patients from 0.11 with glatiramer acetate alone to 0.03 with combination therapy [82]. Taken together, these studies show that the efficacy of FDA-approved drugs can be heightened if the drugs are administered with the right timing in the right combinations.

While the therapies listed above have shown success in reducing the negative side effects of MS, there is substantial room for improvement. All FDA-approved therapies are given via injection, which is an undesirable route of administration for the patients. Additionally, the negative side effects of the treatments, which can range from flu-like symptoms to cardiotoxicity to death, pose uncomfortable and serious health risks for patients. Cost of treatment is also an important issue, as over $14 billion are spent per year in the United States alone on MS treatment [61]. The cost of treating a MS patient is approximately $47,000 per year [61]. In a 2008 survey, 983 MS patients aged 21-64 were questioned about their treatment regimens [83]. 96.3% of the population had health insurance, but 16% of the patients reported lack of health care coverage for their MS medication and 22.3% of the patients reported not filling a prescription or cutting pills in half due to high drug costs [83]. It is clear that more effective and less expensive disease-modifying therapies with minimal side effects need to be explored to improve treatment options for MS patients.

1.2. Experimental Autoimmune Encephalomyelitis

Experimental Autoimmune Encephalomyelitis (EAE) is a popular and widely studied model of MS. EAE can be induced in mice or rats through active immunization with a myelin peptide, through passive transfer of activated myelin-specific immune cells [84], or through a viral infection [85]. In actively induced EAE, a myelin peptide injected into the animal produces a T-cell mediated autoimmune reaction that closely mimics MS [8, 41]. The pro-inflammatory diseases are similar, as levels of IFN-γ, interleukin-1beta

(IL-1β), and tumor necrosis factor-alpha (TNF-α) are upregulated in EAE and MS and both are characterized by CNS demyelination and neurodegeneration [67, 86]. The similarities that EAE and MS share make EAE an ideal model for testing potential disease therapies for MS [2, 84].

1.2.1. Models of EAE

EAE dates back to the 1920's, when researchers tried to inject human spinal cord homogenate into rabbits to induce spinal cord inflammation [87]. Many models of EAE have since emerged, and different myelin peptide-animal strain combinations can be used to induce various disease courses. Mice, rats, and monkeys are used to study EAE [88]. Monkeys are beneficial to use because of their genetic and immunological similarities to humans [89], but cost limits the amount of MS research conducted with monkeys. SJL mice can be injected with proteolipid protein (PLP) 139-151 to induce a relapsing form of EAE intended to mimic RR-MS [90]. Injecting Biozzi ABH mice with spinal cord homogenate produces an EAE disease course similar to PR-MS in humans [91]. The mice develop RR-EAE followed by a steady increase in disease progression [91]. Injecting myelin basic protein (MBP) or spinal cord homogenate into Lewis rats produces a chronic form of EAE [92]. Injection of C57BL/6 mice with myelin oligodendrocyte glycoprotein (MOG) is a common model due to a desirable genetic background in C57BL/6 mice. Moreover, this combination also produces a chronic disease course [92] that includes the three main phases of MS, inflammation, demyelination, and neurodegeneration [93]. The C57BL/6 model is also desirable to use because it produces both T and B cell responses similar to what occurs in MS, where many other EAE models are only T cell-mediated diseases [23, 92, 94]. Although MOG makes up <0.1% of the CNS myelin, MOG is found on the outer surface of the oligodendrocytes and is therefore an easy target for the immune system [33].

To administer EAE with a myelin peptide injection, the myelin peptide is dissolved in an aqueous solution which is emulsified in Complete Freund's Adjuvant (CFA). CFA is made up of heat-killed mycobacterium tuberculosis and mannide mono-oleate in paraffin oil [95]. CFA inhibits degradation of the antigen and increases the production of myelin peptide-specific antibodies [95]. In addition to the myelin peptide in CFA, animals are usually given 2 intraperitoneal injections of pertussis toxin [96, 97]. Pertussis toxin is a crucial component to EAE induction, and increasing dosages induces more uniform and severe forms of EAE [98]. Pertussis toxin increases permeability of the BBB, which allows lymphocytes to enter the CNS [99]. Pertussis toxin also propagates the proinflammatory stage of EAE by stimulating the release of interleukin-6 (IL-6), Th17, and transforming growth factor-beta (TGF-β) [100].

It is possible to induce EAE by isolating immune cells and antibodies from animals injected with a myelin peptide and injecting the cells and antibodies into a new animal, a method called adoptive transfer [92]. Adoptive transfer is useful in studying extensive axonal damage and inflammatory brain lesions, as adoptive transfer EAE produces a more severe form of EAE than the standard myelin peptide injection [92]. $CD4^+$ T cells, notably the Th1 and Th17 subsets, are most commonly used to passively transfer EAE [23]. However, EAE can also be induced with $CD8^+$ T cell populations either isolated from MOG-injected C57BL/6 mice and enriched in culture with additional MOG stimulation or isolated from *shiverer* mutant mice that lack MBP [23].

A form of EAE can also be induced with Theiler's murine encephalomyelitis virus (TMEV) infection [85]. TMEV is a non-enveloped, positive-sense, single-stranded RNA virus [85]. Injection of the virus intracerebrally produces a demyelinating disease of the CNS in susceptible strains [85]. In EAE induced with a myelin peptide, demyelination precedes axonal damage, but a TMEV infection results in axonal damage followed by

demyelination [85]. C57BL/6 mice are not very susceptible to TMEV, but in Wld mice TMEV causes a biphasic paralytic disease with demyelination present during the first phase of disease, but absent after 5 weeks during the chronic phase [85].

1.2.2. Insights into MS using EAE Models

EAE models have served an invaluable role in the laboratory analysis and characterization of MS. However, various therapies have been highly successful at inhibiting development or progression of EAE but have failed to alleviate symptoms of MS in humans. EAE studies can also fail to accurately predict toxicity of MS treatments, most notably Natalizumab treatment which had no complications in EAE models but led to fatal cases of progressive multifocal leukoencephalopathy in humans [101]. These issues are likely due to the fact that EAE is studied in an small inbred population of mice for a short duration of time, while MS is a lifelong disease that affects a large heterogeneous population around the world [101]. Additionally, only about 5% of all small molecule therapeutics studies are passed by the FDA due to toxicity concerns [101]. Prospective MS therapies that were advantageous In EAE but not successful in the clinic include TNF-α [102-107] and IFN-γ [3, 108-110]. Particularly disappointing were the studies on TNF blockade, as monoclonal antibodies directed against the cytokine or fusion proteins that blocked the TNF receptor were successful treatment for Crohn's disease and rheumatoid arthritis, but not MS [103]. In EAE models, anti-TNF antibodies and fusion proteins inhibited or ameliorated disease symptoms [102, 104], and injection of TNF exacerbated EAE symptoms [105]. Soluble TNF is elevated in MS and post-mortem studies demonstrate that concentration of TNF is positively correlated with MS lesion severity [106], but TNF blockade surprisingly increased relapse rate in humans compared to placebo-treated controls [107]. Similar to the TNF studies, IFN-γ decreases symptoms of EAE but worsens MS in humans. IFN-γ that is produced by

both the innate and adaptive immune systems is similar to TNF-α in its ability to regulate intracellular infection and tumor progression [111]. IFN-γ can also stimulate cells of the CNS, most notably microglia, to produce MHC class I and II molecules, enabling the cells to become APCs and promoting the immune response [108]. Mice unable to produce IFN-γ develop a more severe form of EAE compared to mice that are able to produce the cytokine [3]. Mice that are genetically manipulated to temporally produce IFN-γ in the CNS showed an increase in oligodendrocyte survival when IFN-γ production was stimulated [109]. Thus, IFN-γ is thought to be protective in EAE. However, when MS patients are given IFN-γ, relapse rate increases [110].

Although there has been much false hope generated from treatments that were successful in EAE studies but did not translate into efficacious MS treatments, all 6 FDA-approved therapies have been successful at ameliorating EAE symptoms. Two treatments, glatiramer acetate and Natalizumab, were developed from EAE studies [112]. Therefore, it is still beneficial and relevant to test potential MS therapies in EAE models.

1.3. Opioids

1.3.1. Opioid Peptides

Opioids are endogenously produced peptides that are found throughout the body and are extensively dispersed throughout the CNS [113]. Endogenous opioids were discovered by Hughes and colleagues in 1975 [114]. Opioids can act at neurotransmitters to regulate pain, enforce reward, and modulate neuroendocrine function [113, 115]. Nearly 20 unique endogenous opioids have been identified, all of which are derived from three precursor proteins: pro-enkephalin, pro-opiomelanocortin, and pro-dynorphin [113, 116]. The four types of endogenously produced opioids are enkephalins, endorphins, endomorphins, and dynorphins [115, 117]. These peptides

differ in action and receptor affinity but have a high degree of sequence homology. Enkephalins, endorphins, and dynorphins contain the amino acid sequence Tyr-Gly-Gly-Phe, while endomorphins contain the amino acid sequence Tyr-Pro-Trp/Phe-Phe [116, 117].

Endogenous opioids are ubiquitous, and each endogenous opioid has a unique distribution throughout the body. Endomorphin-1 is present mainly in the brain, while endomorphin-2 is primarily localized to the spinal cord [116]. The highest concentration of enkephalins in the body is in the corpus striatum, with [Met^5]-enkephalin (Met-enk) nearly 10-fold more concentrated than [Leu^5]-enkephalin (Leu-enk) [118, 119]. Immunohistochemical analysis of enkephalin distribution in developing and mature rat brain showed high levels of enkephalins present in the developing brain, but undetectable levels in mature rat brains [120]. β-endorphin is synthesized in the pituitary gland and hypothalamus and systemically released, but β-endorphin does not easily cross the BBB [121]. Enkephalins and endorphins can also be found in a variety of tumors, including breast, prostate, and liver [122]. Dynorphin is primarily located in areas of the brain associated with decision making and reward, such as the ventral tegmental area, the nucleus accumbens, and the prefrontal cortex [123].

Opioid expression can change under various conditions. β-endorphin expression markedly increases in response to formalin-induced pain and inflammation [124], along with strenuous activity [125]. Spinal cord prodynorphin mRNA levels increase in response to chronic and acute inflammation [126]. Antagonizing the receptor for dynorphin signaling can lead to decreased dopamine release [123], which in turn can control expression of dynorphin and enkephalins [127]. Changes in behavior and mood alter the effects of opioid peptides, along with opioid receptor availability.

1.3.2. Opioid Receptors

1.3.2.1. Opioid Receptor Distribution

There are three major classes of opioid receptors: μ, δ, and κ. All 3 receptor subtypes are widely distributed throughout the CNS, the autonomic nervous system, the peripheral nervous system, and various tissues and organs [115, 128]. Different concentrations of the 3 opioid receptors throughout human body indicate that each receptor has a specific and unique function [115]. Mu (μ), delta (δ), and kappa (κ) opioid receptors are seven transmembrane G-protein coupled, and all have different affinity for the various endogenous and synthetic opioid peptides [116]. All are located in the cell membrane, and opioid receptors function by converting extracellular signals into intracellular messages [129]. Endomorphins have a very high selectivity for μ opioid receptors [116]. Enkephalins bind with the highest affinity to δ opioid receptors [116]. β-endorphin has equal affinity for μ and δ opioid receptors [116]. Dynorphins bind to κ opioid receptors with the highest affinity [116]. μ, δ, and κ opioid receptors are present in tumors originating from a variety of organs, including breast, prostate, neck, tongue, ovarian, uterus, rectum, stomach, liver, lung, lymph nodes, and pharynx [122].

All 3 receptor subtypes are widely distributed throughout the CNS [128]. μ opioid receptors have high levels of expression in the basal ganglia, cortical structures, thalamic nuclei, spinal cord, and nuclei in the brainstem [130, 131]. δ opioid receptors are found throughout the brain [131]. κ opioid receptors are located in the limbic system and the spinal cord [131]. In the CNS, μ opioid receptors are primarily located on the cell membrane, but δ and κ opioid receptor immunostaining indicates intracellular receptor localization [132]. Oligodendrocytes express μ and κ opioid receptors [133].

Binding analyses have demonstrated that opioid profiles change with age and under various physiological conditions. δ and κ opioid receptor capacities are 7.8 and

3.6 fold higher, respectively, in newborn human cerebellum compared to mature adult cerebellum [134]. μ opioid receptor capacity in adults is one half the binding capacity of μ opioid receptors in newborn cerebellum [134]. Animals with peripheral inflammation experienced increased nociception in response to morphine compared to control animals, indicating μ opioid receptor profile is altered under inflammatory conditions [126].

1.3.2.2. Opioid Receptor Function

Opioid receptors differ in affinity for various opioid ligands. μ receptors have an affinity for endogenous enkephalins, β-endorphin, and dynorphin A [131], along with exogenous morphine [Martini Whistler], methadone, and fentanyl [131]. μ opioid receptors can be divided into 2 subtypes - μ1 and μ2 receptors. Activation of μ1 opioid receptors causes strong analgesia and euphoria, while μ2 receptors are related to respiratory depression, prolactin release and sedation [131]. The use of morphine for treating chronic pain is not recommended, as tolerance to opioids and desensitization can develop easily with G-protein-coupled receptors [129]. μ opioid receptor phosphorylation by protein kinase C, protein kinase A, tyrosine kinases, and G-protein coupled receptor protein kinases promotes receptor desensitization [129]. δ opioid receptor activation can also produce analgesia, but to a much lesser degree than μ receptor activation [135]. δ receptors have a very strong affinity for endogenous enkephalins, and a weaker affinity for β-endorphin [131]. Activation of δ opioid receptors with the selective agonist SNC80 leads to improvements in symptoms of depression, anxiety, pain, cardiac disorders, and Parkinson's disease [136]. Agonists for δ opioid receptors can also convey protection against neuronal mitochondria dysfunction that occurs under conditions of ischemia and hypoxia [137]. κ receptors have strong affinity for endogenous dynorphin A [131]. Agonists of κ opioid receptors cause spinal

analgesia, sedation, dysphoria, and respiratory depression [131]. Administration of the endogenous dynorphin A can also cause decreased dopamine production [138]. Depression, cocaine addiction, and dysregulated feeding behavior are potential clinical uses for κ opioid receptor antagonists [138].

The interaction of opioids with their opioid receptors can be inhibited by the opioid receptor antagonist naltrexone (NTX) or naloxone (NAL). NAL was synthesized in 1960, and was unique from existing opioid receptor antagonists available at that time because it did not produce dysphoric side effects [139]. However, the half-life of NAL is only 30 min [140], so it could not be a treatment for opioid addicts that would provide a long-lasting opioid receptor blockade. NTX was synthesized in 1963 to serve as a more potent and longer-lasting opioid receptor antagonist [139]. Reports on the half-life of NTX range from 8 hours [140] to 9.7 – 10.3 hours, depending on route of administration [141]. Both NTX and NAL can cross the BBB [142]. NTX is orally effective, but NAL is not [140]. NTX earned FDA approval for use in the treatment of alcohol and opiate addiction in 1994 [143]. The patent for NTX expired in 1985 [143].

1.3.3. Opioids and Immunology

Groundbreaking work in 1979 by Wybran et al. demonstrated that opioid receptors are present on immune cells, and that opioids (namely Met-enk and morphine) can affect immune cell function [144]. All 3 traditional opioid receptors, μ, δ, and κ, are present on immune cells and have been cloned from primary cultures of lymphocytes and macrophages [145-150]. The roles of opioids in immunity are conflicting, as some reports suggest that opioid peptides suppress the immune system from functioning normally while others observe opioid-mediated stimulation of the immune system. Opposing reports and conclusions are likely due to the employment of different model systems.

Inflammation in vivo and stimulation of lymphocytes in vitro can affect opioid and opioid receptor expression. Concanavalin A (Con A) stimulation of mouse T cell lines increases the expression of proenkephalin A mRNA [151], and supernatants of phytohemagluttinin (PHA) -stimulated cell lines (human peripheral blood lymphocytes, rat mononuclear cells) have high Met-enk immunoreactivity [152-154]. Following an injection of CFA into the rat paw, there is an upregulation in μ opioid receptor expression in the ipsilateral lumbar dorsal root ganglia within 24 hours [155].

Humoral immunity can be regulated by opioid agonists and antagonists. Plaque forming cell (PFC) response and hemagluttinin production are markers of humoral immunity activity levels [156]. Administration of the opioid receptor agonists Met-enk and Leu-enk in animals injected with sheep red blood cells (SRBC) led to increased PFC response and higher anti-hemagluttinin levels in the serum 4 days after the SRBC injection compared to vehicle-treated controls [156]. Conversely, administration of ICI 174864, a δ opioid receptor antagonist, or NTX caused a decrease in PFC response from spleen cells and lower hemagluttinin antibody production [156]. Administration of either antagonists with the Met-enk or Leu-enk inhibited the effects of the agonists. These experiments indicate that μ and δ opioid receptors can regulate humoral immunity [156]. Morphine administration inhibits B cell antibody generation both in vitro [157-159] and in vivo [158]. Morphine-mediated inhibition of antibody production in vivo is reversible with NTX [158].

Activation of opioid receptors can also regulate cell-mediated immunity. Administration of opioid receptor agonists in vitro and in vivo suppresses T cell, macrophage, and natural killer (NK) cell function. Administration of the δ opioid receptor agonist deltorphin inhibits proliferation of purified populations of $CD4^+$ and $CD8^+$ T cells and inhibits IL-2 production in $CD4^+$ T cells [160]. Cultured macrophages are unable to

phagocytose sheep erythrocytes following administration of Met-enk, Leu-enk, or morphine [161, 162]. Injections of β-endorphin into mice cause immunosuppression [163]. Met-enk decreases NK cell activity in the spleen of athymic mice after 28 days of treatment [164]. Conversely, administration of the opioid receptor antagonist NTX causes an elevation in NK cell activity in the peripheral blood [164].

Timing of opioid administration and slight differences in opioid peptide structure can cause opposing affects on the immune system. The paper documenting Wybran's initial discovery of opioid receptors on T cells reported morphine to suppress and Met-enk to increase T cell rosette formation [144]. Dynorphin and B-endorphin stimulate superoxide formation in neutrophils and macrophages, while Met-enk and Leu-enk inhibit superoxide formation in neutrophils [165, 166]. When neutrophils and monocytes are pretreated with opioid peptides, migration and chemotaxis of the cells are inhibited [167, 168]. Conversely, when opioids are administered to activated monocytes and neutrophils, migration and chemotaxis of the cells increase [169-172]. Opioids only have been shown to affect migration of immune cells, as administration of an array of opioids specific for classical opioid receptors had no effect on the migration of cancer cells [173].

Administration of opioid receptor antagonists in vivo alters the rate of lymphocyte proliferation in vitro. T lymphocytes isolated from the blood of both rats and humans were stimulated in culture with Con A or PHA. Human subjects either were given a single infusion of 0.4 mg NAL or took a 50 mg NTX tablet every night for 7 days, and blood samples were taken before and after the treatment regimen. Rats were given either a single dose of 5 mg/kg NAL or NTX, or a dose of 5 mg/kg NAL or NTX for 7 days, and blood samples were collected after the treatment regimen. In both rats and humans, acute treatment with opioid receptor antagonists caused an increase in the rate of lymphocyte proliferation. Chronic treatment led to a decrease in the rate of

lymphocyte proliferation. Binding analysis was only completed on NAL samples, but the number of β-endorphin receptors was significantly upregulated following chronic NAL treatment as compared to controls. [140]

The role of the endogenous opioid Met-enk has been tested in models of EAE. Preliminary studies by Jankovic and Maric demonstrated that a high dose of Met-enk (5 mg/kg) suppressed EAE development in Wistar and Lewis rats [174]. Daily administration of 5 mg/kg Met-enk prevented paralysis in Wistar rats and significantly delayed the onset of paralysis in Lewis rats [174]. Conversely, a low dose of Met-enk (0.2 mg/kg) had no effect on EAE development and pathogenesis [174]. The authors concluded that Met-enk had immunomodulatory properties and might be a useful treatment for MS. In a separate experiment, daily administration of 5 mg/kg Met-enk inhibited adoptive transfer of EAE in a Lewis rat model [175]. Follow-up research from this group demonstrated that location of Met-enk administration did not alter efficacy. Met-enk was administered via surgically implanted cannulae into the lateral ventricles, and a dosage of 1 mg/kg decreased clinical and histological symptoms of EAE [176]. This group conducted more studies on immunomodulatory properties of Met-enk, but no further studies were completed to examine and more comprehensively illustrate the effects of Met-enk in EAE.

1.4. The OGF-OGFr Axis

1.4.1. NTX and OGF Regulate Cell Proliferation

In addition to its well-known analgesic properties, the endogenous opioid peptide Met-enk has regulatory effects on cell proliferation. Studies by Zagon and McLaughlin dating back to 1986 have demonstrated that Met-enk negatively regulates cell growth. Because none of the other natural or synthetic opioid peptides possess the inhibitory growth properties of Met-enk, the peptide has also been given the name opioid growth

factor (OGF) [177-180]. OGF is an endogenously produced pentapeptide that negatively regulates growth in a receptor-mediated fashion [177-180]. OGF's actions are reversible upon the addition of a general opioid receptor antagonist such as NTX [177-180]. NTX competitively binds to each of the classical opioid receptors, but the traditional G-protein coupled receptor cascade that is activated upon opioid receptor agonist binding is not initiated [131]. However, the interaction of OGF and NTX with a unique nuclear receptor causes changes in growth regulatory processes.

Multiple experiments and observations led to the discovery of the unique growth properties of OGF and NTX. In 1983, two dosages of NTX were shown to have opposite effects on the growth of neuroblastoma in mice [181]. Hot plate tests using morphine with a NTX challenge showed that a high dose of NTX, 10 mg/kg, provided continuous 24-hour opioid receptor blockade, while a low dose of NTX, 0.1 mg/kg, caused intermittent 4-6-hour opioid receptor blockade [181]. The high dose of NTX increased tumor incidence and rate of death and decreased time to tumor formation, while the low dose of NTX decreased tumor incidence and death and increased time before tumor formation [181]. It was well-known that OGF was present in the CNS and could function as a neurotransmitter, but this was the first paper to suggest a role for opioid systems in neuro-oncogenesis. Similar studies were completed in a rat model of neuroblastoma with findings parallel to those in the mouse study – a low dose of NTX inhibited and a high dose of NTX stimulated cancer cell growth [182]. These experiments demonstrated that opioid receptor blockade affected proliferation, but it was unknown if opioid receptor agonists could regulate cell growth. The NTX dosage experiment was repeated in mice, and again animals that experienced complete opioid receptor blockade with the high dose of NTX had decreased latency to tumor development and accelerated mortality while animals with the low dose of NTX experiencing intermittent opioid receptor

blockade had a delay in tumor formation and an increase in survival rate compared to sterile water-treated controls [182].

NTX-mediated opioid receptor blockade leads to an increase in endogenous opioid and opioid receptor production. Administration of 50 mg/kg NTX into rats causes a 67-183% increase in OGF levels from 5 min post-injection to 24 hours post-injection in the caudate putamen as compared to control rats [183]. Following a 1 mg/kg injection of NTX, levels of OGF in the cerebellum were reduced by approximately 80% at 5 min, 30 min, 2 hr, and 4 hr, but a 35% increase was observed at 8, 16, and 24 hours [183]. There were no changes in OGF levels in the cerebellum of rats given 50 mg/kg NTX or in the plasma of animals given a high or low dose of NTX, demonstrating that location may vary, but in response to NTX, endogenous production of OGF increases. In an in vivo cancer study, both high and low NTX-treated groups had increased levels of β-endorphin and OGF in tumor tissue [184].

Previous studies proving that complete blockade of opioid receptors causes an increase in cancer progression suggest that the interaction of endogenous opioids with their receptors could be a beneficial interaction in preventing cancer progression. To determine if enkephalins could regulate cancer cell growth, mice were injected with neuroblastoma cells to induce tumor formation and were given daily injections of either Leu-enk or OGF [185]. The mice given daily injections of OGF experienced delays in tumor formation and decreased mortality rates while animals given Leu-enk did not differ from control-treated mice, suggesting that the key opioid that regulates tumor growth is OGF [185].

The OGF-OGFr axis is also present and functioning in the eye. Re-epithelialization of an injured cornea is expedited in Type 1 diabetic rats treated with NTX compared to saline treated diabetic rats [186]. OGF and OGFr

immunohistochemical analysis of the cornea demonstrated that the receptor is present in the paranuclear membrane cytoplasm, in the nuclear membrane, and in the nucleoplasm adjacent to heterochromatin [187].

1.4.2. The Discovery of the OGFr

Following the discovery that OGF and NTX are negative and positive regulators of growth, respectively, the question arose as to what receptor they utilize. Past experiments established that administration of classical opioid receptor agonists does not alter cell proliferation [185, 188]. Animals given β-funaltrexone, a μ-specific opioid receptor antagonist, had no changes in tumor incidence and formation compared to saline-treated control animals [188]. Additionally, rats given daily injections β-funaltrexone did not differ from control animals in their brain weight or development [189], supporting the idea that NTX's influence on growth is not mediated through the μ opioid receptor. COS-7 cells, a cell line derived from African green monkey kidney [190], are devoid of classical opioid receptors [191-193]. However, OGF administration causes a decrease and NTX administration causes an increase in COS-7 cell proliferation, suggesting the involvement of a non-classical receptor that can bind to both OGF and NTX [194].

Binding analyses completed in homogenates of neuroblastoma tumors from mice demonstrated the presence of a receptor with specific affinity for OGF. No other opioids selective for the classical opioid receptors could displace OGF from this receptor, with all other opioids having at least 100-fold weaker affinity for the receptor. This unique binding site was saturable, stereoselective, and specific for drug displacement. These findings, coupled with previous immunohistochemical proof of OGF in tumors and characterization of a function role of OGF, led to the discovery of the zeta opioid receptor. [195]

The previously termed zeta opioid receptor that interacts with OGF to regulate cell proliferation was cloned and sequenced, and it was found that it shared no structural homology with classical opioid receptors, it was not a G-coupled receptor like the classical opioid receptors, and it was located in the nuclear membrane instead of the cell membrane like the classical opioid receptors [196]. These key differences led to the proposal that the receptor be given a new name, opioid growth factor receptor (OGFr) [196]. OGFr has been cloned and sequenced in humans, rats, and mice [197]. There is substantial sequence homology between the three species, especially at the N terminal end of the 580, 634, and 677 amino acid rat, mouse, and human receptor, respectively [197]. Seven exons and six introns make up the 9 kb gene for OGFr [197]. The chromosomal location for the gene is 20q13.3, and defects in this chromosomal location have been associated with autism, newborn epilepsy, and myeloproliferative disorders [197]. There are 4 binding subunits of the OGFr of molecular weights 32, 30, 17, and 16 kilodaltons [198].

OGF halts cell growth through a unique cell signaling cascade. When OGF binds to OGFr, the bipartite nuclear localization signal of OGFr interacts with importin karyopherins to cause active nuclear import of the peptide-receptor complex through nuclear pores [197]. Deletion of the nuclear localization signals NLS 383-386 and NLS 456-460 on OGFr decreases receptor localization to the nucleus by 80% [199]. Localization into the nucleus takes 8 hours [199]. In squamous cell carcinoma of the head and neck, OGF-OGFr interactions induce p16 overexpression, which suppresses cells in the G0/G1 phase [200]. In pancreatic adenocarcinoma, transport of the OGF-OGFr complex into the nucleus induces an overexpression of p21, which also halts the cell at the G1/S checkpoint [201].

Regulation in growth through OGF or NTX interacting with OGFr is not due to apoptosis or necrosis [202] or changes in cell differentiation [203]. OGF, NTX, and other classical opioid receptor agonists do not alter the metastatic properties of migration, invasion, and adhesion in cancer cells [173]. When OGF binds to OGFr, growth, mitosis, and DNA synthesis rates decrease by stalling cell proliferation in the G0/G1 phase [204]. NTX, on the other hand, increases cell growth, mitosis, and DNA synthesis, and it increases the number of cells in the S and M phases [204]. OGF can act in both an autocrine and paracrine nature [205]. The effects of NTX at OGFr are stereospecific; a high dose of (+)NTX that provides 24-hour opioid receptor blockade does not affect neuroblastoma incidence compared to control animals, while the same high dose of (-)NTX increases tumor incidence and size compared to controls [206].

1.4.3. Distribution and Expression of OGFr

OGFr is present in cells that are dividing and developing, but the receptor is absent from post-mitotic cells [197]. In mice, rats, or humans, studies on OGFr have demonstrated receptor transcript or expression in myocardial and epicardial cells [207-209], the cerebrum [209], cerebellum [210], skin [211], eye [212], lung, liver, and triceps surae muscle [209]. Binding of OGFr is not recorded in the brain and cerebellum of adult rats [213], but Northern blot analysis demonstrates that OGFr mRNA is expressed in the rat brain and cerebellum throughout development and adulthood [210]. OGF decreased labeling index as measured by tritiated thymidine incorporation in the developing nervous system external germinal layer (gives rise to neurons) and the medullary layer (gives rise to glia) [214], and in the retina [215], indicating functioning growth receptors in these areas. The ontogeny of OGFr can be altered by administration of exogenous peptides. Administration of NTX at a high dose caused an increase in the binding capacity of the OGFr in the whole brain and cerebellum of rats

and an increase in the number of layers of germinal cells in the rat cerebellum as compared to vehicle-treated controls [213]. Administration of OGF also inhibits the growth of *S. aureus*, *P. aeruginosa*, and *S. marcesans*, demonstrating that OGFr originated billions of years ago [177].

1.4.4. OGFr and Development

Continuous opioid receptor blockade affects body and organ growth in developing animals. Newborn rats that experienced continuous opioid receptor blockade for three weeks through daily injections of a high dose of NTX (50 mg/kg), which led to an increase in cerebellum size, along with an increase in the number of glial cells and neurons in the cerebellum [216]. Subsequent developmental studies in newborn rats showed that continuous opioid receptor blockade with daily injections of 50 mg/kg NTX for 21 days led to increased body weight, increased weight of brain, heart, kidneys, liver, and skeletal muscle, and faster development of eye opening and walking ability compared to control treated newborn rats [217, 218]. Conversely, daily injections of a low dose of NTX (1 mg/kg) led to decreased body weight, decreased weight of brain, kidneys, liver, and skeletal muscle, and slower development of eye and ear opening and walking ability compared to controls [217, 218]. These studies revealed that opioid receptor blockade critically affects rat body, organ, and behavior development.

Prenatal exposure to a NTX or OGF can also affect growth, organ development, behavior, and mortality. Pregnant rats given a high dose of NTX to mediate continuous opioid receptor blockade gave birth to pups with higher overall body weight and higher wet and dry weights of brain, heart, kidney, liver, and skeletal muscle as compared to pups from rats injected with saline [219]. Gestation, course of pregnancy, litter size, and animal viability did not differ between groups [219]. These data show that opioids play

an important role in prenatal ontogeny regulation [219]. Post-natal rats from mothers given daily injections of a high dose of NTX had less grooming, rearing, wet dog shakes, and defecation compared to rats from control mothers [220]. Developmentally, animals exposed to NTX in the womb had accelerated rates in incisor eruption, ear opening, and eye opening [220]. This indicates that endogenous opioid interactions play a crucial role in development both physically and behaviorally [220]. Rats exposed to 10 mg/kg OGF during pregnancy had 25% smaller litters and 4 times the number of stillborns compared to saline-treated pregnant rat counterparts [221]. Pregnancy duration and course were not affected, and there were no differences between the groups in food and water intake, maternal weight gain, and nociceptive response [221]. Rats exposed to OGF gave birth to pups that remained smaller than control pups for 3 weeks after birth [221].

Further postnatal studies testing the effects of NTX on rat brain development demonstrated that complete opioid receptor blockade with daily injections of a high dose of NTX stimulated brain development and differentiation, while intermittent opioid receptor blockade with a low dose of NTX impeded brain development compared to control rats give daily injections of sterile water [222]. Thymidine incorporation studies established that newborn rats injected with a high dose of NTX had significantly higher cell proliferation in the developing CNS 12 hours after the NTX administration compared to control animals [223]. Conversely, rats given a either a low dose of NTX or a high dose of OGF had significantly decreased cell proliferation in the developing CNS [223]. This study showed that manipulation of the endogenous opioid systems can alter the development of the CNS. In addition to a higher rate of cell proliferation in the CNS, rats given a high dose of NTX have an increased number of dendritic spines in the pyramidal cells of the hippocampus, the granule cells of the dentate gyrus, the pyramidal cells of the cerebral cortex, and the purkinje cells of the cerebellum [224].

Analysis of OGFr expression demonstrates a large change in expression levels throughout development. OGFr levels in newborn are 1/20th of the levels in 2-19 day old humans. However, OGFr expression level decreases after early development, because it is undetectable in adult cerebellum. [134]

1.4.5. OGF-OGFr Axis and Cancer

Administration of OGF decreases the rate of cancer cell proliferation in both *in vivo* [178, 196, 207, 225-227] and *in vitro* [228] cancer model systems. This negative growth regulation is mediated by OGFr, which is present in all cancer types listed above, and can be reversed with the opioid receptor antagonists naloxone or NTX [178-180, 225, 229, 230]. Administration of a high dose of NTX that leads to continuous opioid receptor blockade increases the rate of cancer formation *in vivo* [231] and increases the rate of cancer cell proliferation *in vitro* [228]. Conversely, a low dose of NTX that mediates a 4-6 hr opioid receptor blockade inhibits the appearance and growth of cancer *in vivo* [232].

Phase I clinical trials have shown that OGF is a safe and efficacious treatment for pancreatic cancer [233]. OGF could also be an ideal therapy for pancreatic or other cancers in humans when given in combination with existing cancer treatments. When paclitaxel, an FDA-approved anti-cancer drug, is given in conjunction with OGF, growth of SCCHN decreases more than control treatment or either treatment alone in both *in vivo* and *in vitro* cancer models [234, 235]. Similarly, OGF given in conjunction with gemcitabine inhibits the growth of pancreatic adenocarcinoma in both *in vivo* and *in vitro* systems [236].

1.5. Gap in the Knowledge

It is known that endogenous opioids possess immunomodulatory properties, but their role in the progression of EAE and/or MS is unknown. This project was designed to

determine if endogenous opioids alter the severity or course of EAE, with the idea that potential findings could be translated into a successful therapy for MS.

1.6. Hypothesis

The *hypothesis* of this research was that endogenous opioid systems play a role in EAE pathogenesis. The *short term goal* of this study is to determine how modulation of OGFr with an agonist or antagonist can alleviate EAE symptoms. To test the hypothesis and attain this goal, mice will receive a series of MOG injections to induce EAE. Daily administration of an OGFr agonist (OGF) and high and low dosages of an OGFr antagonist (NTX) will begin at the time of disease induction. The NTX treatments were chosen to alter the availability of opioid receptor to interact with opioid peptide. OGF treatment was chosen to determine if specific receptors activated by the peptide play a role in disease progression. The effects of OGF and NTX on *in vitro* proliferation of immune cells will also be examined. The *long term goal* of this study is to discover a novel therapy for the treatment of MS. The proposed work is *innovative* because the immunomodulatory properties of OGF make it a potential candidate for MS therapy. The potential of LDN as a successful MS therapy has been implicated in select literature [143, 237, 238], but no animal studies have been conducted. This work will be *beneficial to human health* because if OGF or NTX alleviates the behavioral and histological symptoms of EAE, it could serve as a useful biotherapy for the treatment of MS.

CHAPTER 2: METHODS

2. Methods

2.1. EAE Induction

Active EAE was induced in mice as previously described [70, 239-242] with minor modifications. Female 7-10 week old C57BL/6 mice (Harlan Laboratories, Frederick, MD) received 200 µL intramuscular flank injections of 300 µg MOG 35-55 (Penn State University College of Medicine Core Facility) and 500 µg heat-killed Mycobacterium tuberculosis (Difco Laboratories, Lawrence, KS) dissolved in equal parts of phosphate buffered saline (PBS, Penn State University) and complete Freund's adjuvant (CFA; Sigma Aldrich, St. Louis, MD). Care was taken to ensure the formation of a successful water-in-oil emulsion [95]. The 200 µL injection was divided between the left and right flank, with each side receiving a 100 µL intramuscular injection. Intraperitoneal injections of 500 ng pertussis toxin (List Biological Laboratories, Campbell, CA) dissolved in 200 µL PBS were administered immediately after the first MOG injection on Day 0, and 48 hours later. Animals received booster intramuscular flank injections of the MOG mixture on Days 3 and 6. Animals were lightly anesthetized with 3% isoflurane (Penn State University) for the MOG injections. Animals receiving injections of vehicle only (CFA, PBS, Mycobacterium tuberculosis) with Pertussis toxin on days 0 and 2 served as Control+Vehicle mice. All mice were housed 5 per cage in an environment of 21 ± 0.5˚C with a relative humidity of 50 ± 10%. The room had a complete exchange of air 15-18 times per hour and a 12-hour light-dark cycle with no twilight. Water and food were continuously available. Animals were acclimated to the facility one week prior to disease induction. All procedures have been approved by the Penn State Hershey IACUC (protocol number 2006-055). 6 individual EAE experiments were conducted to test the effects of vehicle, LDN, OGF, or HDN treatment. Animals

were sacrificed at 10 days in 1 experiment, 20 days in 2 experiments, 30 days in 2 experiments, and 60 days in 1 experiment.

2.2. Treatment Groups

Daily 0.2 mL intraperitoneal injections of vehicle (PBS), 10 mg/kg NTX (HDN), 0.1 mg/kg NTX (LDN), or 10 mg/kg OGF began on Day 0. New solutions of NTX and OGF were prepared each week to ensure freshness [243], and solutions were stored at 4˚C. Injections were given at the same time each day (approximately 1 P.M. Eastern Time) for the duration of the experiment.

2.3. Weight and Behavior

To monitor EAE progression, body weight was recorded 2-3 times per week. Confirmation of EAE was made by daily assignment of disease score. Disease severity was evaluated on a scale of 0-5 with 0.5 gradations for intermediate score: 0, no clinical signs; 1, loss of tail tone; 2, wobbly gait (sea lion like); 2.5, single hind limb paralysis; 3, complete hind limb paralysis; 4, hind and fore limb paralysis; 5, death [244-247]. Animals were blindly assigned disease scores at the same time every day.

To measure disease incidence, animals were considered EAE-positive if they received a disease score ≥ 1 for two consecutive days. Remissions occurred when an animal with a disease score ≥ 1 returned to a disease score of 0 before the sacrifice time point. Relapses were characterized as an animal going from a disease score ≥ 1, back to 0, then returning to a disease score ≥ 1. Disease index was calculated according to Suen and colleagues [245]. Disease index is the mean daily clinical score for all animals in a treatment group divided by the average day of disease onset and multiplied by 100. For those animals injected with MOG that did not display behavioral symptoms of EAE before the time of sacrifice, day of disease onset was assigned as 1 day after the sacrifice time point.

2.4. Sacrifice and Tissue Preparation

At the designated time point (10, 20, 30, or 60 days post-EAE induction) animals were sacrificed. Mice were deeply anesthetized with 0.1 mL injections of a sterile water-based cocktail made up of ketamine (30 mg/kg), xylazine (5 mg/kg), and acepromozine (2 mg/kg), and were perfused intracardially with either 4% paraformaldehyde or 10% neutral buffered formalin for approximately 5 minutes. Whole spinal columns were extracted and placed in fixative for 48 hours at 4˚C. Using a dissecting microscope and fiber-optic lamps, spinal cords were dissected out of the columns with special care to keep the sciatic nerve attached to the cord. Spinal cords were placed in plastic tissue cassettes and processed through a series of increasing alcohol concentrations (Shandon Citadel 1000, Thermo Scientific, Waltham, MA), xylene, and hot paraffin wax. Spinal cords were then divided into three sections, with cuts made at the level of the sciatic nerve (L5), and 1 mm rostral to the sciatic nerve cut. The three new sections were embedded into paraffin blocks (Microm EC 350, Thermo Scientific, Waltham, MA). In Figure 2.1, heavy black lines indicate where cuts were made to divide the cord into three sections and red “X”’s indicate the side of each section that was embedded down. Spinal cords embedded in paraffin blocks were cut into 10 µm sections (Microtome, American Optical Corporation, Southbridge, MA) for immunohistochemical analysis.

2.5. Immunohistochemistry

2.5.1. Astrocyte Activation

2.5.1.1. Staining Protocol

A glial fibrillary acidic protein (GFAP) primary antibody was employed to measure astrocyte activation in spinal cord sections. Sections were passed through xylene, 100% ethanol (EtOH), 95% EtOH, 70% EtOH, 50% EtOH, and distilled water (5 minutes each)

for deparaffinization and rehydration. A blocking solution of 4% fetal bovine serum (FBS; HyClone, Logan, UT) in 1% normal goat serum (NGS, VWR, West Chester, PA) with 0.1% Triton X-100 (Sigma Aldrich, St. Louis, MO) was added to sections for 15 minutes at room temperature, followed by a 1 hour incubation of GFAP rabbit primary antibody (Dako, Glostrup, Denmark) diluted 1:500 in 1% NGS with 0.1% Triton X-100 at 4°C. Sections were rinsed 3 times for 5 minutes in Sorensen's phosphate buffer, then blocked with 4% FBS in 1% NGS for 15 minutes at room temperature. A horseradish peroxidase (HRP) -conjugated goat anti-rabbit secondary antibody (Millipore, Billerica, MA) diluted in 1% NGS was added to sections for 45 minutes at 4°C. Sections were washed twice for 15 minutes in 1% NGS. To detect HRP, a diaminobenzidine (DAB) solution, made up of 0.005g 3,3'-DAB (Sigma Aldrich, St. Louis, MO) in 5 mL 0.15M PBS with 20 µL H_2O_2, was added to slides for 1 hour at room temperature. Slides were washed 3 times in dH_2O, counterstained for 10 seconds in hematoxylin (Harleco, Lawrence, KS), dehydrated through a series of alcohols for 5 minutes each (50%, 70%, 95%, 100%), fixed in xylene for 5 minutes, and coverslipped in Cytoseal.

2.5.1.2. Quantification of Astrocyte Activation

Using a 40x objective and an Olympus BH-2 brightfield microscope, the number of activated astrocytes were counted. In order for a cell to have been considered an activated astrocyte, the cell had a nucleus and brown positive reaction product in at least two processes extending from the nucleus (Figure 2.2A). The number of cells that were located in the 0.0529 mm^2 grid projected onto the slide by an eyepiece reticule was counted, and the number of astrocytes experience counted in the grid was multiplied by 18.9 to reach the unit of number of astrocytes per mm^2. Three grids were counted per spinal cord section, and two nonconsecutive spinal cord sections in the L4-L6 region

were examined. Counts were completed by the same individual who was blinded to the treatment group of each animal.

2.5.2. Demyelination

2.5.2.1. Staining Protocol

To detect areas of demyelination, spinal cord sections were stained with luxol fast blue (LFB). 10 µm sections were incubated for 5 minutes each in xylene, 100% EtOH, and 95% EtOH for deparaffinization and partial rehydration. Slides were stained in a LFB solution composed of 200 mL 95% EtOH, 0.2g LFB (Roboz Surgical Instrument Co., Washington, D.C.), and 1 mL glacial acetic acid (EM Science, Gibbstown, NJ) overnight at 57˚C. The following day, excess stain solution was rinsed off in 95% EtOH, and slides were placed in dH_2O. To differentiate between gray and white matter, slides were placed in a lithium carbonate solution for 30 seconds and a 70% EtOH solution for 30 seconds. Slides were checked microscopically for differentiation. If differentiation was incomplete, the lithium carbonate and 70% EtOH steps were repeated until the luxol fast blue stain had faded in the gray matter and the spinal cord gray and white matter were clearly indistinguishable. To counterstain, slides were placed in either a 0.1% cresyl echt violet (Sigma Aldrich, St. Louis, MO) or a 1% filtered neutral red (Fisher Scientific, Pittsburgh, PA) solution for 2 minutes. After microscopically determining the counterstain was effective, slides were rinsed in distilled water, then passed through 95% EtOH for 1 minute and 100% EtOH for 1 minute before fixing in xylene for 5 minutes and coverslipping with Cytoseal, a xylene-based resinous medium (Richard-Allan Scientific, Kalamazoo, MI).

2.5.2.2. Quantification of Demyelination

To measure demyelination, the spinal cord sections were divided into 4 sections by a horizontal and a vertical line that intersected through the central canal (see Figure

2.3). Two spinal cord sections per animal were evaluated. Data were analyzed in 2 ways: 1) The number of spinal cord sections with no demyelination (no demyelination present in any of the quadrants), or 2) Each section was assigned a number of 0, 1, 2, 3, or 4, indicating the number of quadrants that had demyelination present [248]. Analysis was completed by the same individual who was blinded to the treatment group of each animal.

2.5.3. Neuronal Damage

2.5.3.1. Staining Protocol

A primary antibody directed against nonphosphorylated neurofilament H, SMI-32, was used to measure neuronal damage in spinal cord sections. Sections were passed through xylene, 100% EtOH, 95% EtOH, 70% EtOH, 50% EtOH, and dH_2O (5 minutes each) for deparaffinization and rehydration. A blocking solution of 4% FBS in 1% NGS with 0.1% Triton X-100 was added to sections for 15 minutes at room temperature, followed by a 1 hour incubation of SMI-32 mouse primary antibody (Covance, Madison, WI) diluted 1:500 in 1% NGS with 0.1% Triton X-100 at 4°C. Sections were rinsed 3 times for 5 minutes in Sorensen's phosphate buffer, then blocked with 4% FBS in 1% NGS for 15 minutes at room temperature. A HRP-conjugated goat anti-mouse secondary antibody (Millipore, Billerica, MA) diluted in 1% NGS was added to sections for 45 minutes at 4°C. Sections were washed twice for 15 minutes in 1% NGS. To detect HRP, a solution made up of 0.005 g 3,3'-DAB in 5 mL 0.15 M PBS with 20 µL H_2O_2 was added to slides for 1 hour at room temperature. Slides were washed 3 times in dH_2O, counterstained for 10 seconds in hematoxylin, dehydrated through a series of alcohols for 5 minutes each (50%, 70%, 95%, 100%), fixed in xylene for 5 minutes, and coverslipped in Cytoseal.

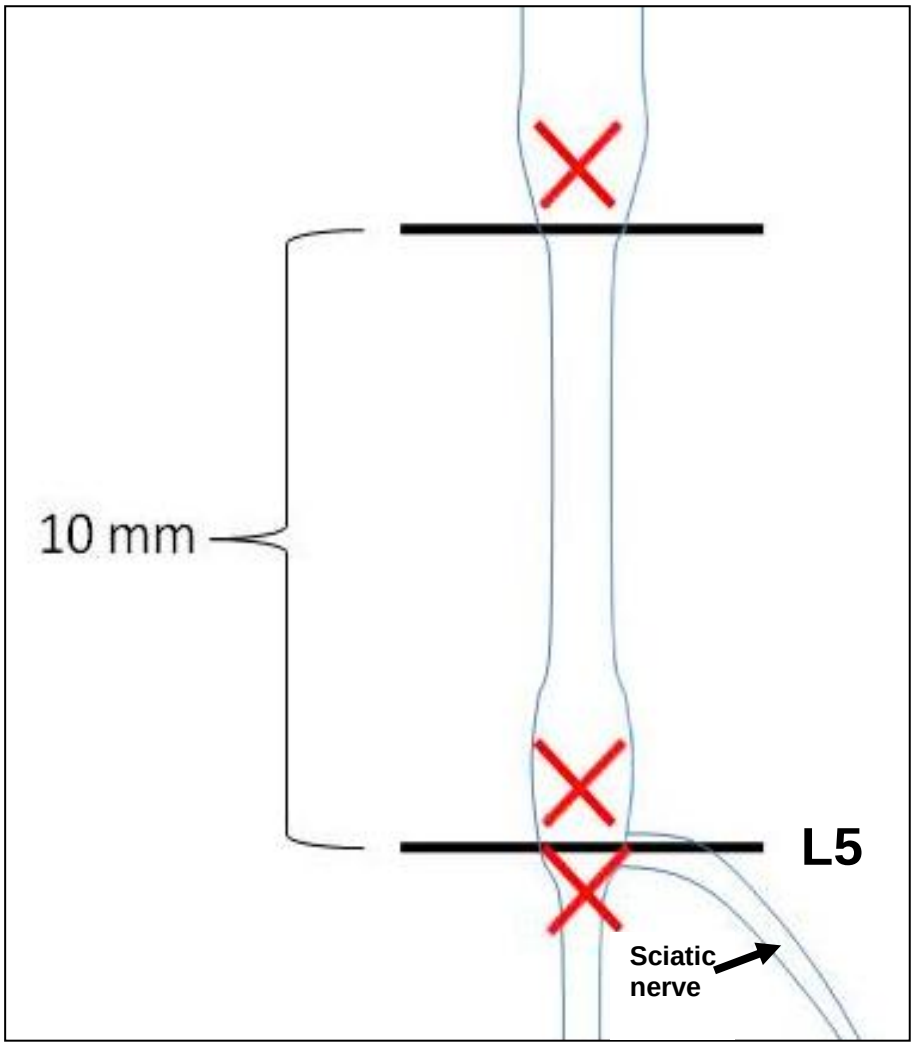

Figure 2.1: A schematic of the mouse spinal cord dissection procedure. Shown is a drawing of a mouse spinal cord and sciatic nerve to demonstrate where cuts were made (heavy black lines) and which end of each section was embedded into the paraffin (Red X's). The most caudal cut was made where the sciatic nerve innervates the spinal cord, L5. The histological experiments described below utilize sections surrounding the caudal cut, ranging from L4 - L6.

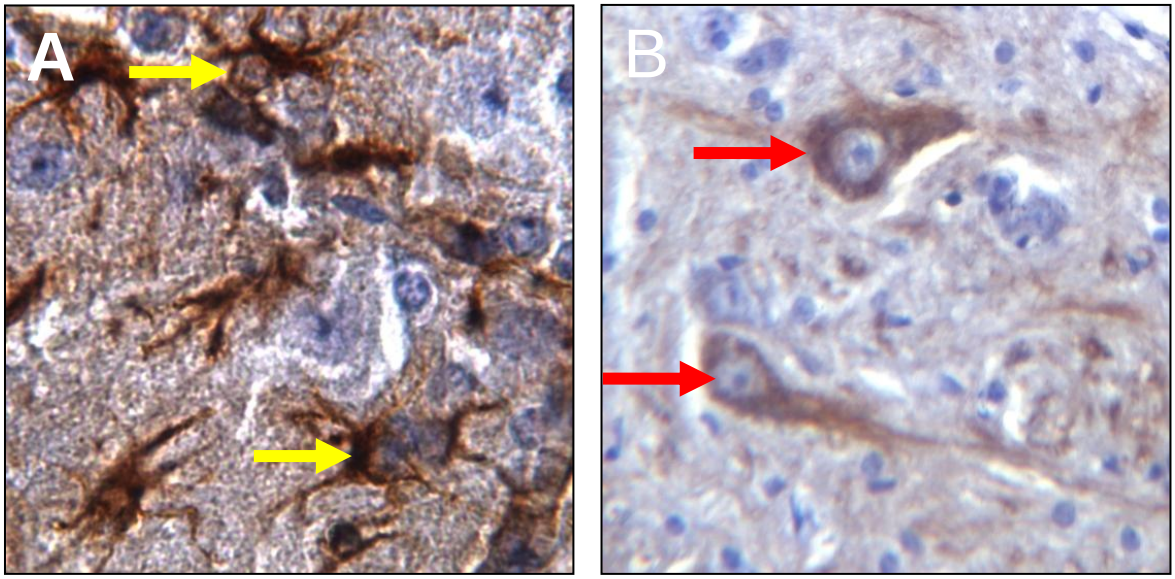

Figure 2.2: The criteria for GFAP and SMI-32 positivity in immunohistochemical analysis. (A) To be considered an activated astrocyte, cells were required to have a defined nucleus, and at least 2 brown processes extending from the nucleus. Yellow arrows point to examples of cells that qualified as activated astrocytes. (B) To be considered a damaged neuron, cells were required to have a defined nucleus and brown cytoplasm surrounding the nucleus. Red arrows point to cells that qualified as damaged neurons. 40x magnification

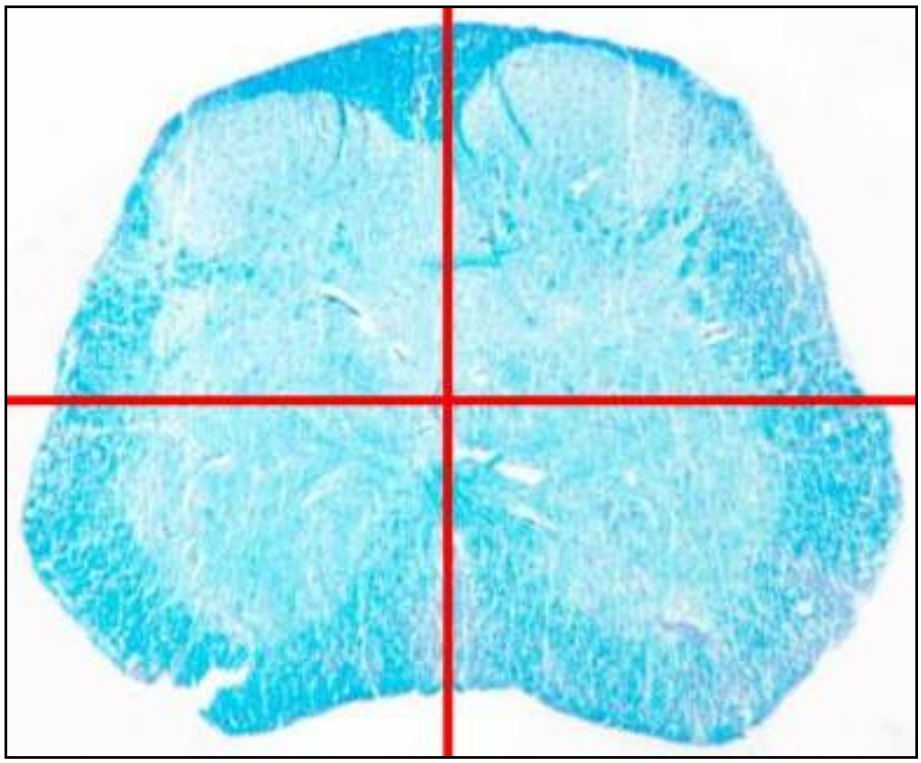

Figure 2.3: The method for LFB quadrant quantification. 10 µm spinal cord sections were stained with LFB and divided into quadrants (red lines). To quantitate demyelination, the number of quadrants that contained demyelination was determined in two L4 – L6 sections per animal.

2.5.3.2. Quantification of Neuronal Damage

The number of damaged neurons was counted in the grey matter of two spinal cord sections in the L4-L6 region from each mouse spinal cord using an Olympus BH-2 brightfield microscope. To be considered a damaged neuron, the cell had to have a distinct nucleus and nucleolus, and have brown positive reaction product in the cytoplasm surrounding the nucleus (Figure 2.2B). Counts were completed by the same individual who was blinded to the treatment group of each animal.

2.6. Cell Culture – Immunology

Lymphocytes were isolated from spleens of normal female 8-10 week old C57BL/6 mice. Animals were sacrificed by cervical dislocation and spleens were removed and placed in supplemented Iscove's Modified Dulbecco's Media (IMDM). Supplemented IMDM was made up with 10% (v/v) FBS, 1% (v/v) sodium bicarbonate, and 1% (v/v) penicillin-streptozotocin. Spleens were mechanically dissociated with 60-mesh stainless steel screens (Sigma, St. Louis), pelletted, and placed in tris ammonium chloride for 5 minutes at 37˚C. Cells were centrifuged, resuspended in IMDM, and counted using a hemacytometer using trypan blue dye exclusion. Based on cell counts, lymphocytes were pelletted and resuspended at a concentration of 1×10^7 cells/mL in supplemented IMDM. Cells were then either seeded on coverslips for immunocytochemical studies or cultured in 24-well plates for lymphocyte proliferation studies.

For immunocytochemical experiments, isolated lymphocytes were either left in culture in 1 mL of supplemented IMDM or stimulated with 10 µg/mL phytohemagluttinin (PHA, Sigma, St. Louis) in 1 mL of supplemented IMDM for 48 hours. After the 48 hour incubation, cells were harvested, counted, and resuspended at 1×10^6 cells/mL in supplemented IMDM. 0.5 mL of the cell suspension (500,000 cells) was fixed to slides

with a 4 minute spin at 1000 rotations per minute (Cytospin, Shandon). Cells were immediately fixed and permeabilized with a 15 minute incubation in -20˚C 95% EtOH followed by a 15 minute incubation in -20˚C acetone. Lymphocytes were then stained with antibodies specific for OGF or OGFr according to Zagon and colleagues [194]. Cells were blocked with 4% FBS in 1% NGS with 0.1% Triton-X 100 for 15 minutes, and incubated in primary antibody to OGF or OGFr (C0172 or B0344, Zagon and McLaughlin laboratory, Pennsylvania State University) diluted 1:200 in 1% NGS with 0.1% Triton-X 100 overnight at 4˚C. Sections were rinsed 3 times for 5 minutes in Sorensen's phosphate buffer, then blocked with 4% FBS in 1% NGS for 15 minutes at room temperature. Secondary antibodies of goat anti-rabbit IgG conjugated to rhodamine (Chemicon) were diluted 1:1000 in 1% NGS and incubated at 4˚C for 45 minutes. Some cells were incubated with secondary only to serve as negative controls. All cells were stained for 15 seconds with 4',6-diamidino-2-phenylindole (DAPI) to visualize nuclei. Slides were washed and sealed with a coverslip, and cells were viewed with an Olympus fluorescent microscope. Images were captured with Slidebook software.

For lymphocyte proliferation assays, 1×10^6 splenic-derived lymphocytes were cultured in 1 mL supplemented IMDM in 24-well plates. After 24 hours in culture, cells were either unstimulated or stimulated with 10 µg/mL PHA. Following PHA stimulation, cells were treated twice per day with distilled deionized sterile water, 10^{-5} M OGF (Sigma, St. Louis) in distilled deionized sterile water, or 10^{-5} M NTX (Sigma, St. Louis) in distilled deionized sterile water for 3 days. Wells from each treatment group were counted every 24 hours using a hemacytometer and trypan blue. Throughout the experiment, plates were maintained at 37˚C with 5% CO_2.

For tritiated thymidine incorporation experiments, 1×10^5 splenic-derived lymphocytes were cultured in 100 µL supplemented IMDM in 72-well plates. After 24

hours in culture, cells were either unstimulated or stimulated with 10 µg/mL PHA. Following PHA stimulation, cells were treated twice per day with distilled deionized sterile water or 10^{-5} M OGF (Sigma, St. Louis) in distilled deionized sterile water for 3 days. Following 54 hours of incubation, 1 µCi of ^{3}H-thymidine was added to each well. 18 hours later, the cells from each well were collected and washed using a cell harvester (Brandel, Gaithersburg, MD), and the extent of cell proliferation was determined by liquid scintillation analysis with a scintillation counter (Beckman Coulter, Fullerton, CA). Throughout the experiment, plates were maintained at 37˚C with 5% CO_2.

2.7. Statistical Analysis

Data were analyzed using Student's *t*-test, one-way analysis of variance (ANOVA) with subsequent Newman Keul's post-tests, and correlation analysis to determine levels of significance (GraphPad Prism Software, La Jolla CA). p-values < 0.05 were considered to be significant.

CHAPTER 3: COMPLETE OPIOID RECEPTOR BLOCKADE INVOKED BY HIGH DOSE NALTREXONE AND THE IMPACT ON EXPERIMENTAL AUTOIMMUNE ENCEPHALOMYELITIS

3. HDN

3.1. Rationale of Treatment

Endogenous opioids can regulate immune function [249]. Some experiments favor continuous opioid receptor blockade to decrease immune function and inflammation. In a mouse model of sepsis, administration of NTX inhibited septic shock and caused a decrease in the production of proinflammatory cytokines *in vivo* [250]. *In vitro* monocyte stimulation with LPS caused an increase in OGF production, indicating that OGF could have a pro-inflammatory role [251]. Immunocytochemistry and *in situ* hybridization studies using epithelial and subcutaneous tissue extracted from a rat with CFA-induced inflammation showed that opioid production increases at sites of inflammation and in immune cells [126]. If this interaction contributes to proinflammatory processes, continuous blockade of opioid receptors might decrease inflammation and halt progression of EAE in the first stage. Continuous opioid receptor blockade is possible through the administration of 10 mg/kg NTX. Based on hot plate experiments testing the relationship between dosage of NTX and duration of morphine-induced analgesia, administration of a high dose of NTX (HDN, 10 mg/kg) causes opioid receptor blockade in the mouse for 24 hours [181]. Briefly, in the hot plate experiments, mice were injected with 0.2 mg/kg morphine, and 30 minutes later received injections of 0 (control) or 10 mg/kg NTX. Hot plate tests were administered at 0, 2, 4, 6, 12 and 24 hours post-NTX injection. While control mice with no NTX could not elicit a response to the heat due to morphine-induced analgesia, those mice give HDN responded to the heat for the duration of the experiment, suggesting that HDN blocks opioid receptors for 24 hours. During NTX-mediated opioid receptor blockade, endogenous production of opioids and opioid receptors increases [252].

Continuous opioid receptor blockade with NTX increases the rate of cell proliferation [181, 186, 216, 217]. If HDN mediates an increase in the number of cells that are beneficial to MS patients (e.g. IL-10 secreting Th2 cells), HDN will decrease the damaging effects of the disease. Additionally, although the cytotoxic effects of NK cells are well-documented, some studies have shown that NK cells attenuate EAE progression [253]. Therefore, a HDN-mediated increase in the progression of NK proliferation might alleviate the symptoms of EAE.

NTX therapy would be attractive for MS patients due to route of administration and lowered cost compared to existing therapies. The patent for NTX expired in 1985 [143], so the cost of NTX treatment would be very low compared to the expensive pharmaceutical drugs. Because NTX is orally-effective, the daily, weekly, or monthly injections would be eliminated.

The *hypothesis* of this study was that continuous opioid receptor blockade alters the course of EAE.

3.2. Behavior Results

25 Control+Vehicle, 45 MOG+Vehicle animals, and 32 MOG+HDN animals were observed for behavioral symptoms of EAE across 4 separate experiments. To evaluate EAE severity, animals were assigned disease scores from 0-5 each day. No animal scored above a 3 at any point in these experiments. Control+Vehicle animals did not present with signs of EAE, and all animals injected with MOG that received vehicle or HDN treatment expressed behavioral signs of EAE (disease score ≥ 1) before sacrifice.

Figure 3.1A represents the average disease score of Control+Vehicle, MOG+Vehicle, and MOG+HDN mice from all 4 experiments over 60 days. Control+Vehicle animals not injected with MOG maintained disease scores of 0 throughout the experiment. Mice developed peak EAE at approximately 2-3 weeks post-

EAE induction, as previously described [108]. Disease course did not differ between HDN- and vehicle-treated mice that received MOG injections. Both treatment groups presented with disease symptoms at approximately the same time.

Analysis of individual disease scores at specific time points throughout the studies show little difference between EAE scores in the vehicle and HDN groups (Figure 3.1B). On Day 20, very few animals from either group had disease scores of 0 or 1. Significantly less HDN mice had an EAE score of 2 on Day 20, with 72% of MOG+Vehicle and only 42% of MOG+HDN mice having a wobbly gait. The difference was due to the fact that significantly more HDN mice, 26% compared to 6% in the vehicle group, had the more advanced EAE score of 3 (hind limb paralysis). All HDN-treated animals expressed EAE on days 30 and 60. Only 6% of MOG+Vehicle mice appeared healthy on Day 30, with the majority (83%) demonstrating a wobbly gait. All animals, both HDN and vehicle, received a disease score of 2 on Day 60.

Disease incidence did not vary between MOG+Vehicle and MOG+HDN animals (Figure 3.2A). On Day 15, 42% of MOG+Vehicle and 38% of MOG+HDN mice had behavioral symptoms of EAE. On Day 20, these numbers increased to 89% of MOG+Vehicle and 84% of MOG+HDN mice that were sick. By Day 25, all MOG+Vehicle and MOG+HDN animals had disease scores ≥ 1. 100% disease incidence continued until Day 30, with 1 MOG+Vehicle animal reverting to a disease score of 0. 100% disease incidence was observed on Day 35, but another animal returned to a disease score of 0 on Day 40. This remission continued through Day 45, but by Day 50 both groups returned to 100% disease incidence. Throughout the course of the experiments, 3 out of 45 mice in the MOG+Vehicle group experienced a remission (had a disease score ≥ 1, but returned to a disease score of 0 before the time of sacrifice). Of these 3 remissions, 1 animal relapsed back to having a disease score ≥ 1

before the time of sacrifice. Of the 32 MOG+HDN mice included from 4 experiments, 4 animals reverted back to a disease score of 0, but all 4 animals returned to having a disease score ≥ 1 before the time of sacrifice (Figure 3.2B).

The average day of disease onset for HDN-treated animals was 16.50 ± 0.52, and average day of disease onset for the MOG+Vehicle group was 16.27 ± 0.36 (Figure 3.3A). Disease index was calculated for all animals sacrificed on Days 20, 30, and 60. Disease index data demonstrate no difference between MOG+Vehicle and MOG+HDN treated animals (Figure 3.3B). The disease index for MOG+Vehicle mice is 526.2, while disease index for HDN-treated mice is 529.3. Both groups had a peak average disease score of 2, which was reached on Days 21 and 22 and 31-60 in the MOG+HDN group and on Days 24-27, 31-39, and 50-60 in the MOG+Vehicle group. No animal in the vehicle or HDN group had a disease score of 3, the most severe form of EAE recorded in the experiments, past day 28 and 30, respectively.

3.3. Body Weight Results

Body weight did not significantly differ between groups on Day 0 (Figure 3.4). Control+Vehicle (n = 4), MOG+Vehicle (n = 13), and MOG+HDN (n = 9) mice weighed 18.0 ± 0.6, 18.3 ± 0.3, and 18.2 ± 0.3 grams, respectively, on Day 0. Body weight decreased from Day 0 until Day 6 for Control+Vehicle, MOG+Vehicle, and MOG+HDN mice. All three groups showed a slight increase between Day 6 and Day 10, and by Day 14 body weight was equal to or higher than Day 0 body weight in all groups. Control+Vehicle mice had significantly higher body weights than MOG+Vehicle mice on Day 14 ($p < 0.05$). MOG+HDN mice had significantly higher body weight than MOG+Vehicle mice on Days 36 and 45 ($p < 0.05$). Body weight did not significantly differ between groups on the last day it was measured, Day 50, before animals were

sacrificed. Control+Vehicle mice weighed 21.5 ± 0.6 grams, while MOG+Vehicle and MOG+HDN mice weighed 21.1 ± 0.3 and 21.9 ± 0.5 grams, respectively, on Day 50.

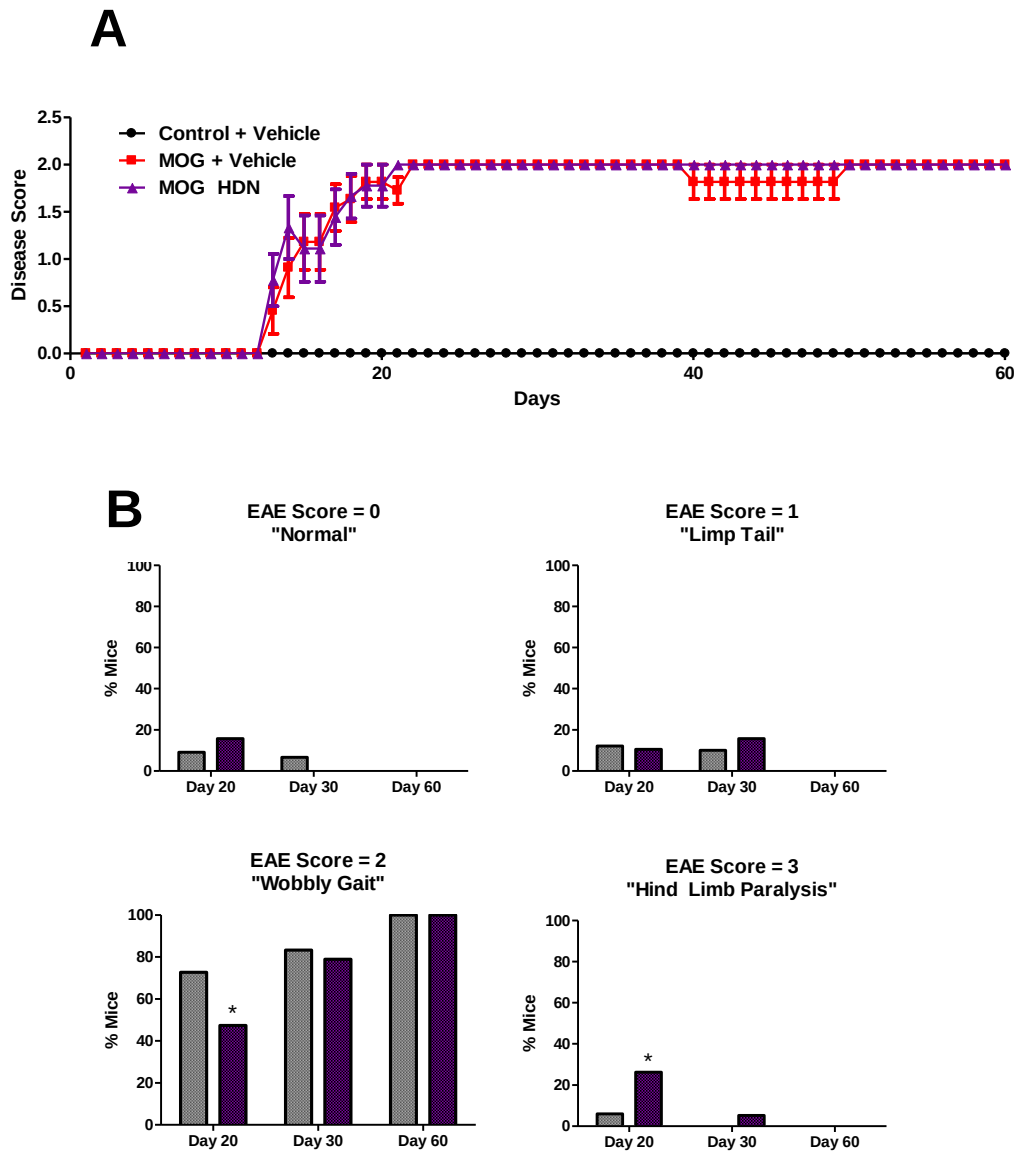

Figure 3.1: The effect of HDN on EAE disease score and distribution. EAE was induced and mice were scored daily on a 0 - 5 scale. (A) Average disease scores for 60 days post-EAE induction. (B) The percentage of MOG+Vehicle (white bars) and MOG+HDN (purple bars) mice receiving the individual disease scores of 0, 1, 2, or 3 on Days 20, 30, and 60. Significantly different from MOG+Vehicle at $p < 0.05$ (*). Control+Vehicle n = 4-25, MOG+Vehicle n=11-45, MOG+HDN n=9-32. N values decrease after the 20 and 30 day time points because some animals were sacrificed for histological analysis at these time points. Data represent means ± SEM from 4-5 independent experiments.

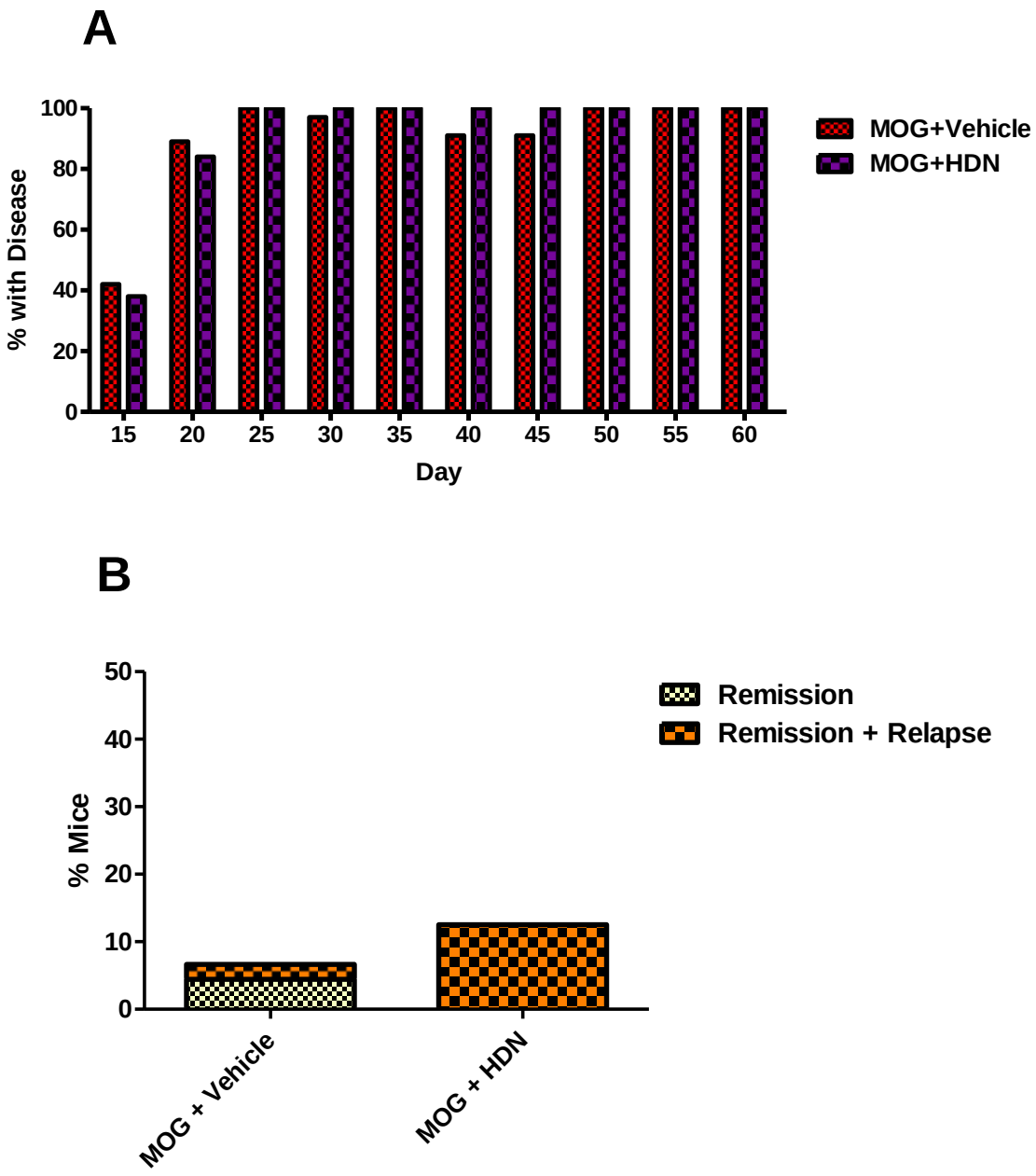

Figure 3.2: The impact of HDN on EAE disease incidence and remissions + relapses. EAE was induced and mice were scored daily on a 0 - 5 scale. (A) Disease incidence of MOG+Vehicle and MOG+HDN mice was calculated by dividing the number of animals with a disease score ≥ 1 by the total number of animals and multiplying by 100. (B) The percentage of MOG+Vehicle and MOG+HDN mice that experienced a remission or a remission with a subsequent relapse before the predetermined time of sacrifice, 20, 30, and 60 days post-EAE induction. MOG+Vehicle n=11-45, MOG+HDN n=9-32. N values decrease after the 20 and 30 day time points because some animals were sacrificed for histological analysis at these time points. Data represent means ± SEM from 4-5 independent experiments.

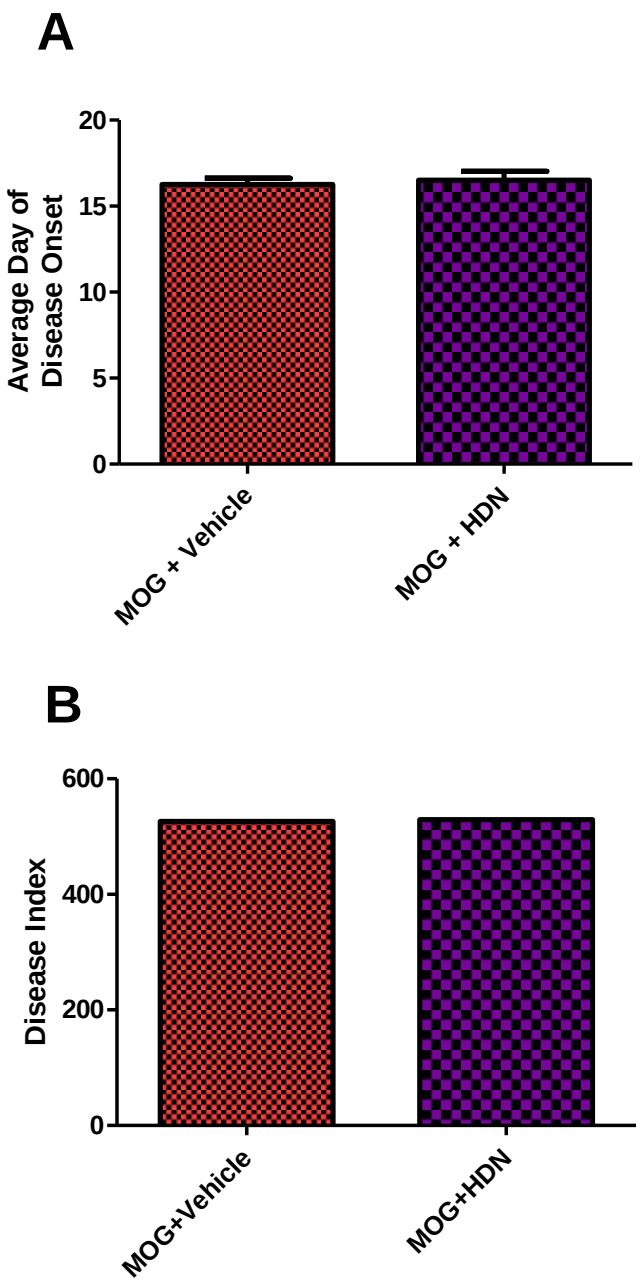

Figure 3.3: The influence of HDN on EAE disease onset and disease index. EAE was induced and mice were scored daily on a 0 - 5 scale. (A) Data correspond to the average day of disease onset in MOG+Vehicle and MOG+HDN groups. The first of 2 consecutive days that a mouse received a disease score ≥ 1 was marked as the animal's day of disease onset. (B) Disease index was calculated by adding up the average daily disease scores, dividing by the average day of disease onset, and multiplying by 100. MOG+Vehicle n=45, MOG+HDN n=32. Data represent means ± SEM from 4-5 independent experiments.

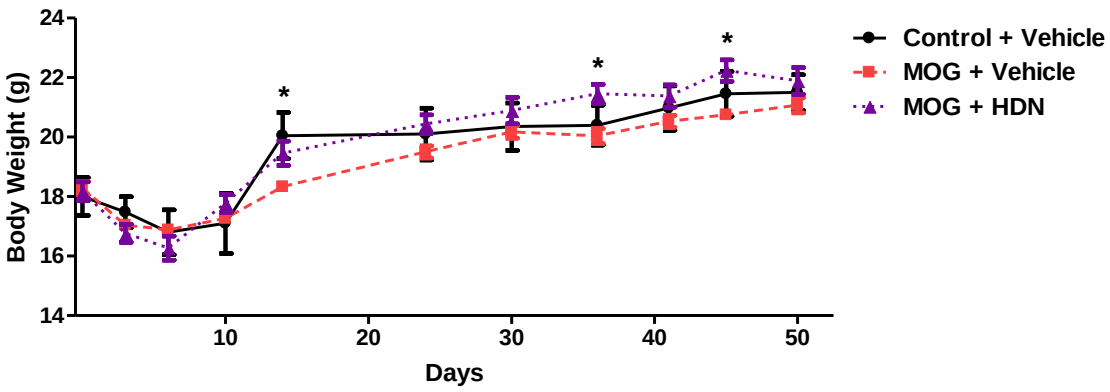

Figure 3.4: Average body weight of Control+Vehicle, MOG+Vehicle, and MOG+HDN mice. Body weight was recorded 1-2 times per week for 50 days post-EAE induction. Significantly different from MOG+Vehicle at $p < 0.05$ (*). Control+Vehicle n = 4, MOG+Vehicle n = 11, MOG+HDN = 9. Data represent means ± SEM.

3.4. Morphology Results

3.4.1. Astrocyte Activation Results

Control+Vehicle, MOG+Vehicle, and MOG+HDN mice were sacrificed on Days 10, 20, 30, and 60. Figure 3.5A shows the number of astrocytes per mm^2 at each time point, while Figure 3.5B shows how astrocyte counts in each treatment group change between the various stages of EAE. On Day 10, Control+Vehicle (n = 4) mice had significantly less activated astrocytes compared to MOG+Vehicle (n = 3) and MOG+HDN (n = 3) mice ($p < 0.001$). Control+Vehicle mice demonstrated 105.5 ± 21.5 activated astrocytes per mm^2, while MOG+Vehicle and MOG+HDN mice had 266.7 ± 20.3 and 282.45 ± 27.3 activated astrocytes per mm^2, respectively. Similar to those results seen on Day 10, at 20 days post-EAE induction the number of activated astrocytes in the spinal cord of Control+Vehicle (n = 8) mice was significantly lower than the numbers in MOG+Vehicle (n = 8) and MOG+HDN (n = 8) mice ($p < 0.001$). Control+Vehicle mice only had 28.9 ± 4.4 activated astrocytes, while MOG+Vehicle mice had 242.9 ± 19.6 and MOG+HDN mice had 248.1 ± 18.3 activated astrocytes per mm^2. On Day 30, the number of activated astrocytes per mm^2 in MOG+Vehicle (n = 6) mice was 289.5% of the number seen in Control+Vehicle (n = 7) mice. MOG+HDN (n = 8) astrocyte counts were elevated by 182.1% compared to Control+Vehicle mice. Control+Vehicle mice averaged 122.4 ± 12.7 activated astrocytes per mm^2 of the spinal cord, while MOG+Vehicle and MOG+HDN mice had means of 354.4 ± 24.8 and 222.9 ± 20.3 activated astrocytes per mm^2, respectively. At 30 days post-EAE induction, counts from Control+Vehicle and MOG+HDN mice were significantly lower than counts observed in MOG+Vehicle spinal cord sections ($p < 0.001$). MOG+HDN counts were significantly elevated over Control+Vehicle counts ($p < 0.001$). At 60 days post-EAE induction, both Control+Vehicle (n = 4) and MOG+HDN (n = 7) activated astrocyte counts were

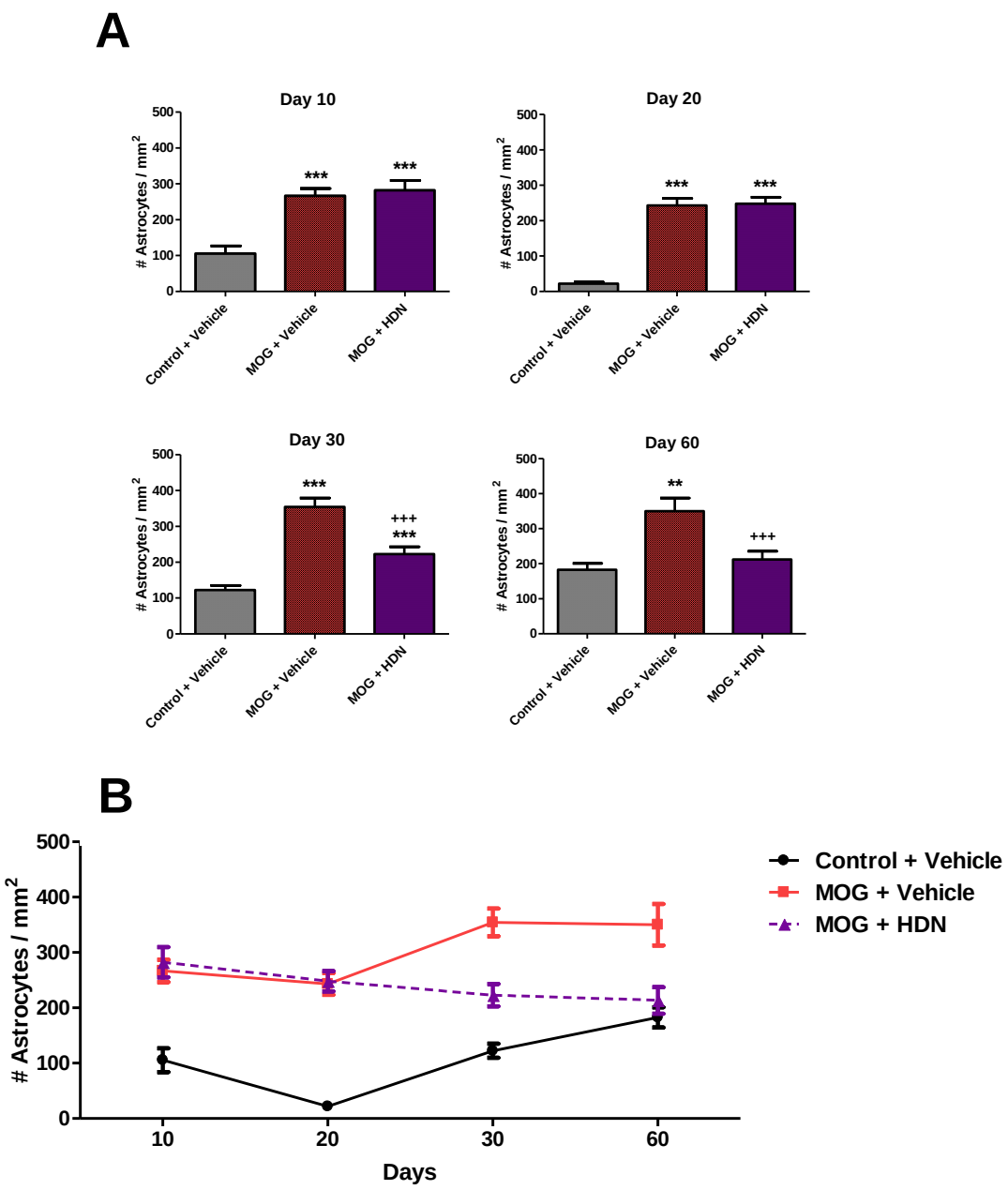

Figure 3.5: The effect of daily HDN administration on EAE mouse spinal cord astrocyte activation. The number of activated astrocytes was counted in three grids per spinal cord of 2 sections per mouse. (A) The number of activated astrocytes per mm^2 in the lumbar spinal cords of mice sacrificed on Days 10, 20, 30, and 60. Significantly different from Control+Vehicle at $p < 0.01$ (**), $p < 0.001$ (***). Significantly different from MOG+Vehicle at $p < 0.001$ (+++) (B) Time course of the number of activated astrocytes on Days 10, 20, 30, and 60 shows how counts change during different stages of EAE. Data represent means ± SEM.

significantly lower than counts in MOG+Vehicle (n = 6) mice ($p < 0.01$ and 0.001). The number of activated astrocytes per mm^2 in Control+Vehicle, MOG+Vehicle, and MOG+HDN mice was 182.7 ± 18.4, 350.2 ± 37.6, and 212.4 ± 23.3, respectively.

3.4.2. Demyelination Results

Mice were categorized as having demyelination if 1 or more quadrants showed demyelination at a given time point. Table 3.1 summarizes data from the LFB staining experiments. Control+Vehicle mice did not demonstrate signs of demyelination at 10, 20, 30, or 60 days post-EAE induction (Figure 3.6). On Day 10, 33% (1/3) mice had 2 demyelinated quadrants in the spinal cord, while spinal cords from MOG+Vehicle animals (n = 4) were free of demyelination. Demyelination was observed on Day 20 in 33% (3/9) of MOG+Vehicle mice and 50% (4/8) MOG+HDN mice. On Day 20 the majority of demyelination for both groups was moderate, with damage in only 1-2 quadrants per spinal cord. At 30 days, 86% (6/7) of MOG+Vehicle mice and 64% (7/11) of MOG+HDN mice had demyelination. Demyelination on Day 30 was the most severe, as the majority of animals experiencing demyelination had 3-4 quadrants damaged. 29% (2/7) of MOG+Vehicle mice had demyelination on Day 60, compared to 25% (2/8) of mice in the MOG+HDN treatment group. All of the demyelination on Day 60 was in only 1-2 quadrants. Figure 3.7A, which charts the "% of mice with 0 Demyelinated Quadrants" over time, shows that both MOG groups experienced an increase in the number of animals with demyelination from Day 10 through Day 30, and a decrease in the level of demyelination between Days 30 and 60. Further categorizing the demyelination as moderate (1-2 quadrants with demyelination) or severe (3-4 quadrants with demyelination) demonstrates that the most profound occurrence of severe demyelination occurs on Day 30 (Figure 3.7B). Some severe demyelination occurs on

Day 20, and interestingly by Day 60 animals only have moderate demyelination in their spinal cords.

	# Mice with…	10 Days	20 Days	30 Days	60 Days
Control+Vehicle	No Demyelination	4	11	9	4
	Demyelination	0	0	0	0
MOG + Vehicle	No Demyelination	4	6	1	5
	Demyelination	0	3	6	2
MOG + HDN	No Demyelination	2	4	4	6
	Demyelination	1	4	7	2

Table 3.1: A summary of animals examined in HDN demyelination studies. Animals were sacrificed and examined for signs of demyelination in the spinal cord. Data represent the number of animals at each time point that had no demyelination present in the spinal cord or that had demyelination in at least 1 quadrant of the spinal cord.

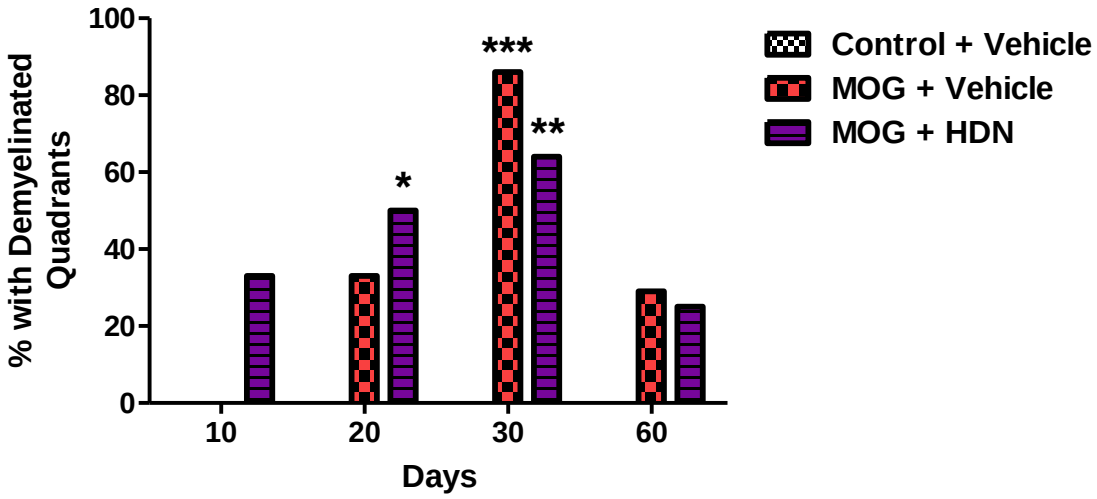

Figure 3.6: The effect of HDN on spinal cord demyelination incidence in EAE mice. Percentage of animals with demyelination in the L4 – L6 section of the spinal cord at 10, 20, 30, and 60 days post-EAE induction. Significantly different from Control+Vehicle at $p < 0.05$ (*), $p < 0.01$ (**), $p < 0.001$ (***).

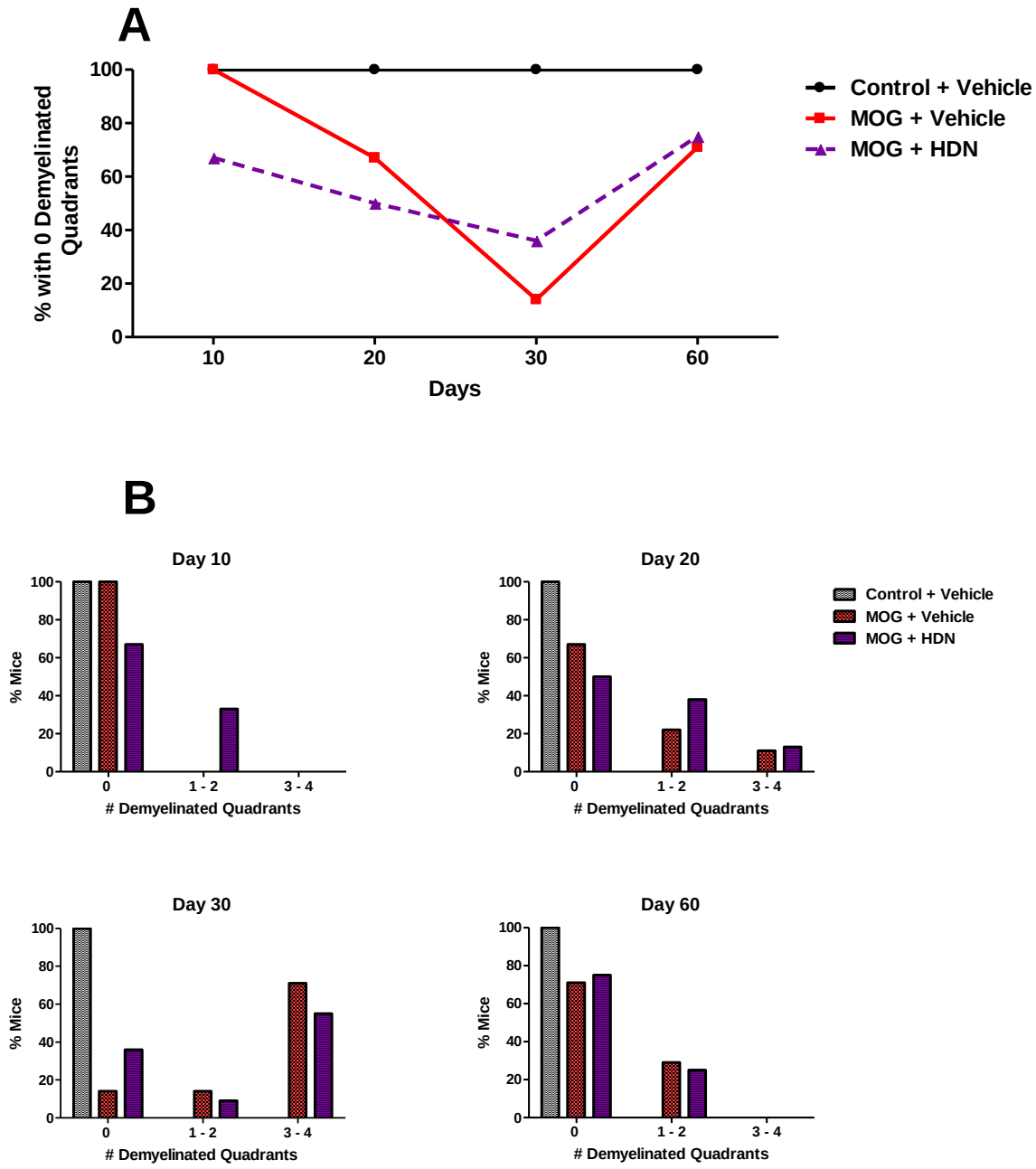

Figure 3.7: The effect of HDN on spinal cord demyelination course and distribution in EAE mice. Two spinal cord sections per mouse were examined for the presence of demyelination. (A) Time course of the percentage of animals in a treatment group with spinal cords free of demyelination on Days 10, 20, 30, and 60 shows how much demyelination, and possibly remyelination, occurs during different the stages of EAE. (B) Histograms of the percent of mice with demyelination in 0, 1-2, or 3-4 quadrants on Days 10, 20, 30, and 60 indicate if animals in a given treatment group have no (0), moderate (1-2) or severe (3-4) demyelination.

3.4.3. Neuronal Damage Results

At 10, 20, 30, and 60 days post-EAE induction, spinal cords from 3 – 9 mice from each treatment group were examined for neuronal damage (Figure 3.8). Control+Vehicle animals (n = 3) had 7.2 ± 1.1 damaged neurons per spinal cord, while MOG+Vehicle mice (n = 3) had 11.6 ± 1.6 and MOG+HDN mice (n = 4) had 11.2 ± 1.3 SMI-32-positive neurons. No significant differences were observed between groups sacrificed on Day 10. The number of damaged neurons in the Control+Vehicle mouse spinal cord decreased to 2.3 ± 0.6 on Day 20. The number of damaged neurons in the Control+Vehicle mice (n = 9) significantly differed from MOG+Vehicle (n = 9) and MOG+HDN (n = 8) counts ($p < 0.001$). MOG+Vehicle and MOG+HDN mice had 13.5 ± 1.3 and 15.5 ± 2.0 damaged neurons, respectively, on Day 20. By Day 30, the number of damaged neurons in the Control+Vehicle mice (n = 5) rose to 11.2 ± 0.8, while the number of damaged neurons in the MOG+HDN (n = 3) animals decreased to 6.7 ± 1.0 MOG+Vehicle mice (n =5) had 20.4 ± 2.3 damaged neurons on Day 30, and MOG+Vehicle counts significantly differed from Control+Vehicle and MOG+HDN counts ($p < 0.001$). By Day 60, the number of damaged neurons did not differ between groups, with counts recorded at 7.3 ± 2.0, 12.4 ± 4.4, and 13.6 ± 2.4 for Control+Vehicle (n = 4), MOG+Vehicle (n = 5), and MOG+HDN (n = 6) mice, respectively.

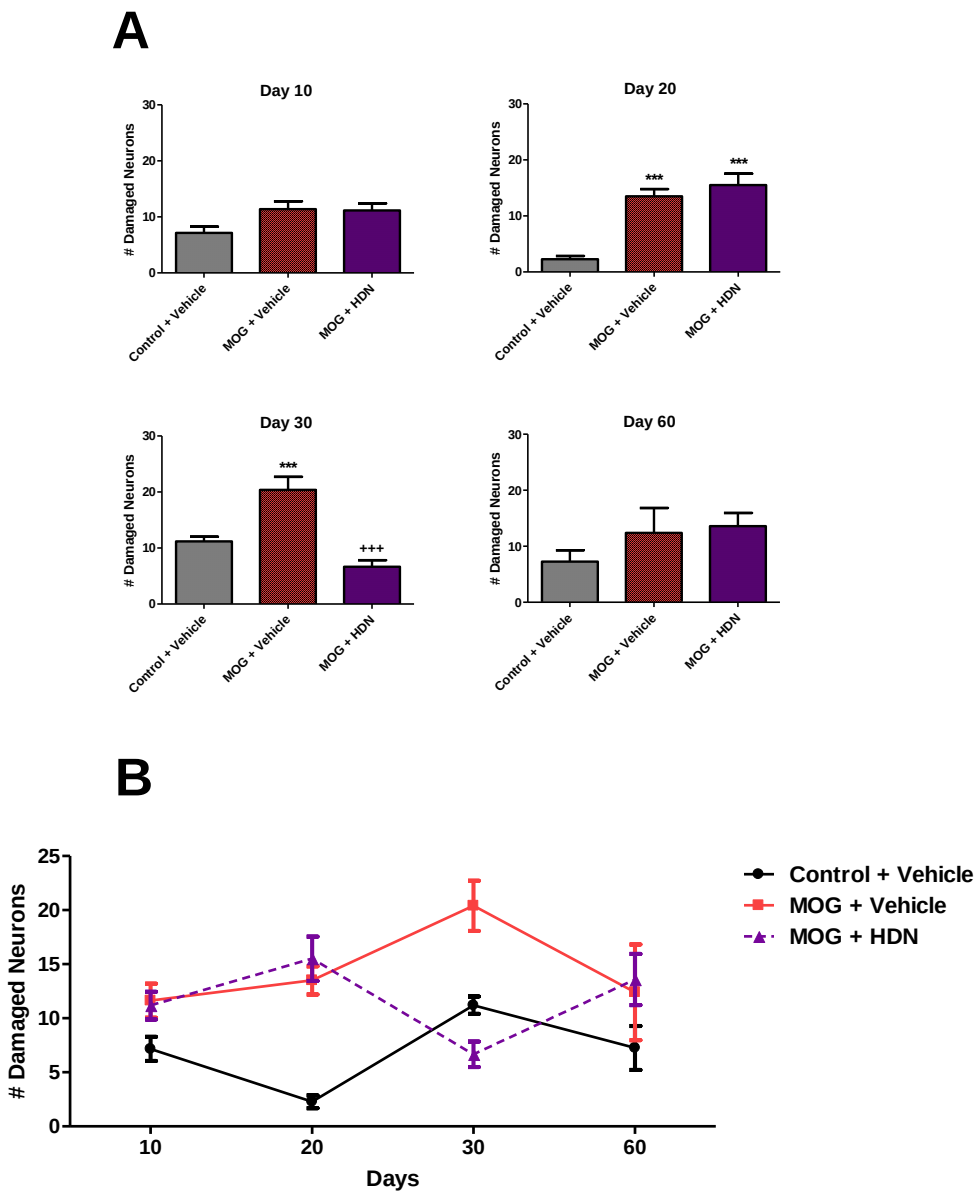

Figure 3.8: The effect of HDN on spinal cord neuronal damage in EAE mice. (A) The number of damaged neurons was counted in the grey matter of 2 lumbar spinal cord sections per mouse on 10, 20, 30, and 60 days post-EAE induction. Significantly different from Control+Vehicle at $p < 0.001$ (***). Significantly different from MOG+Vehicle at $p < 0.001$ (+++) (B) Time course of the number of damaged neurons on Days 10, 20, 30, and 60 shows how counts change during different stages of EAE. Data represent means ± SEM.

3.5. Conclusions

Disease scores were nearly identical in the MOG+Vehicle and MOG+HDN treated animals throughout the 4 experiments. Disease course, incidence, and index were the same regardless of the animals receiving vehicle or HDN injections. The only significant difference observed in all behavioral data was that significantly more ($p < 0.05$) mice in the MOG+HDN group had a disease score of 3 (hind limb paralysis) on Day 20 compared to MOG+Vehicle mice. The disease incidence measured on Day 20 was not different between groups, but MOG+HDN mice had a more severe form of EAE on this day. Average day of disease onset was 16.3 and 16.5 days for vehicle and HDN mice, respectively. Based on behavior data, it can be speculated that continuous opioid receptor blockade produces a more severe form of disease in the initial onset stage of EAE compared to vehicle-treated controls.

Histological data showed no significant differences between MOG+Vehicle and MOG+HDN mice on Days 10 and 20. MOG+HDN mice had significantly fewer activated astrocytes compared to MOG+Vehicle mice on Days 30 and 60 and significantly fewer damaged neurons on Day 30. Based on behavioral data, we expected HDN mice to have equal or higher counts of activated astrocytes and damaged neurons compared to MOG+Vehicle mice. Because MOG+HDN mice had a more severe form of EAE in the onset stage of EAE (Day 20), we expected MOG+HDN mice sacrificed on Day 20 to have more histological signs of disease (i.e. higher counts, more demyelination). A possible explanation for the decreased activated astrocyte counts on Days 30 and 60 is that astrocyte activation is a marker of the first stage of EAE; because HDN increases the rate of disease progression the first signs of EAE would be lower in more advanced disease. This explanation, however, does not account for the decreased number of damaged neurons in MOG+HDN mice compared to MOG+Vehicle mice on Day 30. The

reason for this decrease in the MOG+HDN mice is unknown, as average disease score and disease incidence were the same between groups on Day 30. By Day 60, the number of damaged neurons was the same in the MOG+Vehicle and MOG+HDN mice. From histological measurements it was concluded that astrocyte activation and neuronal damage are not accurate indicators of behavioral manifestations of EAE. Overall, continuous opioid receptor blockade with HDN did not alter disease course in EAE compared to vehicle treatment.

CHAPTER 4: INTERMITTENT OPIOID RECEPTOR BLOCKADE INVOKED BY LOW DOSE NALTREXONE AND THE IMPACT ON EXPERIMENTAL AUTOIMMUNE ENCEPHALOMYELITIS

4. LDN

4.1. Rationale of Treatment

Continuous opioid receptor blockade with HDN treatment did not affect onset of EAE, and it slightly increased the severity of disease as significantly more HDN-treated animals had hind limb paralysis on day 20 as compared to vehicle-treated mice. Based on hot plate experiments testing the relationship between dosage of NTX and duration of morphine-induced analgesia, administration of LDN (0.1 mg/kg) blocks all opioid receptors in the mouse for 4-6 hours [181]. Briefly, in the hot plate experiments, mice were injected with 0.2 mg/kg morphine, and 30 minutes later received injections of 0, 0.1 and 10 mg/kg NTX. Hot plate tests were administered at 0, 2, 4, 6, 12 and 24 hours post-NTX injection. If morphine was able to inhibit the animal from responding to the heat, NTX was not blocking opioid receptors, but if NTX was present, morphine's analgesic properties were inhibited and animals responded to the heat. HDN blocked the opioid receptors for the duration of the experiment, while LDN only blocked the analgesic properties of morphine for the first 4-6 hours of the experiment. During NTX-mediated opioid receptor blockade, endogenous production of opioids and opioid receptors increases [252]. NTX is cleared from the body through enzymatic digestion and excretion in the urine. Following clearance of LDN, we hypothesize that the excess opioid and opioid receptor present in the animals facilitates a supersensitive reaction that will decrease symptoms of EAE. Opioids have known immunomodulatory and growth properties, and either role could contribute to the alleviation of EAE symptoms. For example, *in vitro* inhibition of preproenkephalin translation through administration of anti-sense oligonucleotides causes a 50% increase in T cell proliferation, indicating that opioids suppress immune cell proliferation and inflammation [254]. One opioid, OGF, has been shown to regulate the rate of cell proliferation. If OGF production is

upregulated during LDN-mediated opioid receptor blockade, there could be a subsequent decrease in the rate of cell proliferation in cells that stimulate inflammation in the CNS.

LDN is an effective therapy for Crohn's disease, but the mechanism of action of LDN is unknown [233]. Because Crohn's and MS are both autoimmune diseases, it is possible that cells targeted by LDN in Crohn's disease are those that cause disease progression in MS (e.g. $CD8^+$ T cells, B cells).

The *hypothesis* of this study was that intermittent opioid receptor blockade alters the progression of EAE.

4.2. Behavior Results

Data included in these analyses represent results pooled from 5 independent experiments. 2 experiments were terminated on Day 20, 2 experiments were terminated on Day 30, and 1 experiment was terminated on Day 60 for subsequent tissue analysis of acute, established, and chronic EAE, respectively. Overall, 25 Control+Vehicle, 45 MOG+Vehicle animals, and 44 MOG+LDN animals were observed. To evaluate behavior, animals were assigned disease scores from 0-5 each day. No animal scored above a 3 at any point in the experiments. Control+Vehicle animals did not present with signs of EAE, and all animals injected with MOG that received daily vehicle injections expressed behavioral signs of EAE (disease score ≥ 1) before sacrifice.

Figure 4.1A representing data from all 5 experiments, demonstrates that LDN treatment significantly decreases average EAE disease score compared to vehicle treatment. LDN treatment significantly lowered the average disease score from Day 16, approximately the time of disease onset, until the end of the 60 day study. Control+Vehicle animals not injected with MOG maintained disease scores of 0 throughout the experiment.

Analysis of individual disease scores at specific time points throughout the studies show significant differences between EAE scores in the vehicle and LDN groups (Figure 4.1B). MOG+Vehicle mice had significantly more animals with a disease score of 2 and significantly less animals with a disease score of 0 compared to MOG+LDN on Days 20, 30, and 60 ($p < 0.001$). On Day 20, 57% of LDN animals had a disease score of 0, while only 11% of MOG+Vehicle animals were healthy. Significantly more MOG+Vehicle mice presented with a disease score of 1 on Day 20 compared to the MOG+LDN mice ($p < 0.05$). All vehicle-treated animals received a disease score of 2 on Day 60, while less than 60% of LDN animals had a wobbly gait. There were no differences in the number of animals with hind limb paralysis between the treatment groups at 20, 30, or 60 days.

Disease incidence significantly varied between MOG+Vehicle and MOG+LDN animals (Figure 4.2A). Of the 44 animals treated with LDN, only 30 displayed behavioral signs of EAE before the time of sacrifice, indicating that LDN can completely prevent onset of disease in some animals. On Day 15, only 16% of MOG+LDN mice expressed behavioral symptoms of EAE, compared to 42% of mice that were EAE-positive in the MOG+Vehicle control group. By Day 25, 100% of MOG+Vehicle mice had a disease score ≥ 1, while only 50% of the MOG+LDN mice were sick. The maximum disease incidence reached in the MOG+LDN group, 64%, was reached on Days 30, 40, 55, and 60. The MOG+Vehicle group had 100% disease incidence at the final 60 day time point. Throughout the course of the experiments, 3 out of 45 mice (6.66%) in the MOG+Vehicle group experienced a remission (had a disease score ≥ 1 but returned to a normal score of 0 before sacrifice) (Figure 4.2B). Of these 3 remissions, 1 animal relapsed back to having a disease score ≥ 1 before the time of sacrifice. 30 of the 44 MOG+LDN mice included from 5 experiments presented with behavioral symptoms. Of these 30 animals

that were sick, 7 animals (23.33%) reverted back to a disease score of 0, and 5 of the 7 remissions relapsed back to a disease score ≥ 1 before the time of sacrifice.

Average day of disease onset for LDN-treated animals was 23.57 ± 1.7, and average day of disease onset for the MOG+Vehicle group was 16.27 ± 0.36 (Figure 4.3A). Average day of disease onset was arbitrarily assigned as 1 day after the sacrifice time point for those animals in the LDN group that did not show disease symptoms throughout the experiment compared to the MOG+LDN group. Day of disease onset was significantly higher in the MOG+LDN group compared to MOG+Vehicle ($p < 0.001$). Disease index was calculated for all animals sacrificed at 20, 30, and 60 days by dividing the total of the average daily disease scores by average day of disease onset and multiplying by 100 (Figure 4.3B). Disease index data demonstrate that LDN-treated mice have less than half the disease index of MOG+Vehicle mice, indicating a much less severe disease manifestation in the LDN group. The disease index for MOG+Vehicle mice was 596.2, while the disease index for MOG+LDN mice was only 198.0. The MOG+Vehicle group had a peak average disease score of 2, which was reached at 24-27, 31-39, and 50-60 days post-EAE induction. The MOG+LDN group had a peak average disease score of 1.27, which was reached on Days 40-43 and Day 55. No animal in the vehicle or LDN group had a disease score of 3, the most severe form of EAE recorded in the experiments, past Day 28 and 30, respectively.

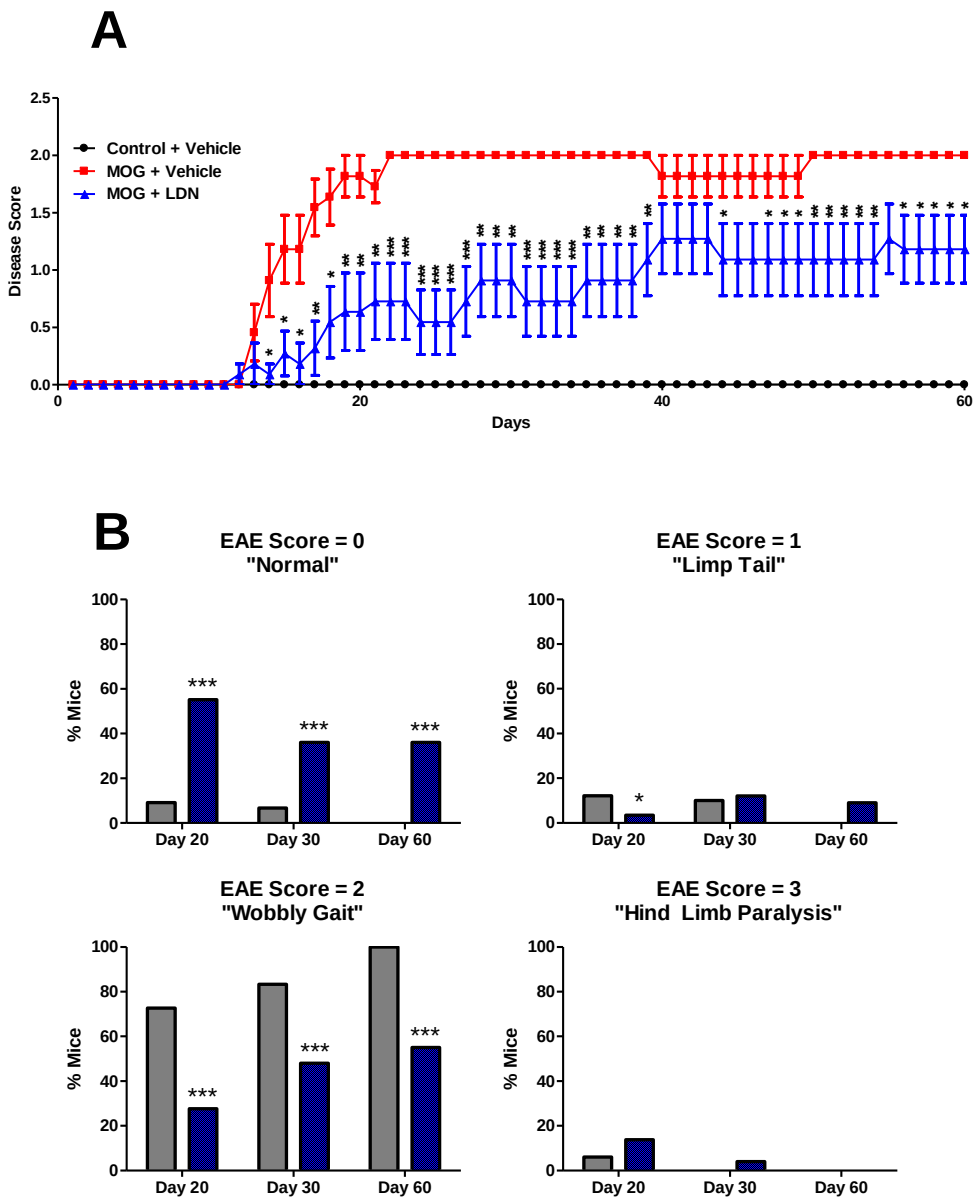

Figure 4.1: The effect of LDN on EAE disease score and distribution. EAE was induced and mice were scored daily on a 0 - 5 scale. (A) Average disease scores for 60 days post-EAE induction. (B) Individual disease scores on Days 20, 30, and 60 for MOG+Vehicle (white bars) and MOG+LDN (blue bars) mice. Control+Vehicle n= 4-25, MOG+Vehicle n=11-45, MOG+LDN n=11-32. N values decrease after the 20 and 30 day time points because some animals were sacrificed for histological analysis at these time points. Data represent means ± SEM from 4-5 independent experiments. Significantly different from MOG+Vehicle at $p < 0.05$ (*), $p < 0.01$ (**), $p < 0.001$ (***).

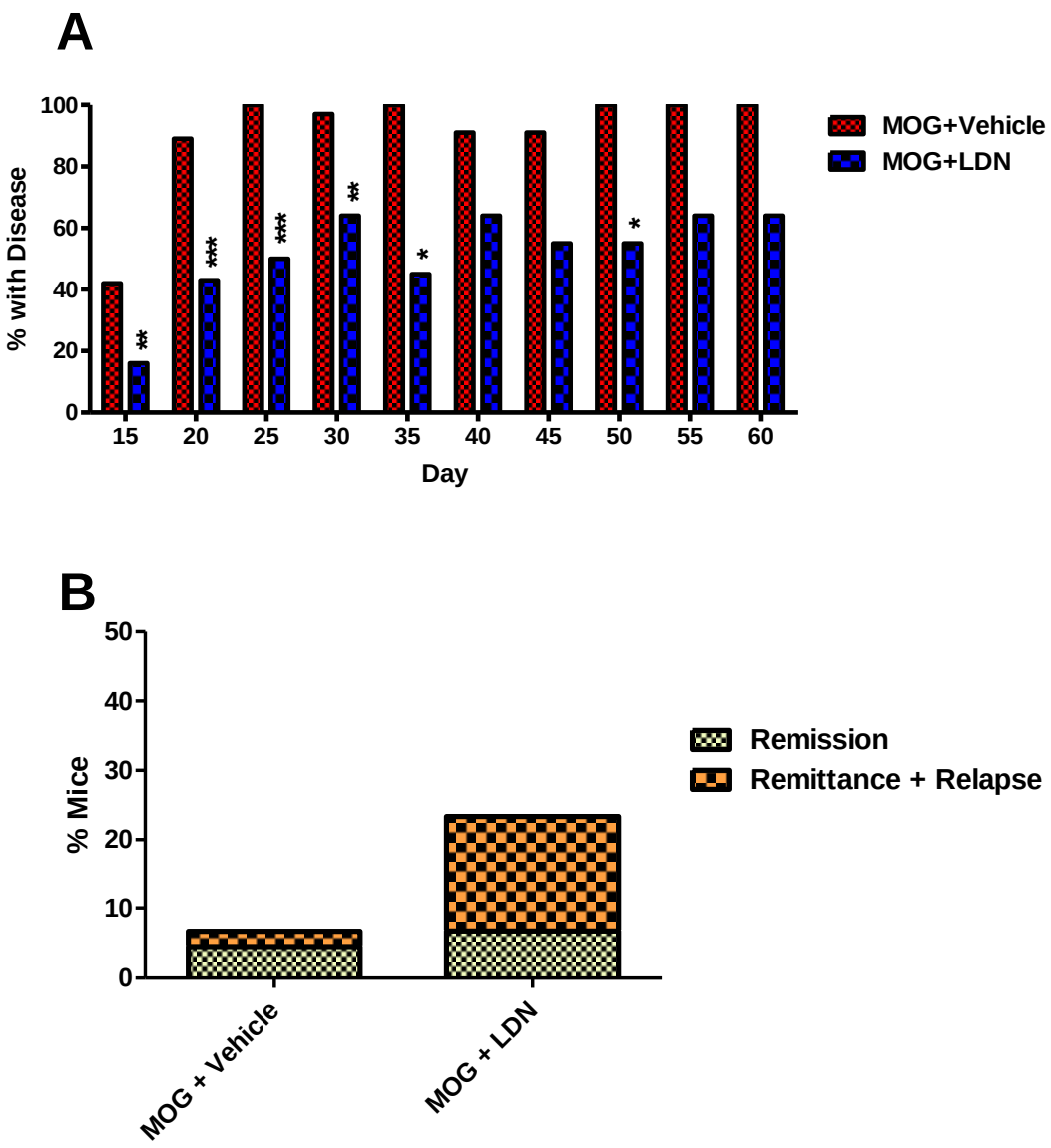

Figure 4.2: The impact of LDN on EAE disease incidence and remissions + relapses. EAE was induced and mice were scored daily on a 0 - 5 scale. (A) Percentage of mice with disease was calculated by dividing the number of animals with a disease score ≥ 1 by the total number of animals and multiplying by 100. Significantly different from MOG+Vehicle at $p < 0.05$ (*), $p < 0.01$ (**). (B) The percentage of MOG+Vehicle and MOG+LDN mice that experienced a remission or a remission with a subsequent relapse before the predetermined time of sacrifice, 20, 30, and 60 days post-EAE induction. MOG+Vehicle n=11-45, MOG+LDN n=11-44. N values decrease after the 20 and 30 day time points because some animals were sacrificed for histological analysis at these time points. Data represent means ± SEM from 5 independent experiments.

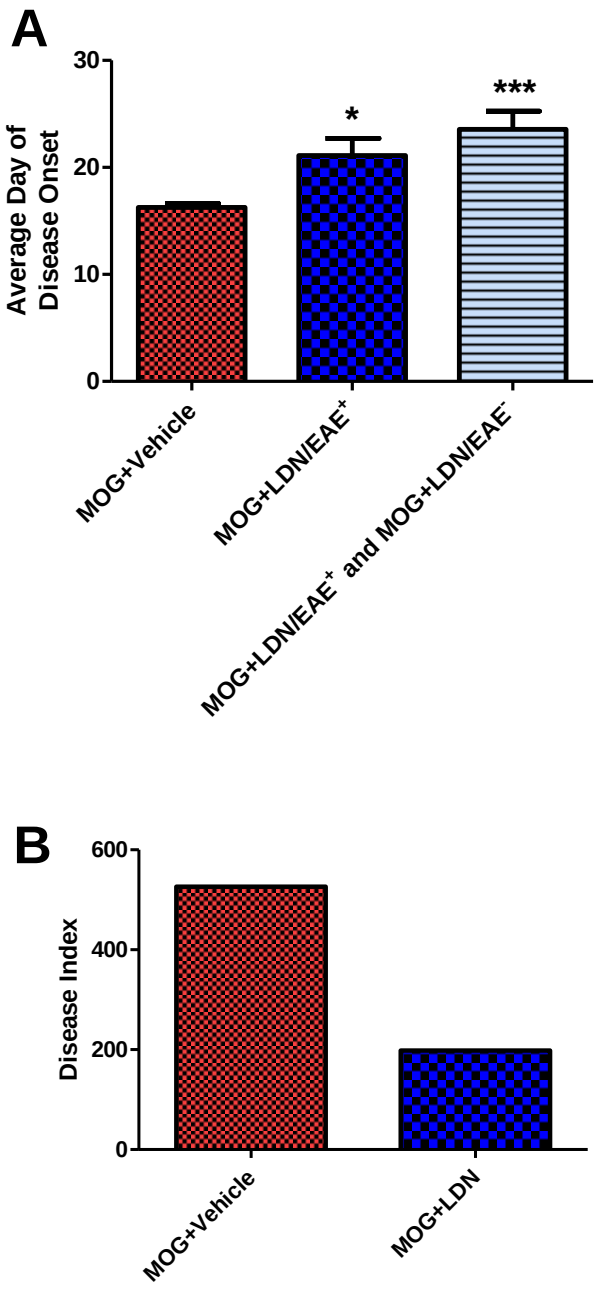

Figure 4.3: The influence of LDN on EAE disease onset and disease index. EAE was induced and mice were scored daily on a 0 - 5 scale. (A) Average day of disease onset for MOG+Vehicle mice, only the MOG+LDN mice that expressed disease before the time of sacrifice (MOG+LDN/EAE$^+$), and all MOG+LDN mice (MOG+LDN/EAE$^+$ and MOG+LDN/EAE$^-$). The first day a mouse received a disease score ≥ 1 was marked as the animal's day of disease onset. Significantly different from MOG+Vehicle at $p < 0.05$ (*) and $p < 0.001$ (***). (B) Disease index was calculated by adding up the average daily disease scores, dividing by the average day of disease onset, and multiplying by 100. MOG+Vehicle n=45, MOG+LDN n=44. Data represent means ± SEM from 5 independent experiments.

4.3. Body Weight Results

Body weight did not significantly differ between groups on Day 0 (Figure 4.4). Control+Vehicle (n = 4), MOG+Vehicle (n = 13), and MOG+LDN (n = 12) mice weighed 18.0 ± 0.6, 18.3 ± 0.3, and 18.0 ± 0.3 grams, respectively, on Day 0. Body weight decreased from Day 0 until Day 6 for Control+Vehicle, MOG+Vehicle, and MOG+LDN mice. All three groups showed a slight increase between Day 6 and Day 10, and by Day 14 body weight was equal to or higher than Day 0 body weight in all groups. Control+Vehicle mice had significantly higher body weights than MOG+Vehicle mice on Day 14 ($p < 0.05$). MOG+LDN mice had significantly higher body weight than MOG+Vehicle mice on Day 45 ($p < 0.05$). Body weight did not significantly differ between groups on the last day it was measured, Day 50, before animals were sacrificed. Control+Vehicle mice weighed 21.5 ± 0.6 grams, while MOG+Vehicle and MOG+LDN mice weighed 21.1 ± 0.3 and 21.7 ± 0.3 grams, respectively, on Day 50.

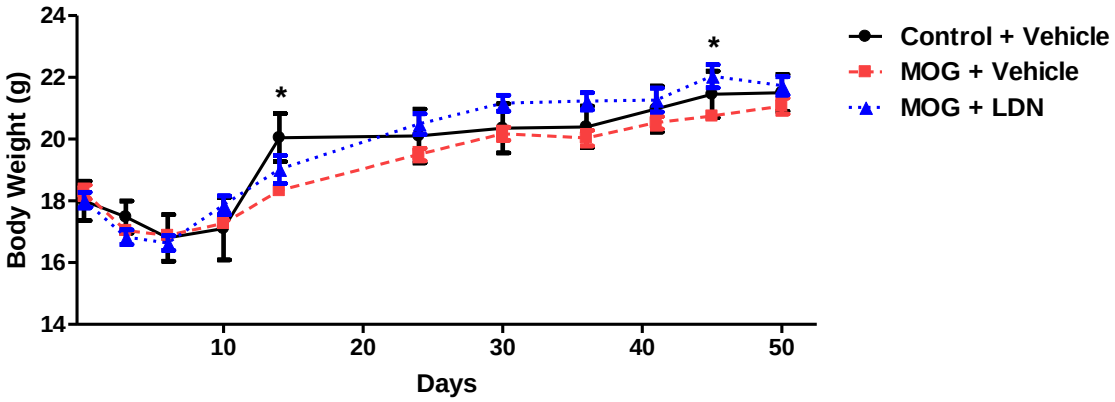

Figure 4.4: Average body weight of Control+Vehicle, MOG+Vehicle, and MOG+LDN mice. Body weight was recorded 1-2 times per week for 50 days. Significantly different from MOG+Vehicle at $p < 0.05$ (*). Control+Vehicle n = 4, MOG+Vehicle n = 11, MOG+LDN = 11. Data represent means ± SEM.

4.4. Morphology Results

4.4.1. Astrocyte Activation Results

Astrocyte activation was examined at 10, 20, 30, and 60 days post-EAE induction (Figure 4.5) At all time points examined, Control+Vehicle mice had significantly less spinal cord astrocyte activation as compared to MOG+Vehicle mice ($p < 0.01$ and 0.001). Astrocyte activation was significantly lower in MOG+LDN animals ($n = 4$) as compared to MOG+Vehicle mice ($n = 3$) on Days 10 ($p < 0.001$), with only 154.35 ± 18.7 activated astrocytes in the LDN-treated mice and 266.7 ± 20.3 activated astrocytes in the vehicle-treated mice. Control+Vehicle mice ($n = 4$) had only 105.5 ± 21.5 activated astrocytes per mm^2 on Day 10. On Day 20, Control+Vehicle ($n = 8$) astrocyte counts decreased to 28.9 ± 4.37, while MOG+Vehicle ($n = 8$) counts remained relatively constant from Day 10 at 242.9 ± 19.6 activated astrocytes per mm^2. LDN animals were divided into those that expressed the disease with behavioral symptoms (MOG+LDN/EAE^+) and those that did not express behavioral signs of EAE and remained healthy (MOG+LDN/EAE^-). On Day 20 spinal cords from MOG+LDN/EAE^+ mice ($n = 7$) had an average of 200.23 ± 26.0 activated astrocytes per mm^2, while sections from MOG+LDN/EAE^- ($n = 7$) had only 92.7 ± 12.8 activated astrocytes per mm^2. Control+Vehicle and MOG+LDN/EAE^+ mice had significantly fewer counts than MOG+Vehicle mice and MOG+LDN/EAE^+ mice ($p < 0.01$ and 0.001) on Day 20. At 30 days post-EAE induction, MOG+LDN/EAE^+ ($n = 6$) and MOG+LDN/EAE^- ($n = 3$) mice had astrocyte counts that did not significantly differ from one another, but both LDN groups had significantly more activated astrocytes than Control+Vehicle ($n = 7$) mice ($p < 0.001$) and significantly fewer activated astrocytes than MOG+Vehicle ($n = 6$) mice ($p < 0.01$ and 0.001). The average numbers of activated astrocytes per mm^2 of spinal cord

tissue in Control+Vehicle, MOG+Vehicle, MOG+LDN/EAE^{+}, and MOG+LDN/EAE^{-} mice sacrificed on Day 30 were 122.4 ± 12.7, 354.4 ± 24.8, 239.4 ± 22.4, and 249.9 ± 24.5, respectively. At 60 days post-EAE induction, the average numbers of activated astrocytes per mm^2 of spinal cord tissue in Control+Vehicle (n = 4), MOG+Vehicle (n = 6), MOG+LDN/EAE^{+} (n = 5), and MOG+LDN/EAE^{-} (n = 2) mice were 182.7 ± 18.4, 350.2 ± 37.6, 334.5 ± 29.3, and 261.5 ± 52.7, respectively. The only significant differences observed at this time point were between Control+Vehicle and MOG+Vehicle ($p < 0.01$), and between Control+Vehicle and MOG+LDN/EAE^{+} ($p < 0.01$).

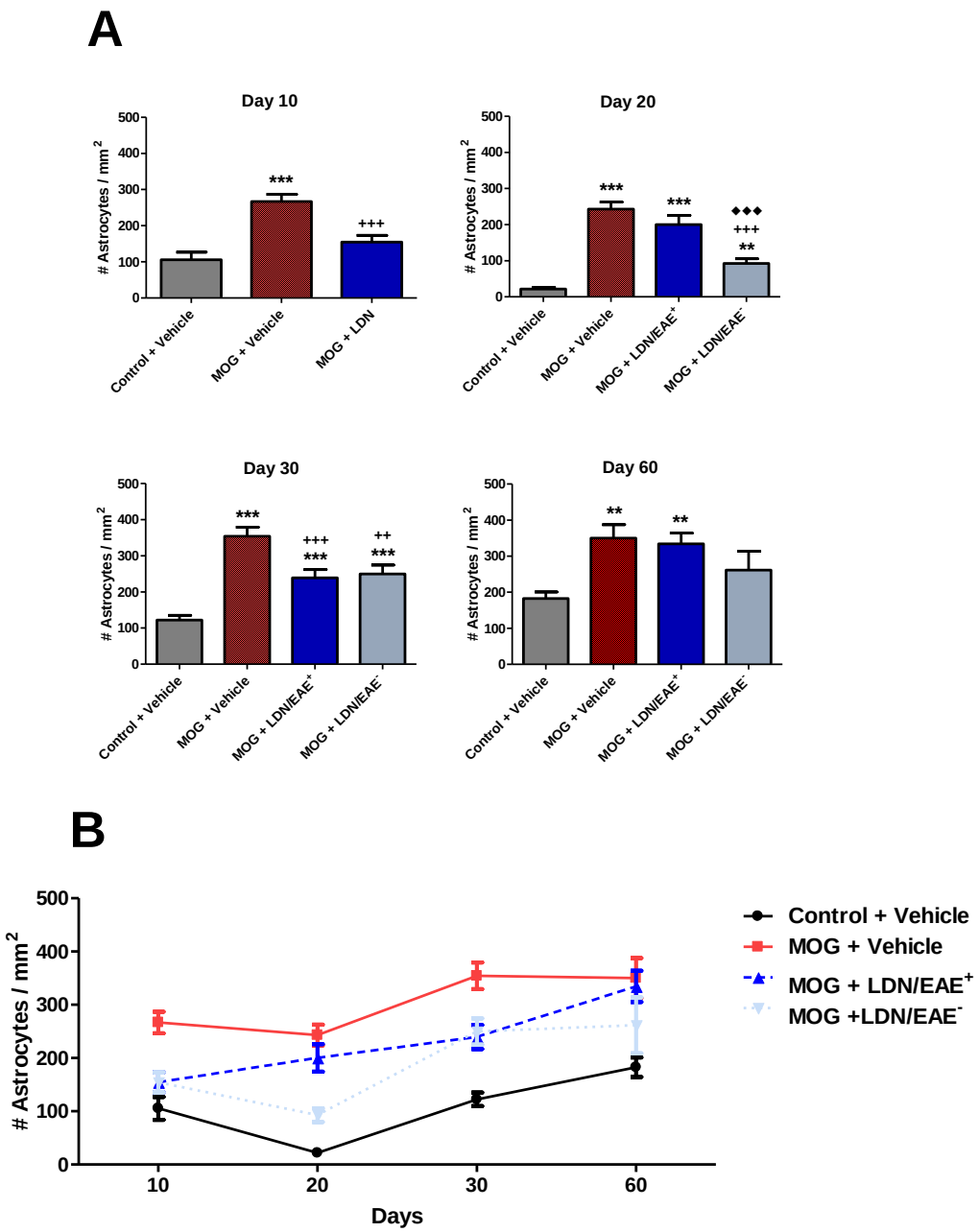

Figure 4.5: The effect of LDN on EAE mouse spinal cord astrocyte activation. The number of activated astrocytes was counted in three grids per spinal cord of 2 sections per mouse. (A) The number of activated astrocytes in the spinal cord on Days 10, 20, 30, and 60 post-EAE induction. Significantly different from Control+Vehicle at $p < 0.01$ (**), $p < 0.001$ (***). Significantly different from MOG+Vehicle at $p < 0.01$ (++), $p < 0.001$ (+++). Significantly different from MOG+LDN/EAE$^+$ at $p < 0.01$ (♦♦♦). (B) Time course of the number of activated astrocytes on Days 10, 20, 30, and 60 shows how counts change during different stages of EAE. Data represent means ± SEM.

4.4.2. Demyelination Results

Mice were categorized as having demyelination if 1 or more quadrants showed demyelination at a given time point. The number of mice observed at 10, 20, 30, and 60 days post-EAE induction are summarized in Table 4.1. Control+Vehicle animals (n = 4-11) did not experience spinal cord demyelination at any of the 4 time points examined. At 10 days post-EAE induction, all spinal cords were free of demyelination (Figure 4.6). On Days 20, 30, and 60, LDN animals were divided into those that expressed the disease with behavioral symptoms (MOG+LDN/EAE^{+}) and those that did not express behavioral signs of EAE and remained healthy (MOG+LDN/EAE^{-}). Demyelination was observed in all groups given MOG injections beginning on Day 20, with 33% (3/9) of MOG+Vehicle, 67% (4/6) of MOG/LDN/EAE^{+}, and 14% (1/7) of MOG+LDN/EAE^{-} mice experiencing demyelination. On Day 30, 86% (6/7) of MOG+Vehicle animals had demyelination, but only 33% (2/6) and 50% (1/2) of the MOG+LDN/EAE^{+} and MOG+LDN/EAE^{-} had demyelination, respectively. No MOG+LDN/EAE^{-} animals had demyelination on Day 60, while 29% (2/7) of MOG+Vehicle and 20% (1/5) of MOG+LDN/EAE^{+} mice had demyelination in their spinal cords. The changes in demyelination over time for each treatment group are shown in Figure 4.7A. Further categorizing the demyelination as moderate (1-2 quadrants with demyelination) or severe (3-4 quadrants with demyelination) demonstrates that the most profound occurrence of severe demyelination occurred on Day 30 (Figure 4.7B). Some severe demyelination occurred on Day 20, and interestingly by Day 60 animals only MOG+LDN/EAE^{+} mice had moderate demyelination in their spinal cords.

	# Mice with…	10 Days	20 Days	30 Days	60 Days
Control+Vehicle	No Demyelination	4	11	9	4
	Demyelination	0	0	0	0
MOG + Vehicle	No Demyelination	4	6	1	5
	Demyelination	0	3	6	2
MOG + LDN/EAE^{+}	No Demyelination	NA	2	2	5
	Demyelination	NA	4	4	1
MOG + LDN/EAE^{-}	No Demyelination	5	6	1	2
	Demyelination	0	1	1	0

Table 4.1: A summary of animals examined in LDN demyelination studies. Animals were sacrificed and examined for signs of demyelination in the spinal cord. Data represent the number of animals at each time point that had no demyelination present in the spinal cord or that had demyelination in at least 1 quadrant of the spinal cord.

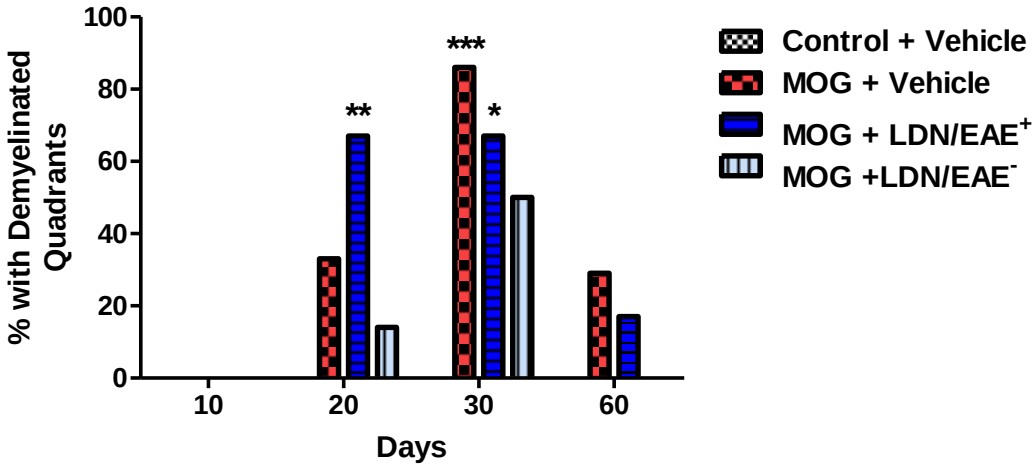

Figure 4.6: The effect of LDN on spinal cord demyelination incidence in EAE mice. Percentage of animals with demyelination in the L4 – L6 section of the spinal cord at 10, 20, 30, and 60 days post-EAE induction. Significantly different from Control+Vehicle at $p < 0.05$ (*), $p < 0.01$ (**), $p < 0.001$ (***).

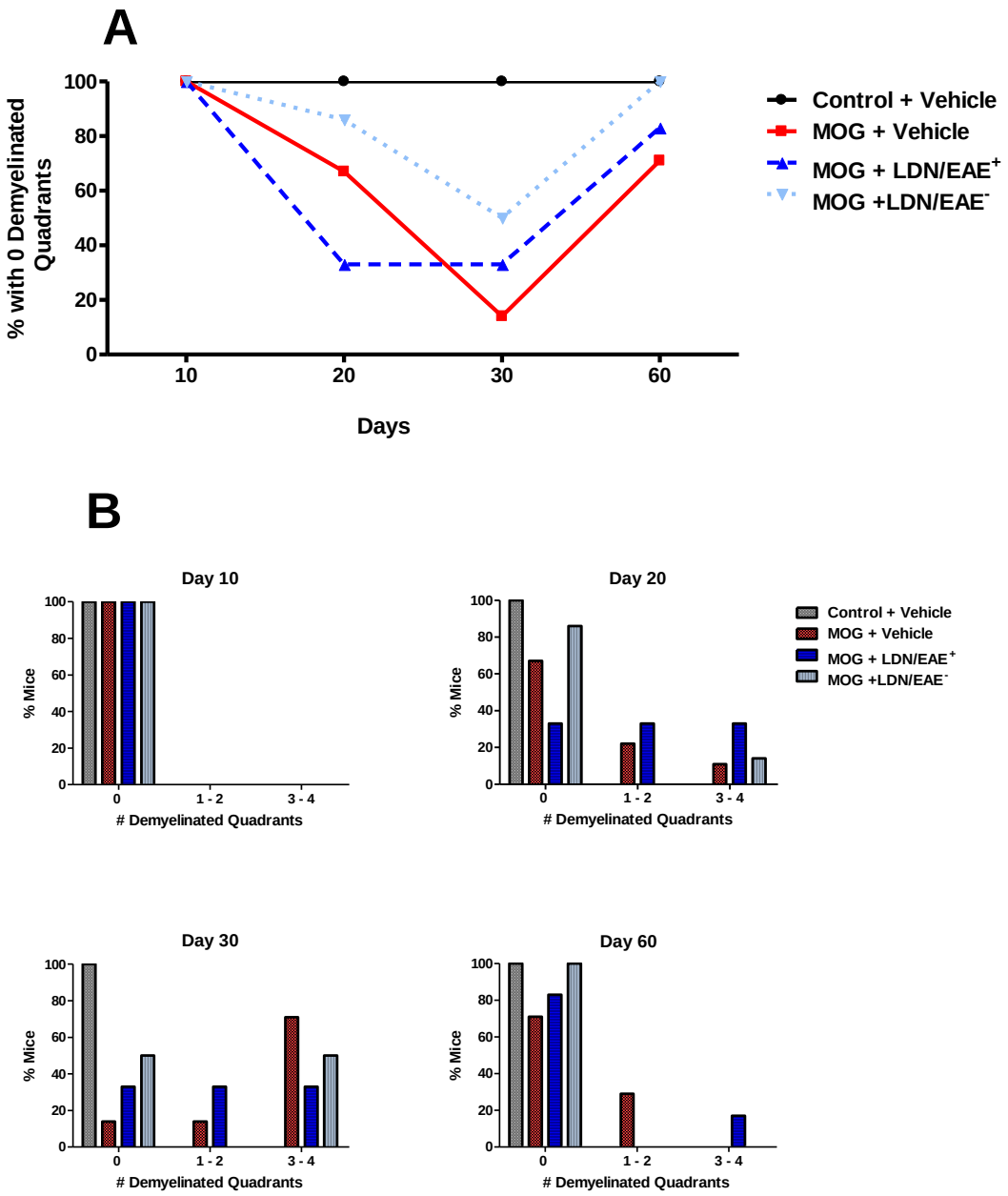

Figure 4.7: The effect of LDN on spinal cord demyelination course and distribution in EAE mice. Two spinal cord sections per mouse were examined for the presence of demyelination. (A) Time course of the percentage of animals in a treatment group with spinal cords free of demyelination on Days 10, 20, 30, and 60 shows how much demyelination, and possibly remyelination, occurs during different the stages of EAE. (B) Histograms of the percent of mice with demyelination in 0, 1-2, or 3-4 quadrants on Days 10, 20, 30, and 60 indicate if animals in a given treatment group have no (0), moderate (1-2) or severe (3-4) demyelination.

4.4.3. Neuronal Damage Results

Neuronal damage was evaluated in spinal cords taken from animals on Days 10, 20, 30, and 60 (Figure 4.8). On Day 10 MOG+LDN mice had similar levels of neuronal damage as compared to mice that did not receive MOG injections. 7.0 ± 1.1 damaged neurons were counted in LDN-treated animals (n = 5) and 7.2 ± 1.1 were counted in Control+Vehicle mice (n = 3). MOG+Vehicle mice (n = 3) had 11.6 ± 1.6 damaged neurons, but this was not significantly higher as compared to Control+Vehicle or MOG+LDN animals. On Days 20, 30, and 60, LDN-treated animals were separated into those that expressed behavioral symptoms of EAE (MOG+LDN/EAE$^+$) and those that did not express behavioral symptoms (MOG+LDN/EAE$^-$). Day 20 data demonstrated a significantly increased number of damaged neurons observed in MOG+Vehicle mice (n = 9) as compared to Control+Vehicle (n = 9), MOG+LDN/EAE$^+$ (n = 7), and MOG+LDN/EAE$^-$ (n = 7) mice ($p < 0.001$). MOG+Vehicle mice had an average of 13.5 ± 1.3 damaged neurons per spinal cord, while Control+Vehicle, MOG+LDN/EAE$^+$, and MOG+LDN/EAE$^-$ averaged 2.3 ± 0.6, 5.3 ± 1.5, and 7.0 ± 1.7 damaged neurons per spinal cord, respectively. Control+Vehicle (n = 5), MOG+LDN/EAE$^+$ (n = 5), and MOG+LDN/EAE$^-$ (n = 3) mice had approximately one-half of the neuronal damage observed in the MOG+Vehicle (n = 5) mouse spinal cords on Day 30, and all were significantly different as compared to MOG+Vehicle values ($p < 0.01$ and 0.001). On Day 30 Control+Vehicle, MOG+LDN/EAE$^+$, and MOG+LDN/EAE$^-$ mice had 11.2 ± 0.8, 11.7 ± 1.9, and 8.3 ± 1.6 damaged neurons, while MOG+Vehicle mice averaged 20.4 ± 2.3 damaged neurons per spinal cord. Day 60 data demonstrate no significant differences in the amount of spinal cord neuronal damage between MOG+Vehicle mice (n = 4), MOG+LDN/EAE$^+$ (n = 6), and MOG+LDN/EAE$^-$ (n = 2) mice. MOG+Vehicle and

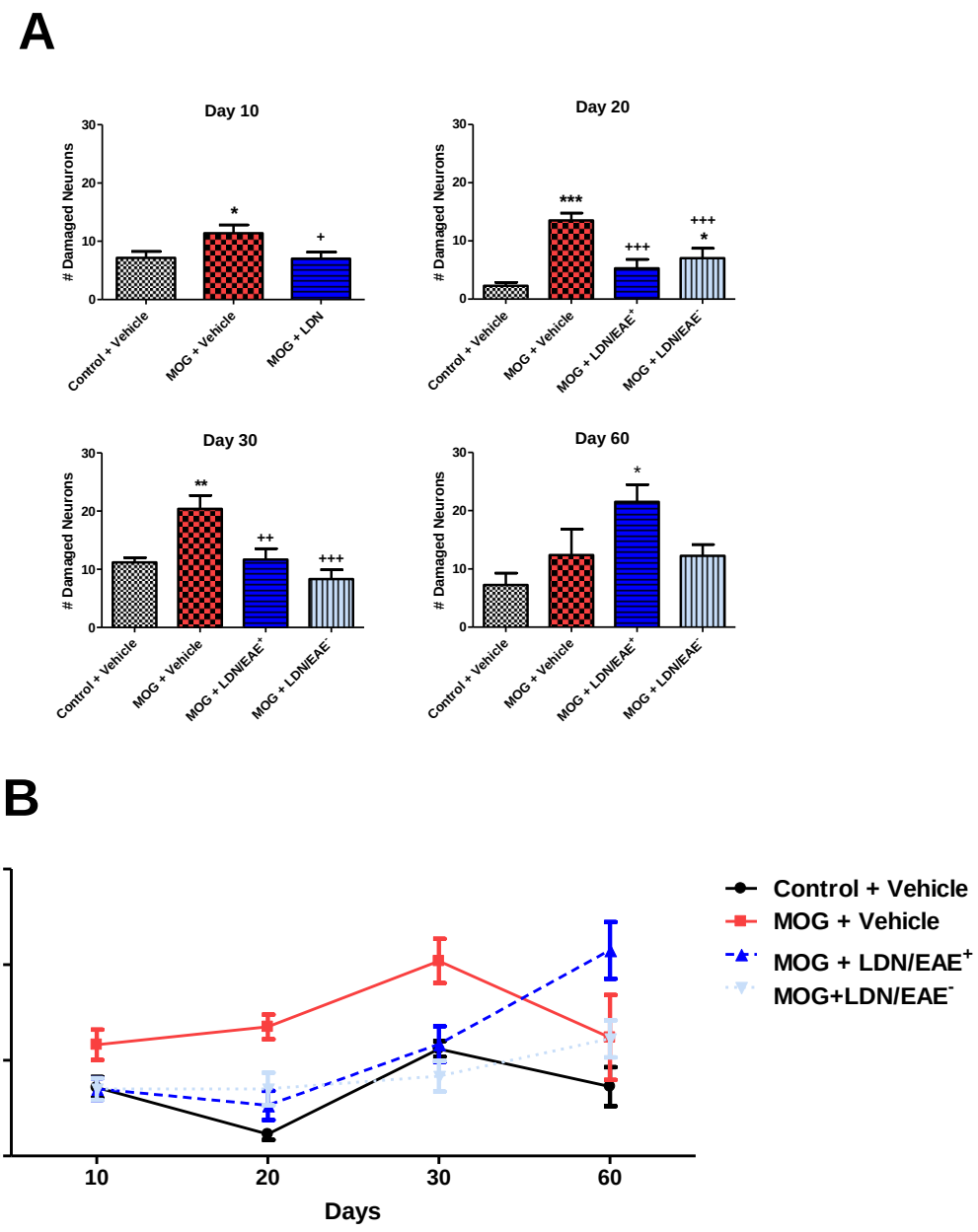

Figure 4.8: The effect of LDN on the amount of spinal cord neuronal damage in EAE mice. The number of damaged neurons was counted in the grey matter of 2 spinal cord of sections per mouse. (A) The number of damaged neurons in the lumbar spinal cord on Days 10, 20, 30, and 60 post-EAE induction. Significantly different from Control+Vehicle at $p < 0.05$ (*), $p < 0.01$ (**), $p < 0.001$ (***). Significantly different from MOG+Vehicle at $p < 0.05$ (+), $p < 0.01$ (++), $p < 0.001$ (+++). (B) Time course of the number of damaged neurons on Days 10, 20, 30, and 60 shows how counts change during different stages of EAE. Data represent means ± SEM.

MOG+LDN/EAE$^-$ animals presented with 12.4 ± 4.4 and 12.25 ± 1.9 damaged neurons on Day 60, respectively. MOG+LDN/EAE$^+$ mice had 21.5 ± 3.0 damaged neurons, which was significantly higher than the 7.25 ± 2.0 damaged neurons observed in Control+Vehicle ($n = 5$) mice ($p < 0.05$). No other significant differences were noted on Day 60.

4.5. Conclusions

Disease scores of MOG+Vehicle and MOG+LDN mice were significantly different throughout the 5 experiments. Disease incidence and disease index were significantly reduced in MOG+LDN mice as compared to MOG+Vehicle mice, indicating that fewer mice were sick and overall severity of disease was lower due to LDN treatment. Average day of disease onset for MOG+LDN mice was significantly later than disease onset for MOG+Vehicle mice. More LDN-treated mice relapsed back to a disease score of 0 than vehicle-treated controls, showing that LDN is capable of reversing behavioral signs of EAE. These behavioral data support the idea that intermittent opioid receptor blockade is able to abolish or diminish the motor deficits that occur in EAE.

Histological data showed significant differences between MOG+Vehicle and MOG+LDN mice on Days 10, 20, and 30. MOG+LDN mice had significantly fewer activated astrocytes as compared to MOG+Vehicle mice on Day 10. This finding was not surprising; astrocytes are a marker of inflammation, which is the first stage of EAE, and LDN mice went on to develop a less severe form of EAE (based on behavioral scores). MOG+Vehicle mice had significantly more activated astrocytes than MOG+LDN mice not behaviorally expressing EAE (MOG+LDN/EAE$^-$) on Day 20 and all MOG+LDN-treated mice (MOG+LDN/EAE$^-$ and MOG+LDN/EAE$^+$) on Day 30. Therefore, there was a correlation between inflammation in the spinal cord and behavioral symptoms of EAE on Day 20. However, there was no correlation on Day 30,

as inflammation in the spinal cord was decreased in LDN-treated mice regardless of behavioral symptoms. MOG+LDN mice not expressing EAE (MOG+LDN/EAE$^-$) had fewer demyelinated quadrants than MOG+Vehicle mice on Days 20, 30, and 60. However, these differences were not significant, probably due to our semi-quantitative methods employed for data analysis. Behavioral symptoms were not indicative of the amount of neuronal damage in the spinal cords. All MOG+LDN-treated mice, both those that were healthy and those that expresses behavioral symptoms of EAE, had significantly less neuronal damage than vehicle-treated controls on Days 10, 20, and 30. Histology and behavior data demonstrated that astrocyte activation and neuronal damage are not accurate indicators of behavioral manifestations of EAE. Overall, intermittent opioid receptor blockade with LDN decreased disease severity and incidence of EAE as compared to vehicle treatment, but disease expression was not indicative of histological damage in LDN-treated mice.

CHAPTER 5: ADMINISTRATION OF EXOGENOUS OPIOID GROWTH FACTOR AND THE IMPACT ON EXPERIMENTAL AUTOIMMUNE ENCEPHALOMYELITIS

5. OGF

5.1. Rationale of Treatment

Various opioid peptides have different effects on immune function [255]. OGF has been shown to downregulate immune responses, as inhibition of OGF production causes an increase in T cell proliferation and IL-6 secretion [254]. Expression of proenkephalin A in $CD4^+$ T lymphocytes occurs in Th2 but not Th1 cells, indicating that OGF might have anti-inflammatory properties [256]. Mice given a single injection of NTX (HDN, 10 mg/kg) one hour prior to sacrifice have elevated IL-2 activity and splenocyte proliferation rates compared to controls [257]. If opioid receptor blockade is proinflammatory, NTX administration could promote the inflammatory processes that lead to demyelination and neurodegeneration. Therefore, some negative side effects could occur during the short term opioid receptor blockade mediated by LDN. Therefore, avoiding NTX administration might be the most beneficial option in EAE treatment.

In addition to the data available on OGF and immune system regulation, it is logical to test the effects of exogenous opioids on EAE based on the HDN and LDN experiments described above. During NTX-mediated opioid receptor blockade, endogenous opioid and opioid receptor production increases. The difference between HDN and LDN is the duration of opioid receptor blockade. HDN blocks opioid receptors in mice for 24 hours, and the continuous opioid receptor blockade observed in HDN animals prevents any of the excess opioid from interacting with excess opioid receptor. In the LDN-treated mice, however, opioid receptors are only blocked for 4-6 hours, creating an 18-20 hour window in which opioids are able to interact with their receptors. HDN treatment had no effect on onset, progression, and histological symptoms of EAE, while LDN delays onset, inhibits EAE in some animals, and improves the histological symptoms of EAE. These results suggest that opioid interactions might play a crucial

role in regulating the immune system, and inhibition of these interactions might contribute to disease pathogenesis. Therefore it is logical and justified to test the efficacy of opioids on alleviating symptoms and progression of EAE. OGF was chosen for a number of reasons. First, our lab is very familiar with the biological properties of the peptide [173, 177, 179, 185, 202-205, 214]. Second, OGF was chosen because it has known immunomodulatory properties [254]. OGF inhibits the effector function of macrophages when administered at high dosages, suggesting that the administration of OGF will decrease CNS inflammation that occurs in MS [258]. Studies have also shown that OGF administration decreases NK activity [259, 260]. Third, experiments completed in other laboratories have shown that OGF (i.e. [Met^5]-enkephalin) can inhibit EAE in rat EAE models [175, 176]. Finally, OGF possesses unique growth properties not found in any other endogenous or exogenous opioid [172, 174, 180, 200, 203, 206, 219, 221-224, 227]. If the effects of LDN and HDN seen above are due to NTX's ability to regulate proliferation, OGF would be the logical opioid candidate to test.

The hypothesis of this study was that administration of exogenous OGF alters the progression of EAE.

5.2. Behavior Results

Data included in these analyses represent results pooled from 5 independent experiments. 25 Control+Vehicle, 45 MOG+Vehicle, and 38 MOG+OGF animals were observed. To evaluate behavior, animals were assigned disease scores from 0-5 each day.

Figure 5.1A represents the average disease score of Control+Vehicle, MOG+Vehicle, and MOG+OGF mice from all 5 experiments over 60 days. Data demonstrate that administration of OGF was successful at significantly decreasing average disease score beginning 17 days post-EAE induction. OGF treatment caused a

significant decrease in average disease score as compared to MOG+Vehicle animals from Days 17-40, 43-44, and 47-60.

Examination of individual disease scores at 3 specific time points demonstrates that OGF inhibited disease severity compared to Vehicle-treated control (Figure 5.1B). The MOG+OGF group had significantly more animals with a healthy disease score of 0 on Days 20, 30, and 60 as compared to MOG+Vehicle mice ($p < 0.001$). Significantly more MOG+Vehicle mice presented with a wobbly gait on Days 20, 30, and 60 compared to MOG+OGF mice ($p < 0.001$). Few animals from each group had disease scores of 1 (limp tail) and 3 (hind limb paralysis), and no significant differences were noted between groups.

Disease incidence data show that significantly fewer animals injected with MOG were sick when given daily injections of OGF compared to vehicle (Figure 5.2A). OGF treatment decreased the time of initial EAE onset by over 50%, as 42% of MOG+Vehicle mice presented with symptoms of EAE by Day 15 but only 16% of MOG+OGF mice had a disease score ≥ 1. MOG+Vehicle animals reached 100% disease incidence by Day 25, but only 33% of MOG+OGF mice were sick at this time point. 56% of MOG+OGF mice were sick on Day 45, and only 44% remained sick at the final Day 60 time point. MOG+Vehicle control mice had 100% disease incidence on Day 60. Throughout the course of the experiments, 3 out of 45 mice in the MOG+Vehicle group experienced a remission (had a disease score ≥ 1, but returned to a disease score of 0 before the time of sacrifice). Of these 3 remissions, 1 animal relapsed back to having a disease score ≥ 1 before the time of sacrifice. 24 MOG+OGF animal presented with disease scores ≥ 1 before the animals were sacrificed 20, 30, and 60 days post-EAE induction, while 14 MOG+OGF mice remained healthy until their time of sacrifice. Starting on Day 20, MOG+OGF mice had significantly fewer sick animals as compared to the MOG+Vehicle

group. Significance was maintained through Day 40, and MOG+OGF mice again had significantly fewer mice sick than MOG+Vehicle from Day 50 until Day 60 ($p < 0.05$). Of the 24 MOG+OGF mice that presented with behavioral symptoms of EAE, 10 reverted back to a healthy disease score of 0 (Figure 5.2B). Of the 10 that reverted back to normal, 4 went on to present with a behavioral disease score ≥ 1.

Average day of disease onset for animals treated with OGF was 23.26 ± 1.98, significantly higher than the 16.27 ± 0.36 average day of disease onset for the vehicle-treated controls ($p < 0.001$) (Figure 5.3A). The peak average disease score for MOG+Vehicle mice was 2, while the peak average disease score in the OGF group was only 1.11. In addition to lowering severity, OGF treatment delayed maximal disease severity. The peak average score was reached in the MOG+Vehicle group by Day 24, but the OGF group did not record peak EAE score until Day 45. Disease index was calculated for all animals sacrificed on Days 20, 30, and 60. Disease index data demonstrate MOG+OGF mice have a lower disease index than MOG+Vehicle animals (Figure 5.3B). The disease index for MOG+Vehicle mice is 526.2, while disease index for OGF-treated mice is 162.3.

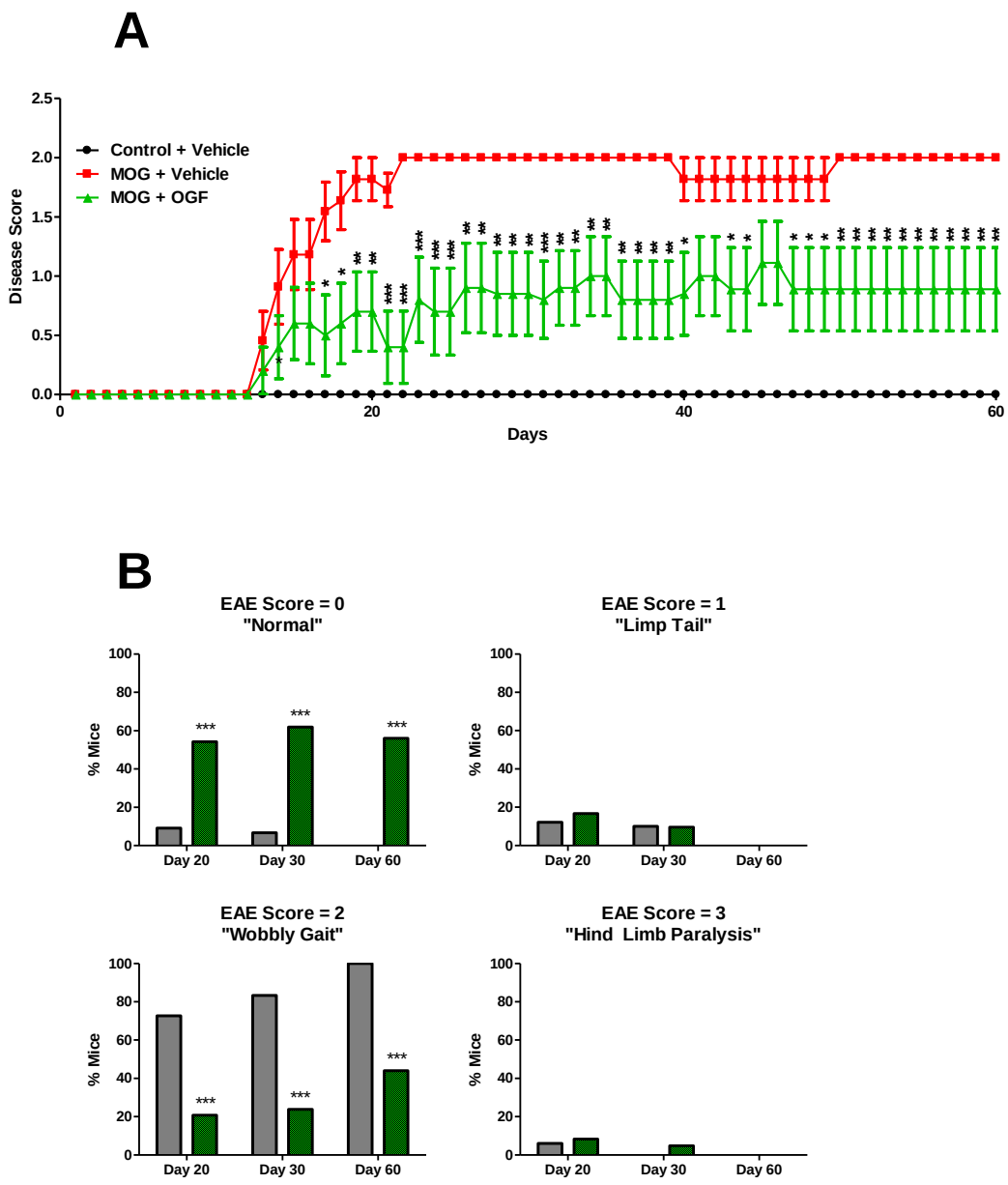

Figure 5.1: The effect of daily OGF administration on EAE disease score and distribution. EAE was induced and mice were scored daily on a 0 - 5 scale. (A) Average disease scores for 60 days post-EAE induction. (B) Individual disease scores on Days 20, 30, and 60 for MOG+Vehicle (white bars) and MOG+OGF (green bars) mice. Control+Vehicle n= 4-25, MOG+Vehicle n=11-45, MOG+OGF n=9-38. N values decrease after the 20 and 30 day time points because some animals were sacrificed for histological analysis at these time points. Data represent means ± SEM from 5 independent experiments. Significantly different from MOG+Vehicle at $p < 0.05$ (*), $p < 0.01$ (**), $p < 0.001$ (***).

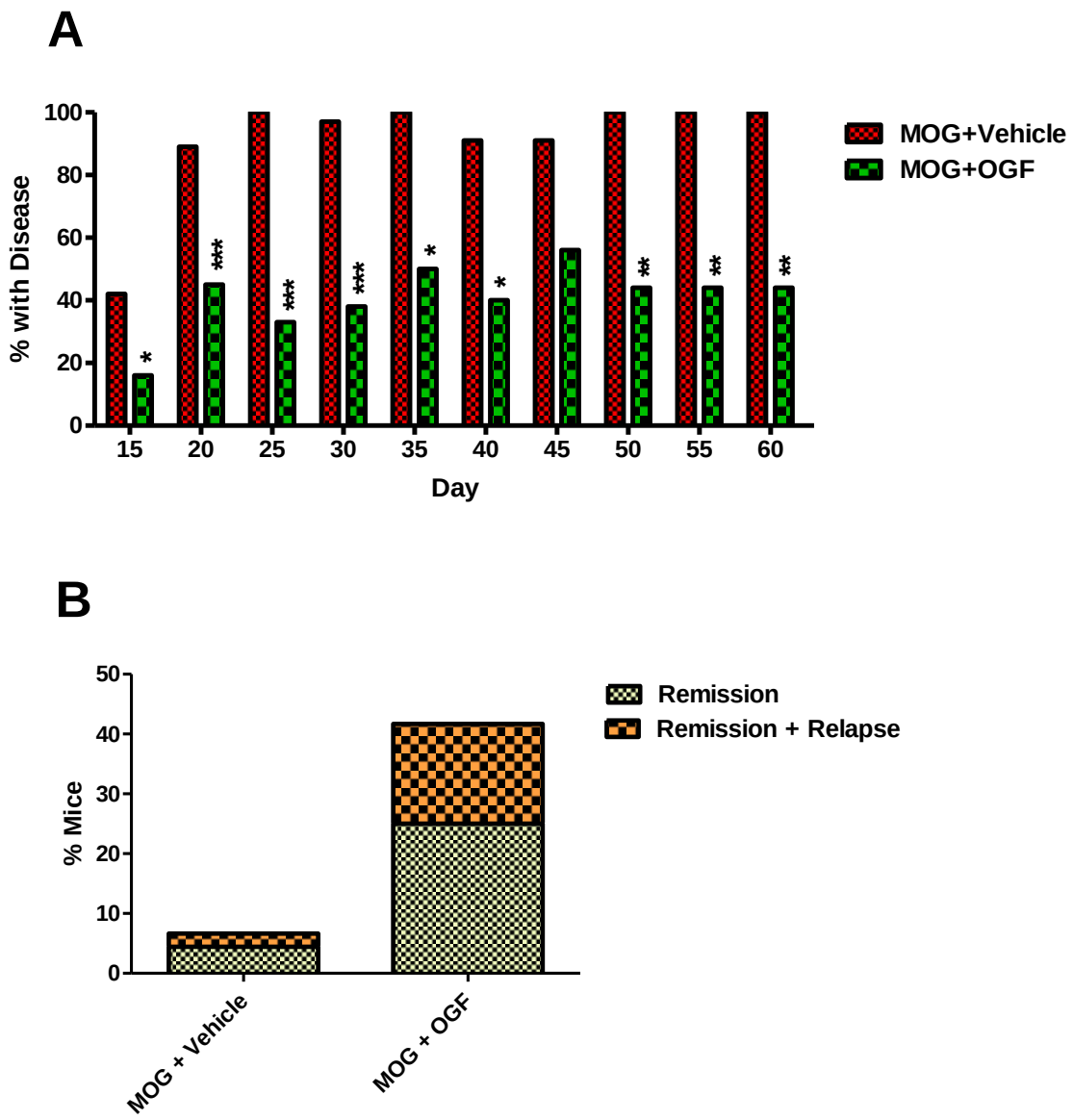

Figure 5.2: The impact of OGF on EAE disease incidence and remissions + relapses. EAE was induced and mice were scored daily on a 0 - 5 scale. (A) Disease incidence of MOG+Vehicle and MOG+OGF mice was calculated by dividing the number of animals with a disease score ≥ 1 by the total number of animals and multiplying by 100. Significantly different from MOG+Vehicle at $p < 0.05$ (*), $p < 0.01$ (**). (B) The percentage of MOG+Vehicle and MOG+OGF mice that experienced a remission or a remission with a subsequent relapse before the predetermined time of sacrifice, 20, 30, and 60 days post-EAE induction. MOG+Vehicle n=11-45, MOG+OGF n=9-38. N values decrease after the 20 and 30 day time points because some animals were sacrificed for histological analysis at these time points. Data represent means ± SEM from 5 independent experiments.

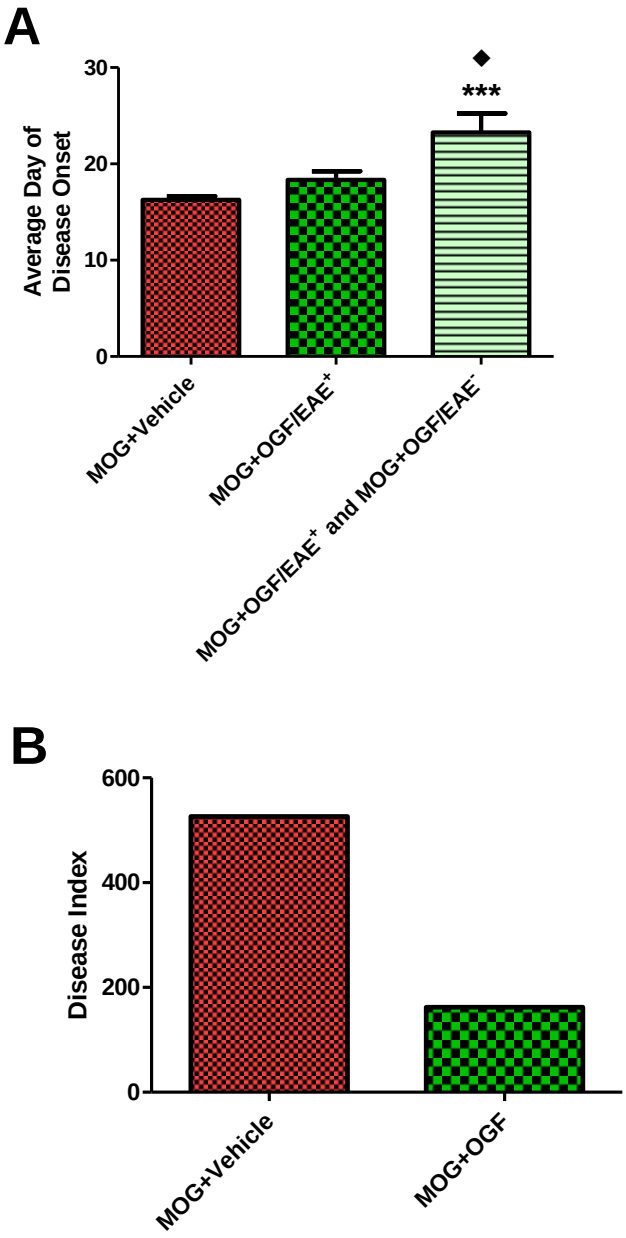

Figure 5.3: The influence of OGF on EAE disease onset and disease index. EAE was induced and mice were scored daily on a 0 - 5 scale. (A) Average day of disease onset for MOG+Vehicle mice, only the MOG+OGF mice that expressed disease before the time of sacrifice (MOG+OGF/EAE$^+$), and all MOG+OGF mice (MOG+OGF/EAE$^+$ and MOG+OGF/EAE$^-$). The first day a mouse received a disease score ≥ 1 was marked as the animal's day of disease onset. Disease onset for MOG+OGF/EAE$^-$ mice was factored in as the day after the time of sacrifice. Significantly different from MOG+Vehicle at $p < 0.001$ (***). Significantly different from MOG+OGF at $p < 0.05$ (♦). (B) Disease index was calculated by adding up the average daily disease scores, dividing by the average day of disease onset, and multiplying by 100. MOG+Vehicle n=45, MOG+OGF n=38. Data represent means ± SEM from 5 independent experiments.

5.3. Body Weight Results

Body weight did not significantly differ between groups on Day 0 (Figure 5.4). Control+Vehicle (n = 4), MOG+Vehicle (n = 11), and MOG+OGF (n = 9) mice weighed 18.0 ± 0.6, 18.3 ± 0.3, and 18.4 ± 0.2 grams, respectively, on Day 0. Body weight decreased from Day 0 until Day 6 for Control+Vehicle, MOG+Vehicle, and MOG+OGF mice. All three groups showed a slight increase between Day 6 and Day 10, and by Day 14 body weight was equal to or higher than Day 0 body weight in all groups. Control+Vehicle mice had significantly higher body weights than MOG+Vehicle mice on Day 14 ($p < 0.05$). MOG+OGF mice had significantly higher body weight than MOG+Vehicle mice on Day 24 ($p < 0.01$). Body weight did not significantly differ between groups for the remainder of the experiment. On the last day body weight was recorded, Day 50, Control+Vehicle mice weighed 21.5 ± 0.6 grams, while MOG+Vehicle and MOG+OGF mice weighed 21.1 ± 0.3 and 21.7 ± 0.4 grams, respectively.

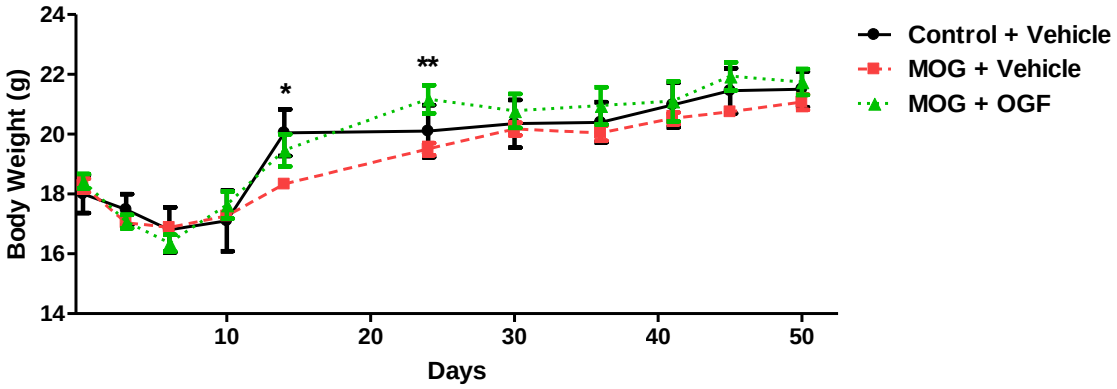

Figure 5.4: The impact of daily OGF administration on body weight in EAE mice. Body weight was recorded 1-2 times per week for 50 days. Control+Vehicle n = 4, MOG+Vehicle n = 11, MOG+OGF = 9. Significantly different from MOG+Vehicle at $p < 0.05$ (*), $p < 0.01$ (**). Data represent means ± SEM.

5.4. Morphology Results

5.4.1. Astrocyte Activation Results

Activated astrocytes were counted in spinal cord sections from mice sacrificed 10, 20, 30, and 60 days post-EAE induction (Figure 5.5A). On Day 10, both Control+Vehicle (n = 4) and MOG+OGF (n = 3) mice had significantly fewer activated astrocytes as compared to MOG+Vehicle (n = 3) mice ($p < 0.05$ and 0.001). Control+Vehicle and MOG+OGF mice had 105.5 ± 21.52 and 185.9 ± 18.29, respectively, activated astrocytes per mm^2 of lumbar spinal cord, compared to 266.7 ± 20.32 activated astrocytes per mm^2 of lumbar spinal cord in MOG+Vehicle mice. On Day 20, Control+Vehicle, MOG+OGF/EAE^+ and MOG+OGF/EAE^- groups had significantly fewer activated astrocytes compared to MOG+Vehicle mice ($p < 0.001$), while mice in the MOG+OGF/EAE^+ and MOG+OGF/EAE^- groups had significantly more activated astrocytes compared to Control+Vehicle ($p < 0.001$). The average numbers of activated astrocytes per mm^2 of spinal cord tissue in Control+Vehicle (n = 8), MOG+Vehicle (n = 8), MOG+OGF/EAE^+ (n = 6), and MOG+OGF/EAE^- (n = 6) mice sacrificed on Day 20 were 28.9 ± 4.4, 242.9 ± 19.6, 117.5 ± 13.8, and 104.5 ± 19.9, respectively. On Day 30, 122.4 ± 12.7 activated astrocytes were observed per mm^2 in the spinal cord of Control+Vehicle (n = 7) mice. The number of activated astrocytes increased by 290%, 244%, and 158% in MOG+Vehicle (n = 6), MOG+OGF/EAE^+ (n = 5), and MOG+OGF/EAE^- (n = 3) mice, respectively, compared to Control+Vehicle mice. MOG+Vehicle, MOG+OGF/EAE^+, and MOG+OGF/EAE^- counts were all significantly increased compared to Control+Vehicle ($p < 0.05$ and 0.001). MOG+OGF/EAE^+ mice had significantly higher counts than MOG+OGF/EAE^- mice ($p < 0.01$). 122.4 ± 12.7, 354.4 ± 24.8, 299.3 ± 26.9, and 193.2 ± 15.5 activated astrocytes per mm^2 were observed in the spinal cords of Control+Vehicle, MOG+Vehicle, MOG+OGF/EAE^+, and

MOG+OGF/EAE$^-$ mice sacrificed 30 days post-EAE induction, respectively. On Day 60, 182.7 ± 18.4 and 350.2 ± 37.6 activated astrocytes were counted per mm^2 in the spinal cords of Control+Vehicle (n = 4) and MOG+Vehicle (n = 6) mice. MOG+OGF/EAE$^+$ mice (n = 5) and MOG+OGF/EAE$^-$ mice (n = 2) averaged 337.7 ± 28.4 and 185.9 ± 48.7 activated astrocytes per mm^2 of spinal cord. MOG+OGF/EAE$^+$ and MOG+Vehicle counts were significantly higher than Control+Vehicle counts ($p < 0.01$), while MOG+OGF/EAE$^-$ counts were significantly lower than counts observed in MOG+Vehicle and MOG+OGF/EAE$^+$ mice. Figure 5.5B shows how the activated astrocyte profile changes for each treatment group at different stages of EAE.

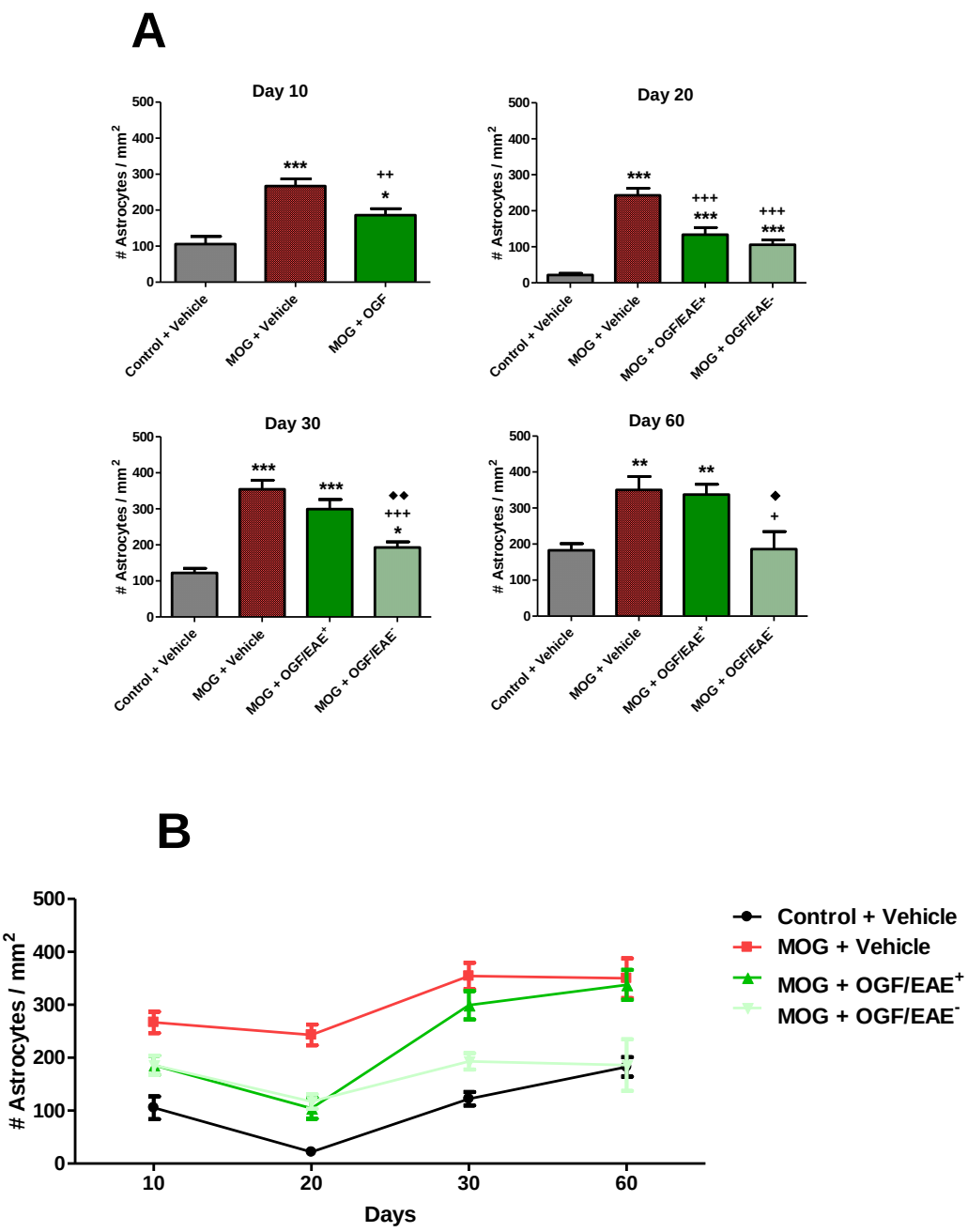

Figure 5.5: The effect of OGF on EAE mouse spinal cord astrocyte activation. The number of activated astrocytes was counted in three grids per spinal cord of 2 sections per mouse. (A) The number of activated astrocytes in the spinal cord on Days 10, 20, 30, and 60 post-EAE induction. Significantly different from Control+Vehicle at $p < 0.05$ (*), $p < 0.01$ (**), $p < 0.001$ (***). Significantly different from MOG+Vehicle at $p < 0.05$ (+), $p < 0.01$ (++), $p < 0.001$ (+++). Significantly different from MOG+OGF/EAE$^+$ at $p < 0.05$ (♦) $p < 0.01$ (♦♦). (B) Time course of the number of activated astrocytes on Days 10, 20, 30, and 60 shows how counts change during different stages of EAE. Data represent means ± SEM.

5.4.2. Demyelination Results

Demyelination profiles changed between treatment groups on Days 10, 20, 30, and 60. Table 5.1 summarizes the number of mice observed in each treatment group at the 4 time points that did or did not have demyelination in the spinal cord. No animal in any treatment group had signs of demyelination on Day 10 (n = 3-4). On Days 20, 30, and 60, OGF-treated animals were separated into those that expressed behavioral symptoms of EAE (MOG+OGF/EAE^{+}) and those that did not express behavioral symptoms (MOG+OGF/EAE^{-}). On Day 20, Control+Vehicle (n = 11) and MOG+OGF/EAE^{-} (n = 8) animals remained free of demyelination in the spinal cord, while 33% (3/9) MOG+Vehicle and 38% (3/8) MOG+OGF/EAE^{+} animals experienced demyelination, respectively (Figure 5.6). By Day 30, 86% (6/7) of mice in the MOG+Vehicle group experienced demyelination in the spinal cord, compared to 100% (6/6) in the MOG+OGF/EAE^{+} group and 60% (3/5) of the MOG+OGF/EAE^{-} mice. Control+Vehicle mice (n = 9) had no demyelination on Day 30. On Day 60, demyelination was detected in 29% (2/7) of the MOG+Vehicle mice and 20% (1/5) of the MOG+OGF/EAE^{+} mice, while spinal cords from Control+Vehicle (n = 4) and MOG+OGF/EAE^{-} (n = 2) mice were free of demyelination. Figure 5.7A shows how demyelination profile changes over time. The increase between Days 30 and 60 suggests a remyelination phenomenon. Further categorizing the demyelination as moderate (1-2 quadrants with demyelination) or severe (3-4 quadrants with demyelination) demonstrates that the most profound occurrence of severe demyelination occurred on Day 30 (Figure 5.7B). Some severe demyelination occurred on Day 20, and interestingly by Day 60 animals only MOG+OGF/EAE^{+} mice had moderate demyelination in their spinal cords.

	# Mice with…	10 Days	20 Days	30 Days	60 Days
Control+Vehicle	No Demyelination	4	11	9	4
	Demyelination	0	0	0	0
MOG + Vehicle	No Demyelination	4	6	1	5
	Demyelination	0	3	6	2
MOG + OGF/EAE^{+}	No Demyelination	NA	5	0	4
	Demyelination	NA	3	6	1
MOG + OGF/EAE^{-}	No Demyelination	3	8	2	2
	Demyelination	0	0	3	0

Table 5.1: A summary of animals examined in OGF demyelination studies. Animals were sacrificed and examined for signs of demyelination in the spinal cord. Data represent the number of animals at each time point that had no demyelination present in the spinal cord or that had demyelination in at least 1 quadrant of the spinal cord.

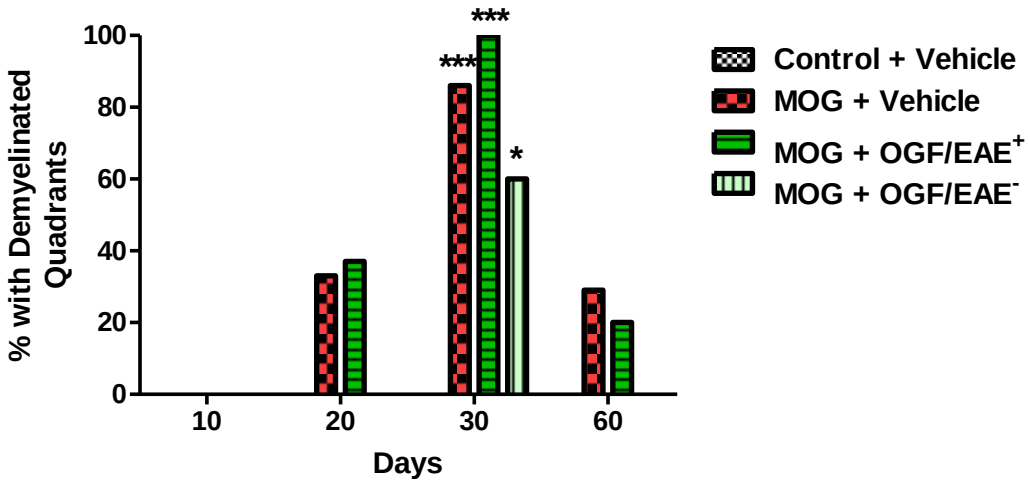

Figure 5.6: The effect of OGF on spinal cord demyelination incidence in EAE mice. Percentage of animals with demyelination in the L4 – L6 section of the spinal cord at 10, 20, 30, and 60 days post-EAE induction. Significantly different from Control+Vehicle at $p < 0.05$ (*) and $p < 0.001$ (***).

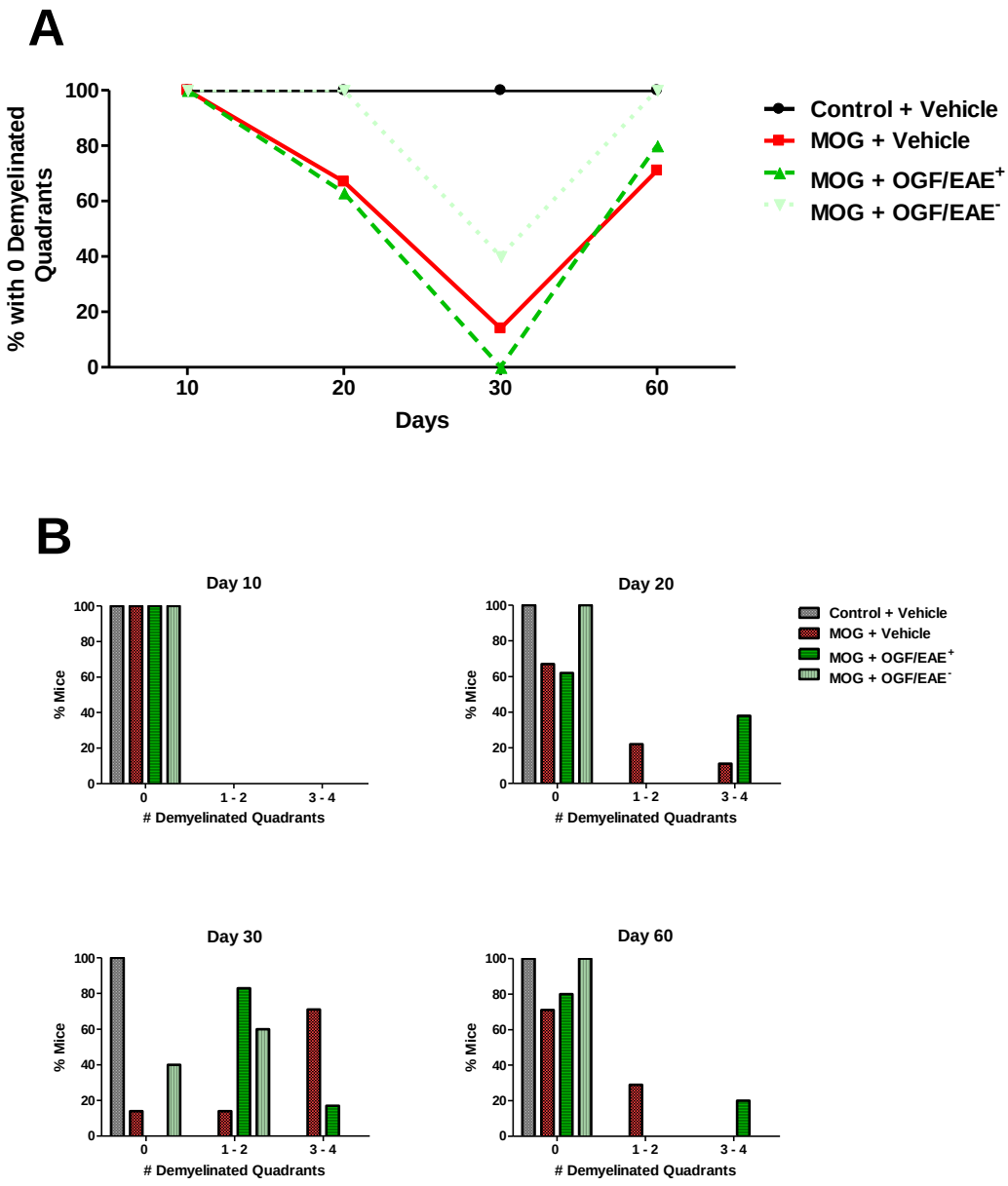

Figure 5.7: The effect of OGF on spinal cord demyelination course and distribution in EAE mice. Two spinal cord sections per mouse were examined for the presence of demyelination. (A) Time course of the percentage of animals in a treatment group with spinal cords free of demyelination on Days 10, 20, 30, and 60 shows how much demyelination, and possibly remyelination, occurs during different stages of EAE. (B) Histograms of the percent of mice with demyelination in 0, 1-2, or 3-4 quadrants on Days 10, 20, 30, and 60 indicate if animals in a given treatment group have no (0), moderate (1-2) or severe (3-4) demyelination.

5.4.3. Neuronal Damage Results

The number of damaged neurons was counted on Days 10, 20, 30, and 60 (Figure 5.8). Control+Vehicle, MOG+Vehicle, and MOG+OGF mice had 7.2 ± 1.1, 11.6 ± 1.6, and 8 ± 1.1 damaged neurons on Day 10, respectively, and none of these values were significantly different (n = 3-4). On Days 20, 30, and 60, OGF-treated animals were separated into those that expressed behavioral symptoms of EAE (MOG+OGF/EAE$^+$) and those that did not express behavioral symptoms (MOG+OGF/EAE$^-$). By Day 20, Control+Vehicle, MOG+OGF/EAE$^+$, and MOG+OGF/EAE$^-$ mice had significantly less neuronal damage compared to MOG+Vehicle mice ($p < 0.01$ and 0.001). MOG+Vehicle (n =9) mice averaged 13.5 ± 1.3 damaged neurons per spinal cord, while Control+Vehicle (n = 9), MOG+OGF/EAE$^+$ (n = 8), and MOG+OGF/EAE$^-$ (n = 7) mice had 2.3 ± 0.6, 8.4 ± 1.3, and 5.6 ± 1.3 damaged neurons, respectively, on Day 20. Day 30 data revealed lower levels of neuronal damage in Control+Vehicle mice (n = 5) compared to MOG+Vehicle mice (n = 5), with 11.2 ± 0.8 damaged neurons in the Control+Vehicle group compared to 20.4 ± 2.3 damaged neurons in MOG+Vehicle mice. However, this difference was not found to be significant. MOG+OGF/EAE$^+$ and MOG+OGF/EAE$^-$ mice had 18.5 ± 4.7 and 14.5 ± 4.5 damaged neurons per spinal cord, respectively, on Day 30. No significant differences were noted between any treatment groups on Day 30. On Day 60, 7.25 ± 2.0, 12.4 ± 4.4, 15.1 ± 3.2, and 6.5 ± 0.5 damaged neurons were found in the spinal cords of Control+Vehicle (n = 4), MOG+Vehicle (n = 5), MOG+OGF/EAE$^+$ (n = 5), and MOG+OGF/EAE$^-$ (n = 1) mice, respectively. No significant differences were observed between treatment groups on Day 60.

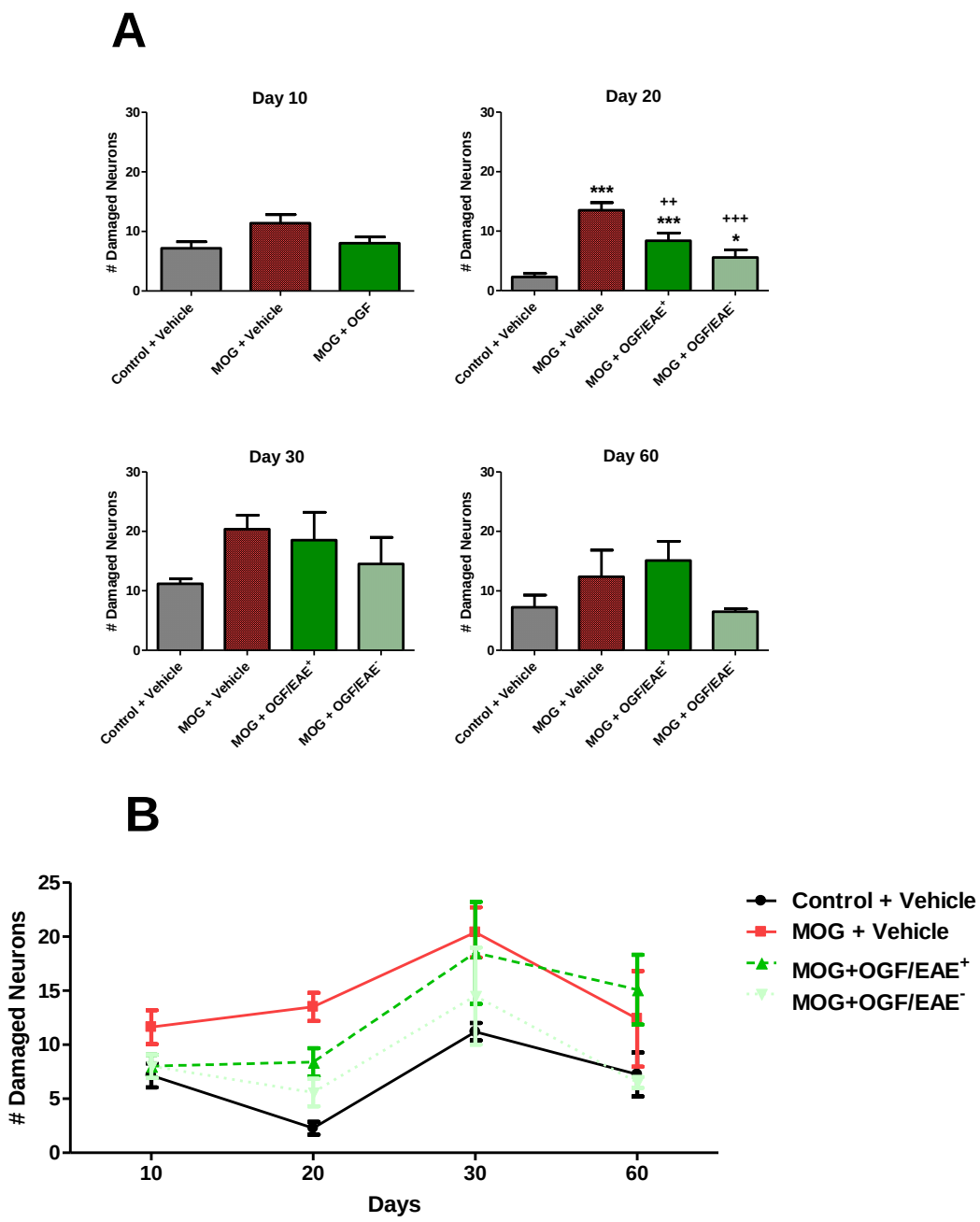

Figure 5.8: The effect of OGF on spinal cord neuronal damage in EAE mice. The number of damaged neurons was counted in the grey matter of 2 spinal cord of sections per mouse. (A) The number of damaged neurons in the lumbar spinal cord on Days 10, 20, 30, and 60 post-EAE induction. Significantly different from Control+Vehicle at $p < 0.05$ (*), $p < 0.001$ (***). Significantly different from MOG+Vehicle at $p < 0.01$ (++), $p < 0.001$ (+++). (B) Time course of the number of damaged neurons on Days 10, 20, 30, and 60 shows how counts change during different stages of EAE. Data represent means ± SEM.

5.5. Conclusions

Disease scores of MOG+Vehicle and MOG+OGF mice were significantly different throughout the 5 experiments. Daily administration of OGF resulted in a decrease in disease incidence and severity compared to MOG+Vehicle mice, indicating that fewer mice were sick and overall severity of disease was lower due to OGF treatment. Average day of disease onset for MOG+OGF mice was significantly later than that for MOG+Vehicle mice. Four times more OGF-treated mice experienced remissions as compared to Vehicle-treated controls, showing that OGF is capable of reversing behavioral signs of EAE. These behavioral data suggest that administration of the exogenous opioid OGF abolishes or diminishes the motor deficits that occur in EAE.

Histological data showed significant differences between MOG+Vehicle and MOG+OGF mice on Days 10, 20, and 30. MOG+OGF mice had significantly fewer activated astrocytes compared to MOG+Vehicle mice on Day 10. This finding was not surprising; astrocytes are a marker of the first stage of EAE, inflammation, and OGF mice went on to develop a less severe form of EAE. MOG+Vehicle mice had significantly more activated astrocytes than all MOG+OGF mice (MOG+OGF/EAE^{+} and MOG+OGF/EAE^{-}) on Day 20. Therefore, there was no correlation between behavior and inflammation on Day 20, as astrocyte counts were decreased in OGF-treated mice regardless of behavioral symptoms. However, there was a correlation between inflammation in the spinal cord and behavioral symptoms of EAE on Day 30 as only healthy MOG+OGF mice (MOG+OGF/EAE^{-}) had lower counts compared to MOG+Vehicle mice. MOG+OGF mice not expressing EAE (MOG+OGF/EAE^{-}) had fewer demyelinated quadrants than MOG+Vehicle mice on Days 20, 30, and 60. However, these differences were not significant, probably due to our semi-quantitative methods employed for data analysis. Behavioral symptoms were not indicative of the

amount of neuronal damage in the spinal cords. All MOG+OGF-treated mice, both those that were healthy and those that expresses behavioral symptoms of EAE, had significantly less neuronal damage than vehicle-treated controls on Day 20. MOG+OGF mice did not have less neuronal damage than MOG+Vehicle mice at any other time point, even in those MOG+OGF mice that did not express behavioral signs of EAE (MOG+OGF/EAE$^-$). Histology and behavior data demonstrated that astrocyte activation and neuronal damage are not accurate indicators of behavioral manifestations of EAE. Overall, administration of exogenous OGF decreased disease severity and incidence of EAE compared to vehicle treatment, but disease expression was not indicative of histological damage in OGF-treated mice.

CHAPTER 6: THE OPIOID GROWTH FACTOR-OPIOID GROWTH FACTOR RECEPTOR AXIS IN SPLENIC-DERIVED LYMPHOCYTES

6. Immunology

6.1. Results

The presence of OGF and OGFr on unstimulated and PHA-stimulated splenic-derived lymphocytes was confirmed with immunocytochemical studies (Figure 6.1). Semi-quantitative analysis of nuclear staining revealed a significant upregulation in the nuclear staining intensity of OGF and OGFr following PHA stimulation compared to unstimulated splenic-derived lymphocytes (Figure 6.2). Subsequent lymphocyte proliferation studies demonstrated that administration of 10^{-5} M OGF twice daily decreases the rate of PHA-stimulated cell proliferation *in vitro* (Figure 6.3A). Data pooled from 3 independent experiments showed that OGF decreases the number of cells in culture at 48 and 72 hours post-PHA stimulation by 24% and 21%, respectively. Differences noted at 48 and 72 hours post-stimulation were significant ($p < 0.001$). PHA-stimulated proliferation of cells treated with NTX did not differ compared to proliferation of vehicle-treated cells (Figure 6.3B). Tritiated thymidine incorporation studies showed that twice daily administration of 10^{-5} M OGF significantly decreases the rate of DNA synthesis in PHA-stimulated splenic-derived lymphocytes (Figure 6.4).

6.2. Conclusions

Our results indicate that the OGF-OGFr axis is present and functioning on splenic-derived lymphocytes. OGFr is located around the nuclear membrane and in the nucleus. Some of the endogenous OGF was likely bound to the OGFr, as positive OGF staining was located both around the nuclear membrane and inside the nucleus. OGF was able to decrease the rate of lymphocyte proliferation after 48 and 72 hours in culture. However, NTX treatment did not cause a difference in proliferation compared to vehicle treatment. Based on studies completed in other cell lines [186, 216, 217], it was expected that NTX would cause an increase in the rate of lymphocyte proliferation

compared to vehicle. However, PHA is a harsh stimulator of lymphocyte proliferation, and it is possible that 10 µg/mL PHA induces cell proliferation at a speed that is the maximum possible rate of proliferation. If this is true, NTX would be unable to increase the lymphocyte proliferation rate above the vehicle proliferation levels. Therefore, it is likely that the model system used in these experiments is not ideal for testing NTX's ability to regulate the rate of lymphocyte proliferation. Further analysis using thymidine incorporation studies showed that administration of OGF decreases the level of DNA synthesis in PHA-stimulated lymphocytes. Therefore, it is likely that the OGF-OGFr axis decreases the rate of cell proliferation through inhibition of DNA synthesis, as observed in other cell types [199-201, 204, 207]. In conclusion, studies demonstrated the presence of OGF and OGFr and function of the OGF-OGFr axis, on the lymphocytes.

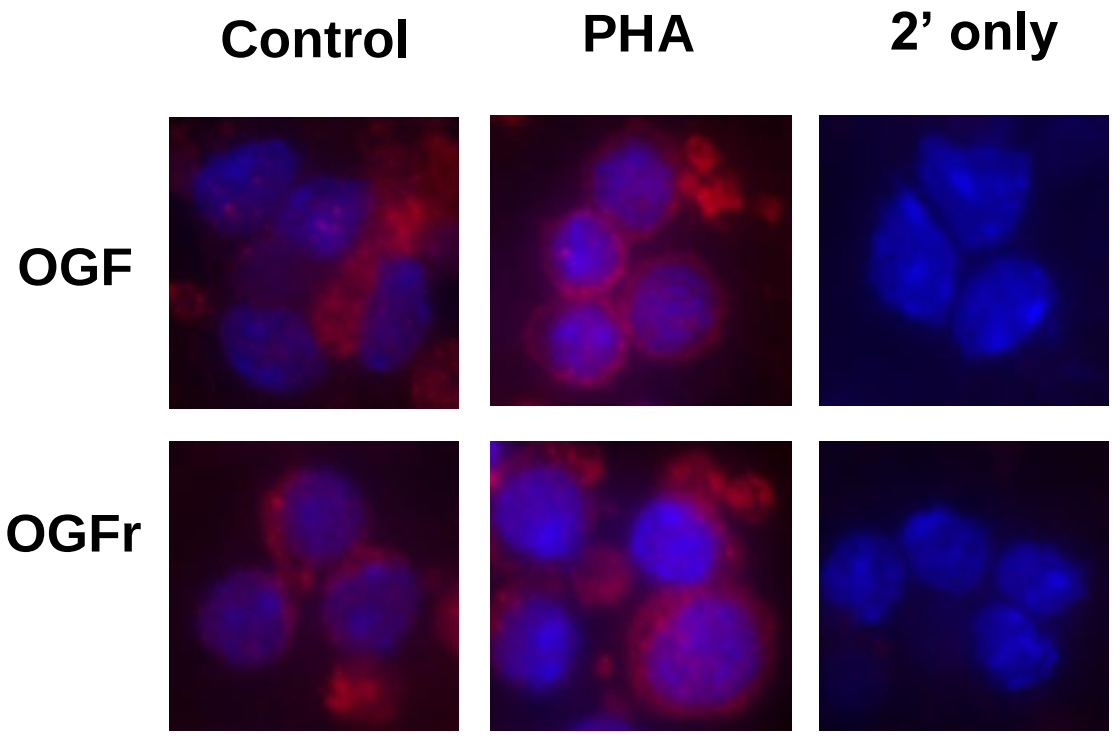

Figure 6.1: Immunocytochemistry for OGF and OGFr on splenic-derived lymphocytes. Cells were either unstimulated (Control) or stimulated with PHA for 48 hours. Nuclei were stained with DAPI, and TRITC-conjugated secondary antibodies were employed to visualize the presence of OGF and OGFr on lymphocytes isolated from the mouse spleens. Negative controls were incubated in the presence of secondary antibody alone. 600x.

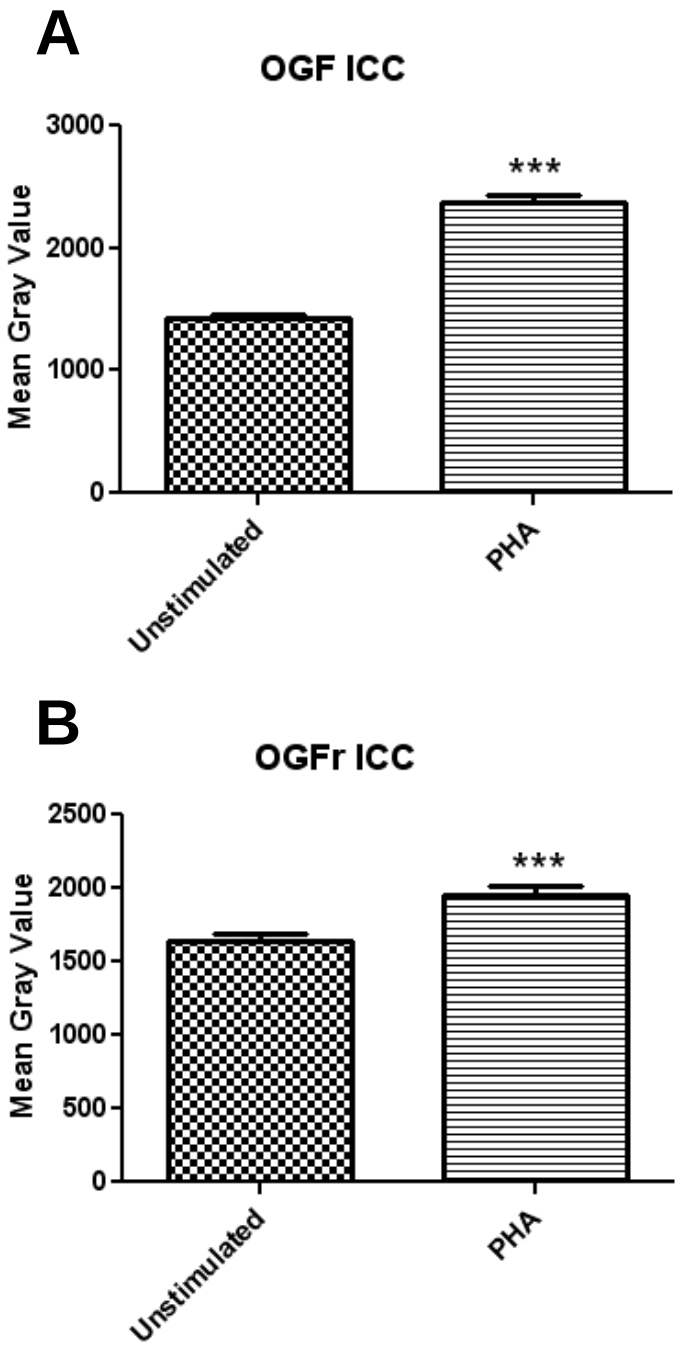

Figure 6.2: OGF and OGFr immunocytochemical staining of mouse lymphocytes. Cultured splenic-derived lymphocytes were either unstimulated or stimulated for 48 hours with PHA, and stained with antibodies directed to (A) OGF or (B) OGFr. Semi-quantitative analysis of OGF and OGFr nuclear staining intensity showing the mean gray value in PHA stimulated lymphocytes compared to unstimulated lymphocytes. Significantly different from Unstimulated at $p < 0.001$ (***).

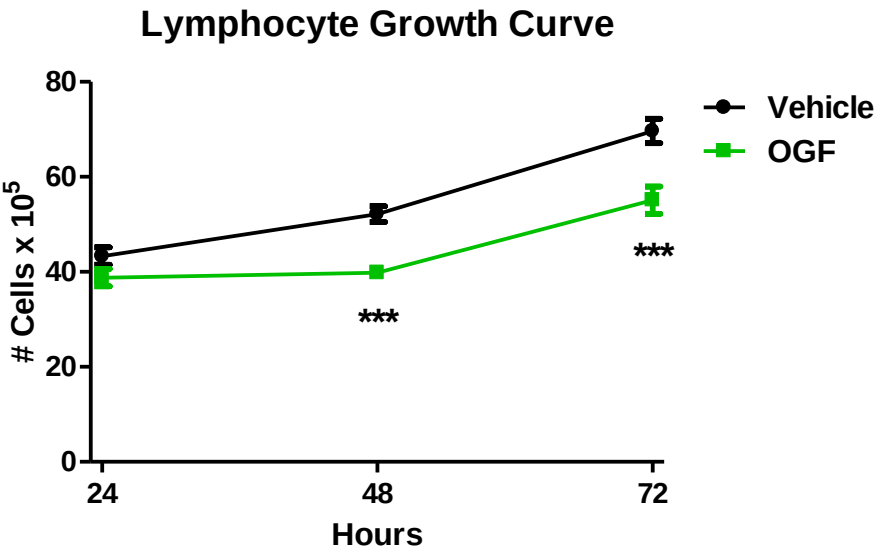

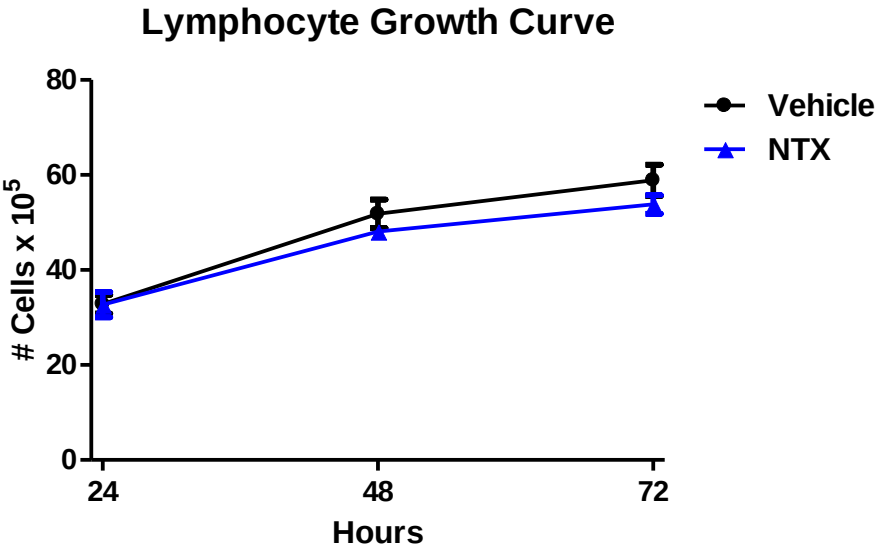

Figure 6.3: The effects of NTX and OGF on lymphocyte proliferation as measured by cell counts. Data from three independent experiments measuring the impact of twice daily administration of (A) 10^{-5} M OGF or (B) 10^{-5} M NTX on splenic-derived lymphocyte proliferation compared to Vehicle-treated controls. Significantly different from Vehicle at $p < 0.001$ (***).

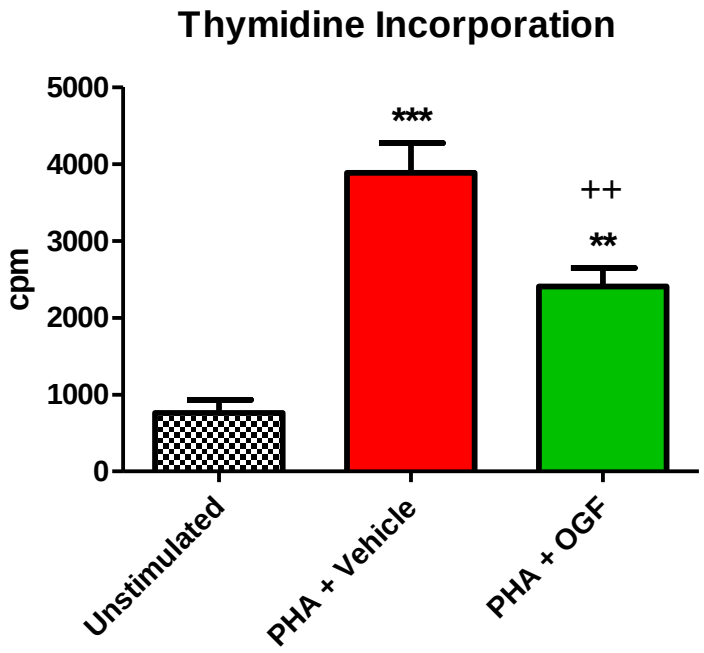

Figure 6.4: The effects of OGF on tritiated thymidine incorporation in splenic-derived lymphocytes. Data from 2 independent experiments show the effects of twice daily administration of 10^{-5} M OGF on the amount of tritiated thymidine incorporation in PHA-stimulated splenic-derived lymphocytes compared to Vehicle-treated controls. Significantly different from Unstimulated at $p < 0.01$ (**), $p < 0.001$ (***). Significantly different from PHA+Vehicle at $p < 0.01$ (++).

CHAPTER 7: DISCUSSION

7. Discussion

7.1. Conclusions

- **Behavioral signs of EAE markedly improve due to LDN or OGF, but not HDN treatment, compared to MOG+Vehicle controls.**
- **LDN and OGF decrease the amount of neuropathological damage in the lumbar spinal cord compared to Vehicle-treated mice with EAE.**
- **While both were effective, OGF was a more effective long-term therapy for the treatment of EAE compared to LDN.**
- **Maximum EAE disease score correlates to the level of demyelination in the lumbar spinal cord.**
- **The OGF-OGFr axis is present and functioning in splenic-derived lymphocytes.**

7.2. Discussion

7.2.1. Control+Vehicle mice had some spinal cord histological damage.

Control+Vehicle mice served as controls in the behavioral and histological analyses. The only difference between the induction injection protocols in Control+Vehicle animals compared to MOG+Vehicle animals is that Control+Vehicle mice injections did not contain MOG. Both groups of animals received equal amounts of heat-killed mycobacterium tuberculosis, CFA, and pertussis toxin. The purpose of including CFA supplemented with additional mycobacterium tuberculosis in the MOG induction injections is to protect the antigen from host clearance and rapid degradation, and to heighten the immune response. The delay in antigen clearance leads to prolonged exposure to MOG, resulting in a sustained immune response to the peptide [95]. CFA can also activate effector cells in the immune system [95]. It is possible for

injections of CFA to cause pain, distress, and inflammation [95]. CFA has also been shown to cause lesions at the injection site and distant granuloma formation [261]. However, Control+Vehicle animals did not demonstrate behavioral symptoms indicative of pain or distress in any of our experiments. The walking gaits of Control+Vehicle mice remained normal, and no animals received a disease score other than 0 at any time during the experiments. This confirms that the gait irregularities observed in MOG groups were due to the MOG and not another component of the injections.

Control+Vehicle spinal cord sections stained positive for baseline levels of astrocyte activation and neuronal damage. Additional experiments were conducted to determine if the astrocyte activation and neuronal damage were caused by the CFA and mycobacterium tuberculosis, the daily intraperitoneal injections, or the handling of the mice. LFB staining for demyelination was not included in these analyses because Control+Vehicle mice did not have any spinal cord demyelination at any time point examined. All mice were handled at the same time every day. To determine if the daily injections of PBS alone caused inflammation or neuronal damage, normal mice were given daily injections with saline for 10 days (Normal+10d PBS). To determine if the CFA and mycobacterium tuberculosis caused astrocyte activation or neuronal damage, other mice were given injections of the CFA, mycobacterium tuberculosis, and PBS only on Day 0 (Control+Vehicle 0d) or on Days 0 and 6 (Control+Vehicle 0&6d). All animals were sacrificed 10 days after the first injection, and the data from these animals were compared to our Control+Vehicle data from animals that received injections of the CFA, mycobacterium tuberculosis, and PBS on days 0, 3, and 6 (Control+Vehicle 0,3,&6d). Results show that giving 3 CFA and mycobacterium tuberculosis injections on Days 0, 3, and 6 cause an increase in the number of activated astrocytes compared to Normal+10d

PBS (Figure 7.1A) and an increase in the level of neuronal damage compared to Normal+10d PBS, Control+Vehicle 0d, and Control+Vehicle 0&6d (Figure 7.1B).

While these are important observations to note, the results included in the present EAE studies are still valid for four important reasons. First, there were no behavioral abnormalities in the Control+Vehicle mice, so any disease scores ≥ 1 and gait abnormalities can be attributed to the MOG injections. Second, although our three injections of CFA and mycobacterium tuberculosis caused an increase in astrocyte activation and neuronal damage compared to only one or two injections, MOG+Vehicle mice had consistently more astrocyte activation and neuronal damage as compared to Control+Vehicle. This indicates that the MOG injection increased inflammation and neuronal damage, both hallmarks of EAE, over the baseline levels observed in Control+Vehicle mice. Third, no demyelination was observed in the Control+Vehicle mice. An immune response mounted to a myelin peptide, MOG in our case, causes demyelination. Therefore, the Control+Vehicle mice do not express the most distinctive and vital symptom of EAE. Fourth, all treatment groups included in the EAE studies received the same amounts of CFA and mycobacterium tuberculosis, and the only differences between groups were either MOG injections or the daily treatment options. Consequently, it is accurate to compare results between groups and attribute findings to MOG or treatment alone. The observations seen in our Control+Vehicle mice will be further discussed in Sections 7.2.4., 7.2.5., and 7.2.6.

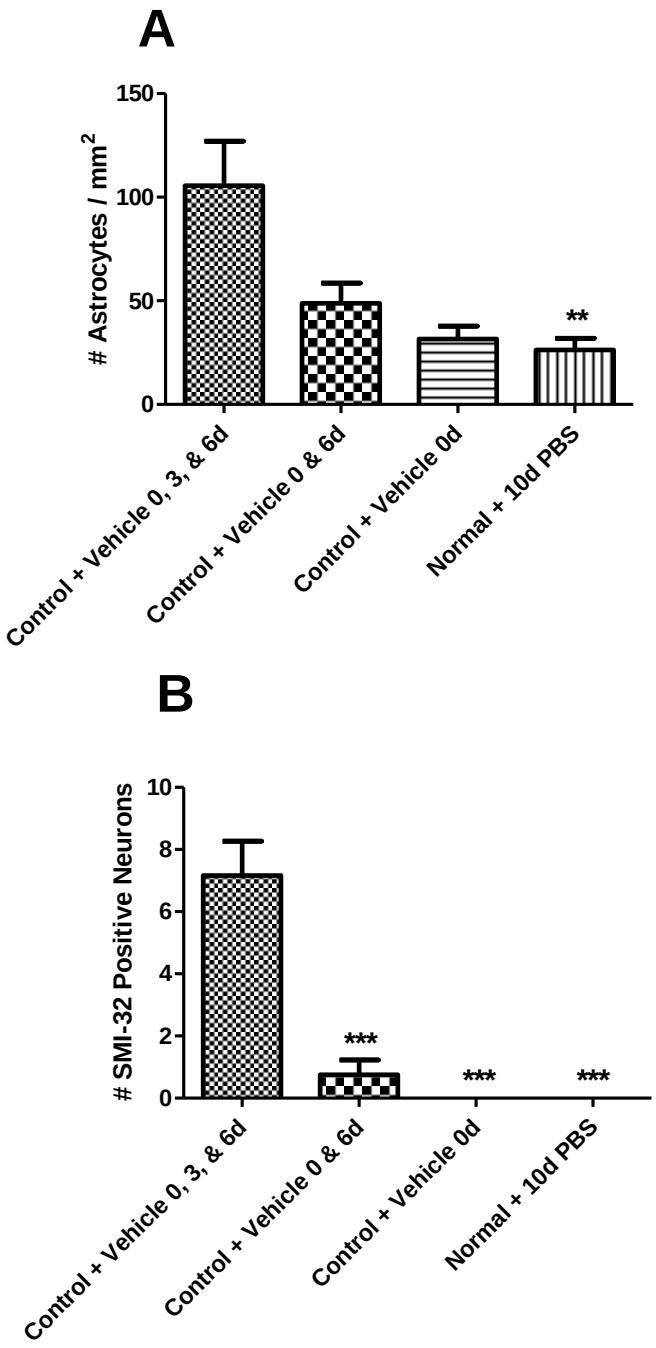

Figure 7.1: Astrocyte activation and neuronal damage as a result of CFA, mycobacterium tuberculosis, and PBS injections. Mice were given 0 (Normal+10d PBA), 1 (Control+Vehicle 0d), 2 (Control+Vehicle 0 & 6d), or 3 (Control+Vehicle 0, 3, & 6d) intramuscular flank injections of CFA and mycobacterium tuberculosis. Mice were sacrificed on Day 10, and the number of activated astrocytes (Figure 7.1A) and damaged neurons (Figure 7.1B) in the lumbar spinal cord were counted. Significantly different from Control+Vehicle 0,3,&6d at $p < 0.01$ (**) and $p < 0.001$ (***), n = 1-4. Data represent means ± SEM.

7.2.2. Behavioral signs of EAE improved with LDN and OGF, but not HDN treatment.

The MOG EAE model was chosen primarily because MOG-induced EAE in C57BL/6 mice produces a chronic disease course. An additional MOG injection was included in the induction protocol to ensure 100% disease incidence in the MOG+Vehicle group. Other laboratories do not reach complete disease incidence with only 1 or 2 MOG injections [262, 263]. A chronic disease course with 100% incidence is ideal for testing a disease therapy, because any remissions or absence of disease can be attributed to the tested therapy (i.e. HDN, LDN, or OGF) and not to the characteristics or side effects of the animal model.

Of the animals given injections of MOG, those treated daily with LDN and OGF had fewer or less severe behavioral symptoms of EAE compared to vehicle and HDN treated mice. Every animal in the MOG+Vehicle and MOG+HDN groups developed behavioral symptoms of EAE (disease score ≥ 1) before the time of sacrifice, while LDN and OGF treatment completely prevented some animals from developing EAE. Significantly fewer animals had disease scores of 2 in both the LDN and OGF groups compared to MOG+Vehicle mice, because the majority of these animals remained healthy. Average disease scores were significantly decreased in MOG+LDN and MOG+OGF mice compared to MOG+Vehicle mice on nearly every day from the time of disease onset until the time of sacrifice, while HDN treated mice had the same disease scores as their vehicle treated counterparts. Disease index, a measure of EAE severity, for MOG+LDN and MOG+OGF mice was less than half the disease index of MOG+Vehicle mice. MOG+HDN and MOG+Vehicle mice had nearly identical disease indices.

It is interesting that LDN and OGF therapy both proved to be beneficial in preventing and diminishing signs of EAE. Both treatments caused a reduction in disease incidence by approximately 50%, caused significant reductions in severity, and increased the relapse rate in a chronic model compared to MOG+Vehicle mice. Slight differences, however, were noted, between the LDN and OGF treatment groups. LDN was more effective at delaying the presentation of behavioral signs of disease. Average day of disease onset for LDN-treated mice was 5 days later than MOG+Vehicle mice and 3 days later than MOG+OGF mice. OGF, however, was slightly more effective at inhibiting long-term disease symptoms and causing reversions back to disease score of 0. At the final 60 day time point, 64% of LDN animals demonstrated behavioral symptoms of EAE, while only 44% of OGF mice were EAE-positive. Only 6.66% of MOG+Vehicle mice experienced a remission before the time of sacrifice. LDN was able to cause 23.33% of mice to return to a disease score of 0, while OGF treatment led to reversions in 41.66% of mice. Therefore, one could conclude that LDN might serve as a better therapy for early stages of MS, while OGF could be a more effective therapy for established disease.

7.2.3. Body Weight was not affected by the treatments.

Upon development of EAE, body weight frequently decreases due to anorexia and inadequate water intake [23, 242]. In these experiments, there was an initial decrease in body weight in all groups, including the Control+Vehicle mice that did not receive injections of MOG. Because all animals received CFA, mycobacterium tuberculosis, and pertussis toxin, the decrease in body weight observed in all groups can be attributed to the components of the vehicle in which the MOG injection was delivered. Though there were some significant differences noted later in the experiment, body weights in each group of animals followed approximately the same course. Regardless

of the treatment group, average body weight was lowest on Day 6. By Day 10, 4 days after the last MOG or Control injection, body weight in all treatment groups had increased back to the average weight recorded on Day 0. Control+Vehicle mice had significantly higher average body weight compared to MOG+Vehicle on Day 14, which correlates to immediately before the time of disease onset (average day of disease onset for MOG+Vehicle mice = 16.27 ± 0.36). However, by the time of acute EAE onset, Day 20, all groups, including the Control+Vehicle mice, had equal body weights. Significant differences in body weight between MOG+Vehicle mice and MOG+HDN, MOG+LDN, or MOG+OGF mice were only noted on 1 or 2 days throughout the duration of the experiment. It is possible that the beneficial effects of LDN and OGF elucidated by behavioral and histopathological measurements were not revealed through body weight measurements because they were overpowered by the detrimental effects of CFA, mycobacterium tuberculosis, and pertussis toxin.

7.2.4. Astrocyte activation does not always correlate with behavioral signs of EAE.

Astrocyte activation occurs in the spinal cords of EAE-positive animals and MS patients alike [246]. Astrocytes promote MS and EAE pathogenesis by secreting pro-inflammatory cytokines and presenting antigen to T cells [246]. Upregulated leukocyte infiltration into the CNS is associated with increased levels of GFAP positivity [264]. Inflammation has been shown to correlate with initial EAE disease severity [42]. Additionally, anti-MOG antibody levels in the spinal cord are positively correlated with GFAP positivity in the spinal cord [264]. Astrocyte activation can also occur in the presence of inflammation without a myelin peptide injection, and animals injected with CFA have inflammation in their spinal cords as measured by immunohistochemistry [265]. Low levels of GFAP are detectable by ELISA of spinal cord homogenates from

normal mice and humans, and GFAP levels are elevated in humans with MS and mice with EAE [266, 267]. Therefore, we expected all animals to demonstrate some GFAP positivity in their spinal cords, but for those animals injected with MOG to have higher GFAP counts than Control+Vehicle mice. As predicted, astrocyte activation was present but significantly decreased in Control+Vehicle animals compared to MOG+Vehicle animals at 10, 20, 30, and 60 days post-EAE induction.

Astrocyte activation was significantly lower in MOG+OGF and MOG+LDN mice compared to MOG+Vehicle animals on Day 10, while HDN-treated mice had a comparable number of activated astrocytes in the spinal cord compared to MOG+Vehicle control mice. These data suggest that inflammation precedes behavioral symptoms, and that inflammation correlates with future behavioral symptoms. MOG+LDN and MOG+OGF mice had significantly reduced average behavioral scores and disease incidence compared to MOG+Vehicle mice, while MOG+HDN behavioral scores and disease incidence did not differ from MOG+Vehicle mice. It is possible that the animals in the LDN and OGF groups did not get sick because the treatment was able to inhibit inflammation, which is the first step in EAE pathogenesis. It is unknown if the treatments inhibited inflammation, or if they inhibited a step that precedes inflammation, such as lymphocyte recruitment into the CNS. However, it is clear that LDN and OGF treatments are beneficial at preventing an initial step of EAE development, astrocyte activation, but that HDN has no effect compared to saline treatment.

Maximum disease score of animals sacrificed 20 days post-EAE induction does not correlate to the number of activated astrocytes in the spinal cord (Figure 7.2). On Day 20, there were significantly less activated astrocytes per mm^2 in MOG+OGF/EAE^+, MOG+OGF/EAE^-, and MOG+LDN/EAE^- mice compared to MOG+Vehicle animals. It is not surprising that MOG+OGF/EAE^- and MOG+LDN/EAE^- mice had significantly lower

activated astrocytes compared to MOG+Vehicle mice, as these EAE^- mice did not display behavioral symptoms. Inflammation initiates disease pathogenesis, so inflammation should be lower in those animals without disease. It is interesting, however, that MOG+OGF/EAE^+ mice had significantly fewer activated astrocytes than MOG+Vehicle mice. Although both groups were made up of animals expressing symptoms of EAE, the OGF group had only 43% of the counts observed in MOG+Vehicle mice. This indicates that regardless of disease expression behaviorally, exogenous OGF treatment decreases inflammation in the spinal cord during the acute stage of EAE onset at 20 days post-induction. Conversely, the MOG+LDN group that expressed behavioral signs of EAE (MOG+LDN/EAE^+) did not differ from vehicle-treated MOG controls at 20 days post-induction. MOG+LDN/EAE^- mice also had significantly lower activated astrocytes than MOG+LDN/EAE^+ mice. Therefore, one may conclude that following LDN treatment, the amount of inflammation measured in the lumbar spinal cord by GFAP IHC correlates to behavioral symptoms around the time of EAE onset. While OGF is beneficial to all animals regardless of disease expression, LDN is only able to inhibit inflammation in some mice. MOG+HDN mice did not differ from MOG+Vehicle mice, showing that continuous opioid receptor blockade does not enhance or repress astrocyte activation induced by MOG.

Maximum disease score of animals sacrificed 30 days post-EAE induction does not correlate to the number of activated astrocytes in the spinal cord (Figure 7.2). On Day 30, there were significantly fewer activated astrocytes per mm^2 in MOG+LDN/EAE^+, MOG+LDN/EAE^-, and MOG+OGF/EAE^- mice compared to MOG+Vehicle animals. Similar to expectations from the 20 day experiments, it was not surprising that MOG+OGF/EAE^- and MOG+LDN/EAE^- mice had significantly lower activated astrocytes compared to MOG+Vehicle mice, as these EAE^- mice did not display behavioral

symptoms. If spinal cord inflammation correlates to behavior, groups expressing EAE (MOG+OGF/EAE$^+$ and MOG+LDN/EAE$^+$) were not expected to have lower activated astrocytes counts than MOG+Vehicle. Therefore, it was surprising that MOG+LDN/EAE$^+$ mice had significantly fewer activated astrocytes in the lumbar spinal cord compared to MOG+Vehicle mice. However, because MOG+OGF/EAE$^+$ mice had fewer activated astrocytes on Day 20, it was especially surprising for MOG+LDN/EAE$^+$ to have fewer on Day 30. It can be concluded from these data that OGF is effective at inhibiting astrocyte activity on Day 20, but by Day 30 the amount of inflammation measured in the lumbar spinal cord by GFAP IHC correlates to behavioral symptoms. LDN, however, is effective at decreasing inflammation in the spinal cord as measured by astrocyte activation in established EAE regardless of behavioral symptoms. The observation of decreased activated astrocyte counts on Day 30 in the MOG+HDN group was intriguing. Because the HDN mice did not differ from MOG+Vehicle in behavior, it was unexpected for MOG+HDN counts to be lower. It could be due to the fact that MOG+HDN mice have increased disease progression and the mice given continuous opioid receptor blockade are already past the initial inflammatory stage of EAE.

At 60 days post-EAE induction, there were very few significant differences in the number of activated astrocytes in the spinal cord between groups. MOG+LDN/.EAE$^+$, MOG+LDN/EAE$^-$, and MOG+OGF/EAE$^+$ astrocyte counts did not differ from MOG+Vehicle counts. MOG+OGF/EAE$^-$ mice had significantly lower astrocyte counts compared to MOG+Vehicle on Day 60, which correlates to the MOG+OGF mice having the lowest disease incidence on Day 60. However, it was interesting that MOG+HDN astrocyte counts remained lower than MOG+Vehicle counts through Day 60. One possible explanation for this finding is the same given on Day 30; that MOG+HDN mice have increased disease progression and the mice given continuous opioid receptor

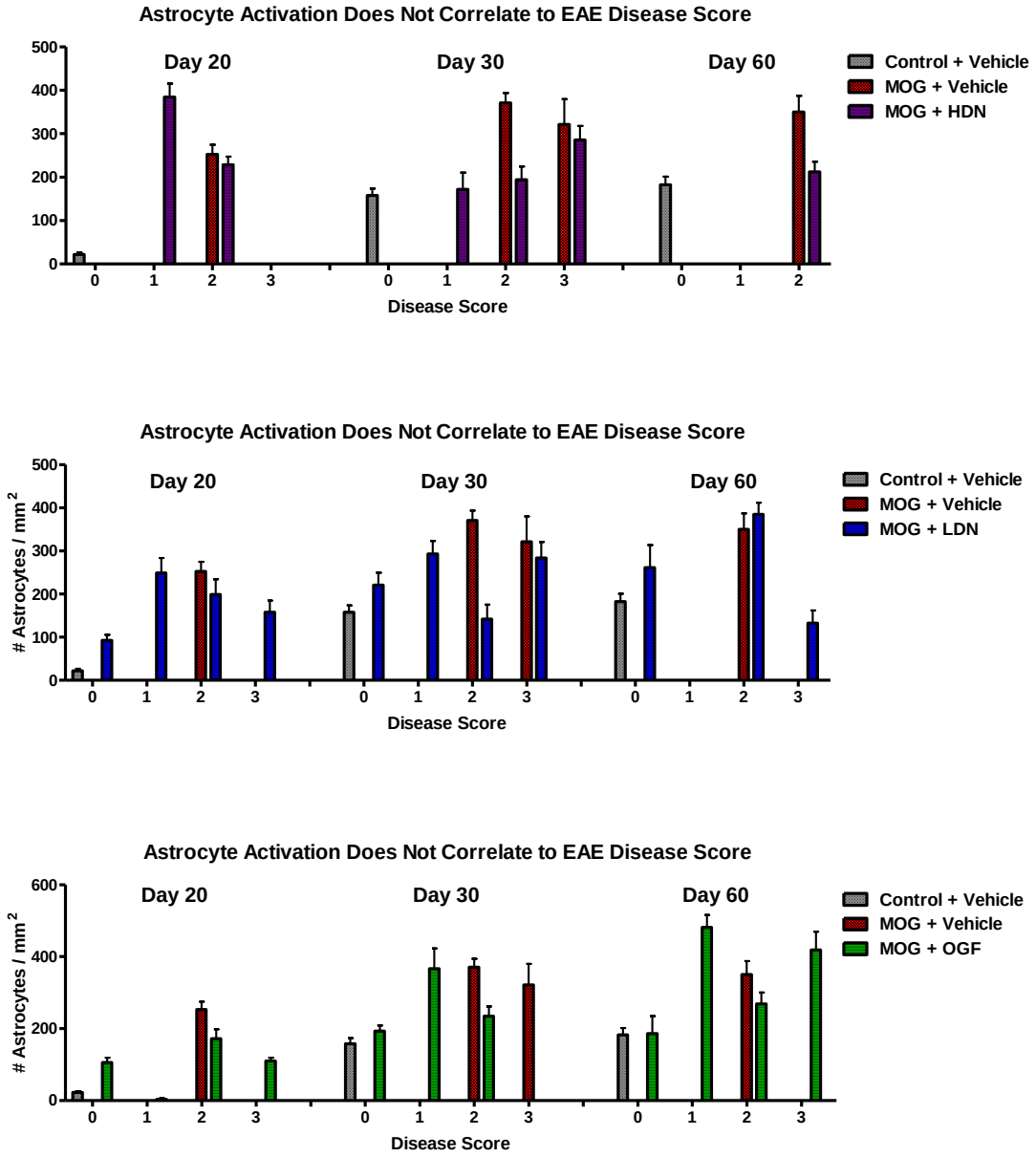

Figure 7.2: The correlation of maximum EAE behavioral scores observed before the time of sacrifice to the amount of astrocyte activation in the lumbar spinal cord of Control+Vehicle, MOG+Vehicle, MOG+HDN, MOG+LDN, and MOG+OGF mice.

blockade are already past the initial inflammatory stage of EAE. Because there were no behavioral implications for the decrease in astrocyte counts observed in the MOG+HDN mice (i.e. disease score and incidence did not differ from that in vehicle-treated counterparts on Day 30 and 60), it is unlikely that the HDN treatment has beneficial anti-inflammatory properties.

Statistical analysis of the amount of astrocyte activation in the spinal cord and the maximum EAE disease score observed before the time of sacrifice showed that there was no correlation between the two measurements in any of the treatment groups. Additionally, there was no correlation between two groups regarding how astrocyte activation changes with different disease scores. Therefore, the maximum disease score an animal reached before the time of sacrifice can not accurately predict the amount of astrocyte activation that the animal will have it its spinal cord.

7.2.5. Demyelination correlates with EAE behavioral scores.

In animal models of CNS damage, motor deficits are largely caused by damage to white matter [268]. Luxol fast blue is a stain that can be used to measure loss of white matter. The stain binds to choline found in phospholipids and lipoproteins in myelin [268]. In the absence of myelin, the stain is unable to hold and the section loses the blue color [268]. Previous research has demonstrated that LFB is a fast and accurate way to quantify demyelination, as results from LFB staining correlate with results from IHC for MOG, MBP, and other myelin proteins [269]. The main problem with the procedure is that LFB is not an easy stain to quantify. Some groups choose to quantify using tracing programs, and demyelination can be expressed as a percentage of white matter [269, 270]. Others choose to employ a blind observer to rate the degree of damage on a numerical scale [269]. These methods did not work for the experiments included in these analyses, as considerable variation and error were noted depending on

the region of the cord observed. Instead, dividing the spinal cord into quadrants as previously described [248] and assessing the number of quadrants that had demyelination present in them turned out to be a reliable, reproducible, and accurate way to quantify demyelination.

Based on our behavioral results, we would expect Control+Vehicle, MOG+LDN/EAE$^-$, and MOG+OGF/EAE$^-$ mouse spinal cords to be free of demyelination. Demyelination was not observed in Control+Vehicle spinal cords at any time point, as anticipated. Some demyelination was observed in MOG+LDN/EAE$^-$ and MOG+OGF/EAE$^-$ mice, but the amount of demyelination was minimal compared to the amount observed in MOG+Vehicle mice. In these studies, loss of myelin correlated with disease severity.

On Day 10, the only animal to show signs of spinal cord demyelination was in the MOG+HDN group. This animal had demyelination present in 2 of the 4 quadrants. Because n values were low for the 10 day study, this finding was not significantly different compared to Control+Vehicle and MOG+Vehicle mice and should be interpreted with caution. However, it is possible that HDN treatment expedites disease progression, thus leading to premature demyelination compared to MOG+Vehicle mice. Because continuous opioid receptor blockade with NTX causes an increase in cell proliferation, it is possible that NTX is affecting the cells that propagate EAE pathogenesis.

On Day 20, the number of spinal cord quadrants with demyelination correlated with disease score for all treatment groups (Figure 7.3). The highest disease score observed in MOG+Vehicle and MOG+HDN mice was 2, and these were the only animals to have spinal cord demyelination. MOG+LDN/EAE$^+$ mice received disease scores of 1, 2, and 3, and the number of quadrants that were demyelinated increased as disease

score increased. Demyelination was observed in the spinal cords of MOG+OGF/EAE^{+} mice with disease scores of 2 and 3, and those animals with hind limb paralysis (disease score = 3) had over twice the amount of demyelination compared to animals with a wobbly gait (disease score = 2). Both MOG+LDN/EAE^{-} and MOG+OGF/EAE^{-} mice averaged less than 1 quadrant with spinal cord demyelination, which was expected as these animals did not showcase any behavioral deficits. Taken together, these data show that the maximum disease score animals reach before sacrifice on Day 20 positively correlates with the amount of demyelination in the lumbar spinal cord. Behavioral symptoms of EAE are a good indicator of the amount of demyelination in the spinal cord, as animals with higher behavioral scores have more demyelination.

Similar trends were observed on Day 30, with behavioral scores correlating to the number of quadrants with demyelination, regardless of which treatment the mice received (Figure 7.3). MOG+Vehicle, MOG+LDN/EAE^{+}, and MOG/HDN mice all received the most severe behavioral scores of 2.5 or 3 before the time of sacrifice, and all of these animals had demyelination in 3-4 quadrants of the spinal cord. OGF treatment prevented any animals that were sacrificed on Day 30 from developing an EAE score of 2.5 or 3, but MOG+OGF/EAE^{+} animals that received a disease score of 2 had more demyelination in their spinal cords compared to those that received a disease score of 1. As expected because of their healthy behavioral scores, MOG+OGF/EAE^{-} mice averaged less than 1 quadrant with spinal cord demyelination. Surprisingly, MOG+LDN/EAE^{-} mice averaged 2 quadrants with demyelination. It was expected that these animals would have minimal or no demyelination due to healthy behavioral scores. However, the n value was only 2 for this group, and only 1 mouse had demyelination. It is possible that this mouse did not exhibit behavioral symptoms because the affected

(demyelinated) areas of the spinal cord were not associated with motor skills and gait function.

There was minimal demyelination in the spinal cords of any animal given MOG injections on Day 60 (Figures 3.7, 4.7, 5.7). The percentage of animals with 0 quadrants demyelination increased between Days 30 and 60 in all groups (except for Control+Vehicle, which maintained 100% through all time points). There are two possible explanations for this finding. First, because different animals were examined at 30 and 60 days, it is possible that the animals sacrificed on Day 30 had a more severe form of EAE compared to those sacrificed 60 days post-induction. In all experiments the EAE induction protocol was identical, but it is possible that circumstances out of the researchers' control (e.g. animal shipping conditions, MOG production, etc.) affected the severity of EAE. Second, and more probable, is that it is possible there is a remyelination phenomenon occurring between Days 30 and 60. The development of EAE in the C57BL/6 MOG models begins around 14 days, and maximum severity is around 3 weeks. By Day 30, the animals have established EAE. In the interim four weeks between the established EAE and 60 days post-induction, it is possible that there is repair of damaged myelin and production of new myelin by oligodendrocytes. A 2008 study completed in the laboratory of Dr. Calabresi reported results similar to our findings. In their study, demyelination shown with an LFB stain was most severe at 30 days post-EAE induction, and recovery of demyelinating areas occurred at later time points (60, 90 days, 7 months, 1 year post EAE-induction) [93].

Statistical analysis of correlation shows that the amount of demyelination observed in the spinal cords of mice correlated to the maximum disease score observed before the time of sacrifice on Days 20 and 30. Regardless of what treatment group was assigned, as behavioral scores increased, the number of quadrants in the spinal cord

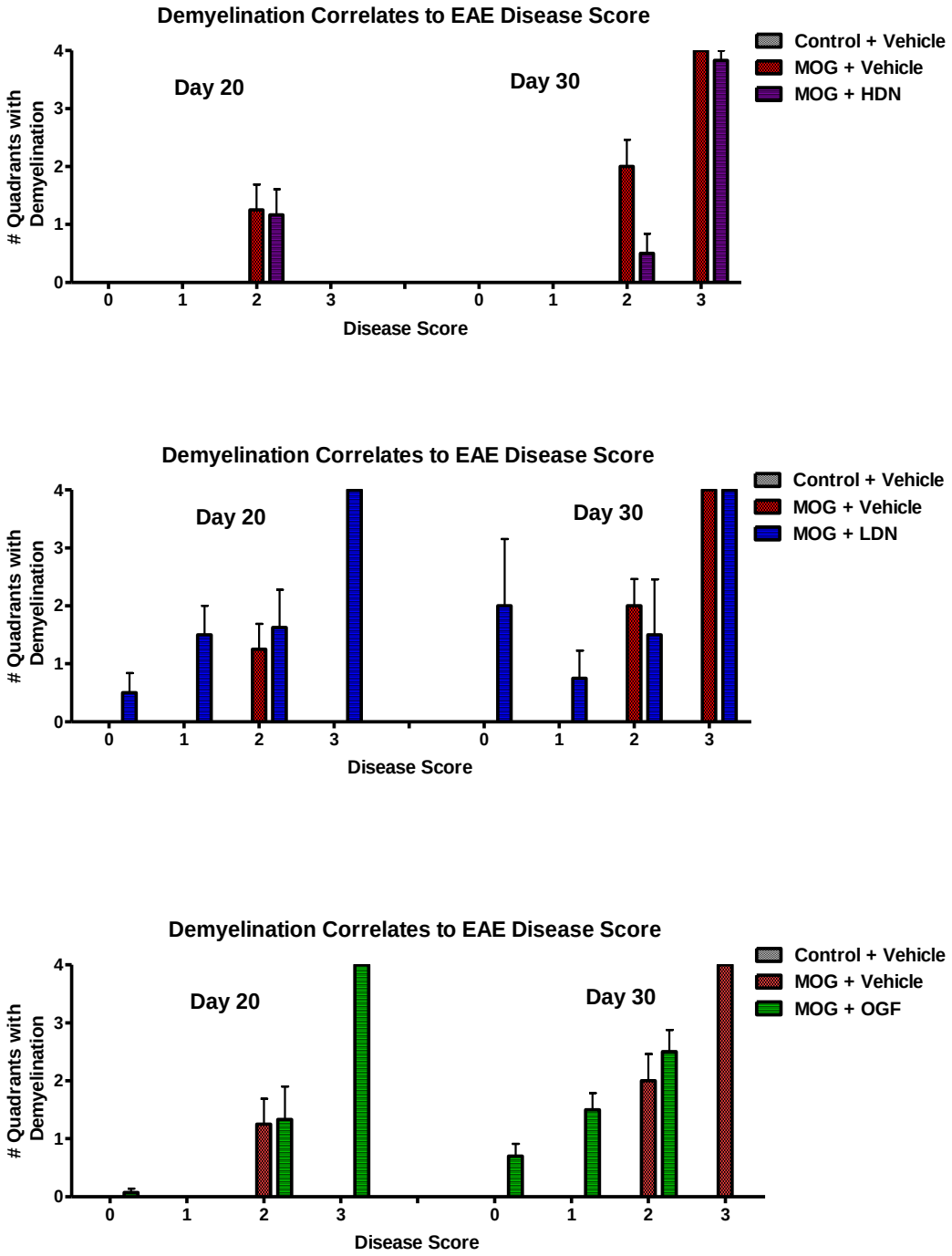

Figure 7.3: The correlation of maximum EAE behavioral scores observed before the time of sacrifice to the number of quadrants with demyelination in the lumbar spinal cord of Control+Vehicle, MOG+Vehicle (Pearson's r = 0.9746, $p < 0.05$), MOG+HDN (Pearson's r = 0.9206, $p < 0.05$), MOG+LDN (Pearson's r = 0.7786, $p < 0.05$), and MOG+OGF (Pearson's r = 0.9096, $p < 0.05$) mice.

with demyelination increased. Correlation results for demyelination and maximum disease score in MOG+Vehicle (Pearson's $r = 0.9746$, $p < 0.05$), MOG+HDN (Pearson's $r = 0.9206$, $p < 0.05$), MOG+LDN (Pearson's $r = 0.7786$, $p < 0.05$), and MOG+OGF (Pearson's $r = 0.9096$, $p < 0.05$) mice were statistically significant. Treatment groups with similar behavioral scores and histopathological results, such as MOG+LDN and MOG+OGF or MOG+Vehicle and MOG+HDN, were expected to have similar correlation of behavior scores and amount of demyelination between groups. MOG+LDN and MOG+OGF mice had comparable results (Pearson's $r = 0.8049$, $p < 0.053$), as did MOG+Vehicle and MOG+HDN mice (Pearson's $r = 0.9117$, $p < 0.088$). These data show that the maximum behavioral score observed in a mouse with EAE is a good indicator of the level of demyelination in that animal's spinal cord.

7.2.6. Neurodegeneration as measured by SMI-32 does not correlate with EAE behavioral scores.

SMI-32 is a monoclonal antibody directed against nonphosphorylated heavy neurofilament (neurofilament H) [271]. Neurofilament H is an important structural protein in the axon, and it becomes dephosphorylated following impairment of axonal integrity [271]. Therefore, SMI-32 is widely used as a marker for neuronal damage [44, 271, 272]. SMI-32 positivity was only measured in the grey matter and not the white matter, because previous reports demonstrate significant heterogeneity in staining of white matter with this antibody [273].

Neurons may become damaged for a variety of reasons, ranging from the presence of pro-inflammatory cytokines like tumor necrosis factor in the CNS [103] to an overabundance of iron and calcium inside the neurons [274]. Other laboratories have reported neuronal damage in the spinal cords of C57BL/6 mice injected with MOG as early as 7 days post-MOG injections [93]. In our studies, neurons could become

damaged as a result of the inflammation and/or demyelination caused by MOG injections. Neuronal damage was also observed in Control+Vehicle animals that only received CFA, mycobacterium tuberculosis, and pertussis toxin (and not MOG) at the time of EAE induction. This was not surprising, as the appearance of neuronal damage in the spinal cord grey matter of CFA-injected mice has been previously documented [273]. On Days 10, 30, and 60, the amount of neuronal damage did not differ between Control+Vehicle and MOG+Vehicle mice. At all time points the MOG+Vehicle group had more neuronal damage than the Control+Vehicle group (162.2%, 182.1%, and 171.0% more on Days 10, 30, and 60, respectively), but these differences were not significant. However, on Day 20 neuronal damage was significantly increased by 593% in MOG+Vehicle mice compared to Control+Vehicle animals ($p < 0.001$).

Data from these experiments show a positive correlation between the maximum disease score reached by an animal and the number of damaged neurons in that animal's spinal cord counted at 20, 30, and 60 days post-EAE induction for MOG+Vehicle mice (Pearson $r = 0.9705$, $p < 0.05$) (Figure 7.3). The number of damaged neurons in the spinal cords of MOG+Vehicle mice increases as the maximum behavior score of the corresponding animals increases. Our reports show, however, that there is no correlation between maximum disease score and the number of damaged neurons counted at 20, 30, and 60 days post-EAE induction for HDN, LDN, or OGF treatment (Figure 7.4). The maximum behavioral score before the time of sacrifice of an animal given OGF or NTX is not an accurate predictor of the amount of neuronal damage that will be found in that mouse's spinal cord. Further statistical analysis shows that there is no correlation between MOG+LDN mice and MOG+Vehicle or MOG+LDN and MOG+OGF mice in the number of damaged neurons associated with each EAE disease score. It was expected that vehicle and LDN treatments would not correlate, as

administration of LDN causes a change in disease course and a decrease in neuronal damage compared to MOG+Vehicle mice. Therefore, it is not surprising that LDN and vehicle treatments differ in the amount of neuronal damage associated with each disease score. It was expected that LDN and OGF data would correlate in how the treatments affect the amount of neuronal damage associated with each behavior score. Both treatments lower average disease scores and decrease neuronal damage, but a correlation was not observed. This is likely due to the fact that LDN is more effective than OGF at lowering neuronal damage compared to MOG+Vehicle mice; MOG+LDN mice had significantly lower counts compared to MOG+Vehicle at 10, 20, and 30 days post-EAE induction, while MOG+OGF mice had lower levels of neuronal damage only on Day 20.

Experiments from Wujek and colleagues [42] using a relapsing model of acute EAE disease demonstrated similar findings in the initial stages of EAE. After the first EAE attack, they found there was no difference between neuronal damage in controls and EAE animals, and they concluded that axonal damage did not correlate to clinical score. However, in end-stage EAE axonal density had a strong correlation with EAE disability score. The animals with severe axonal loss and a high end-stage disease score also had higher numbers of relapses. Discrepancies between Wujek's results and the findings reported here are likely due to different models of EAE utilized in the experiments, as they used the relapsing SJL mouse model and we used the chronic C57BL/6 mouse model.

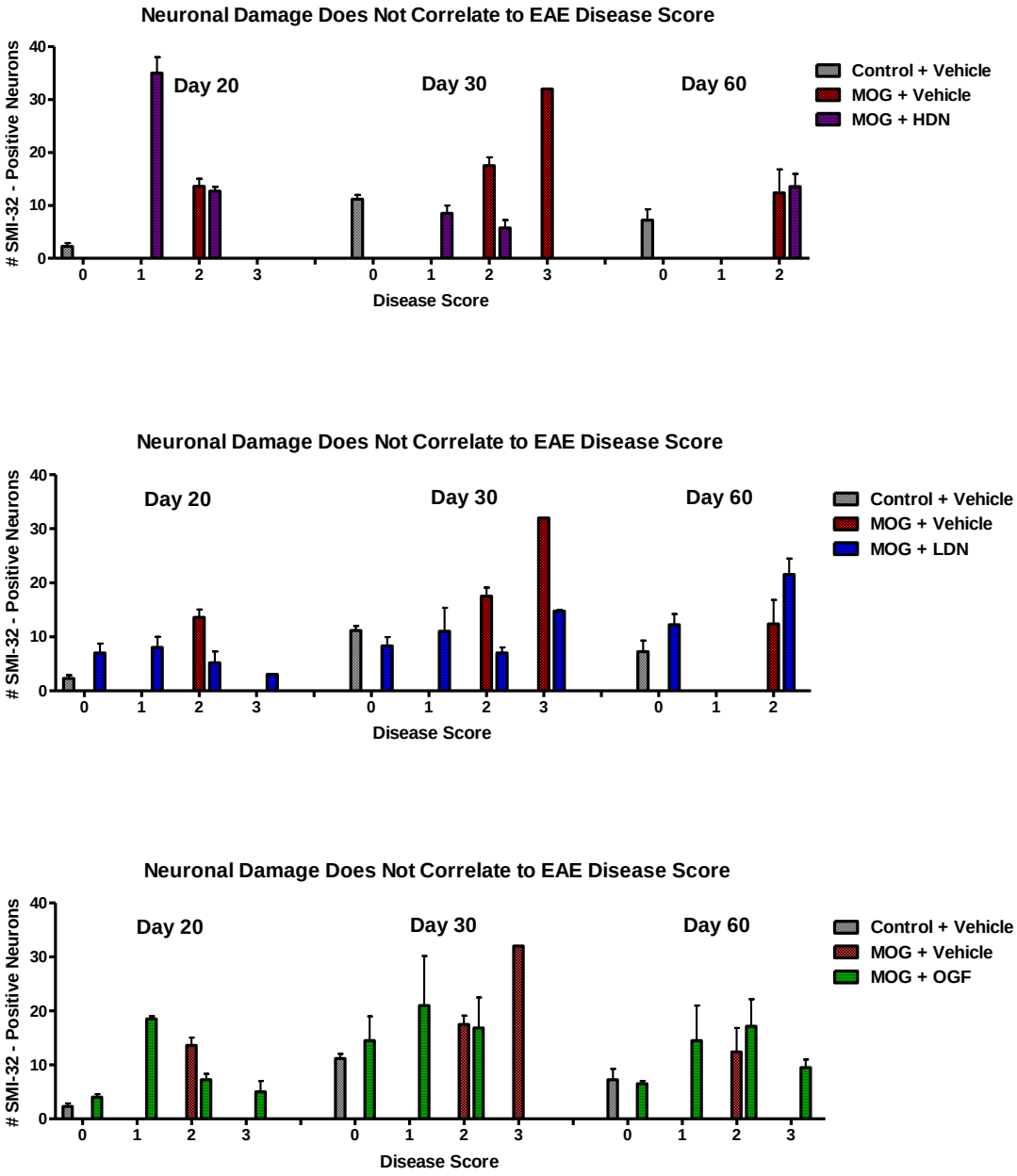

Figure 7.4: The correlation of maximum EAE behavioral scores observed before the time of sacrifice to the amount of neuronal damage in the lumbar spinal cord of Control+Vehicle, MOG+Vehicle, MOG+HDN, MOG+LDN, and MOG+OGF mice.

7.2.7. LDN is effective at treating EAE, but increasing the dosage eliminates the beneficial effects of NTX.

LDN provides intermittent opioid receptor blockade, while HDN causes continuous opioid receptor blockade. It would be reasonable to think that if some NTX is successful at inhibiting the onset and development of EAE, as is the case with LDN, a higher dose would produce even more beneficial results. The results of these experiments indicate the opposite. HDN did not alter the disease course or incidence (Figures 3.1A, 3.2A), and increased the number of animals with paralysis on Day 20 compared to vehicle-treated mice (Figure 3.1B). Immunohistochemical analysis of tissue from HDN-treated animals showed that inflammation as measured by astrocyte activation was decreased on Days 30 and 60 (Figure 3.6A) and neuronal damage was decreased on Day 30 (Figure 3.8A) compared to vehicle-treated controls. This indicates there might have been an improvement in the histological symptoms of EAE, but these changes did not translate into alleviation of behavioral symptoms. Conversely, demyelination, the pathological measurement that most strongly correlates with the behavioral symptoms of EAE, was unchanged at all time points compared to MOG+Vehicle mice (3.7B). Therefore, it can be concluded that HDN treatment does not alleviate the severity of EAE compared to vehicle-treated controls.

However, it is puzzling why astrocyte activation decreased at the 2 latest time points and neuronal damage decreased on Day 30 with HDN treatment. It is possible that the dose of NTX that successfully antagonized opioid receptors in the beginning of the experiment was not sufficient or as effective at antagonizing opioid receptors after a period of prolonged, chronic administration. During the time of NTX-mediated opioid receptor blockade, there is an increase in the production of endogenous opioid receptors [252, 275]. Therefore, the dose that was able to block all opioid receptors may not be

able to antagonize an increased population of opioid receptors. It is possible that in order to maintain the detrimental effects of HDN, the dose of NTX must be increased over time to compensate for either sensitization or increased opioid receptor populations.

7.2.8. If LDN is beneficial, it is possible that HDN could be detrimental.

The experiments outlined in this report using the EAE model of MS provide support for the use of LDN and OGF for the treatment of MS. LDN only blocks opioid receptors for 4 - 6 hours [181], and during this time production of endogenous opioid receptors increases [252, 275]. During the remaining 18 - 20 hours of the day, the excess opioid receptors are free to bind to opioids. Data from the OGF experiments demonstrate that administration of an exogenous opioid decreases the behavioral and histological symptoms of EAE. Therefore, it is likely that the interaction of opioids with opioid receptors is the beneficial component to the LDN treatment that inhibits development and pathogenesis of EAE.

HDN may be detrimental to the health of our EAE mice due to continuous opioid receptor blockade, but our EAE model might be too severe to detect differences between vehicle and HDN treatment. HDN is not harmful because it has toxic side effects, as dosages up to 800 mg caused no negative side effects [139]. It is possible that HDN would be disadvantageous for EAE mice (and MS patients) because of the inhibition of opioid-opioid receptor interactions. Opioid receptors in mice given daily injections of HDN were continuously blocked. Consequently, blockade of this interaction could cause the opposite effect and increase severity of EAE. The model of EAE employed in these experiments was slightly modified from other MOG models. In these experiments, animals were injected 3 times with MOG, as reports from other laboratories have stated that 1 and 2 injections do not cause 100% disease incidence [262, 263].

Therefore, it is possible that continuous opioid receptor blockade with HDN is harmful to mice with EAE, but that exacerbations of EAE were unable to be detected in our model.

7.2.9. LDN has strong potential for use in the clinic.

Anecdotal evidence suggests that LDN might be a beneficial treatment for a variety of autoimmune diseases, including psoriasis, Crohn's disease, and MS [www.LDNers.org, www.lowdosenaltrexone.com]. Internet testimonials from patients using off-label LDN for psoriasis, MS, and Crohn's disease report a decrease in disease progression and an increase in quality of life. The first formal study examining the effects of LDN in a clinical setting tested the treatment in Crohn's disease. A pilot human study demonstrated that 89% of patients with Crohn's disease who were given LDN (4.5 mg per day) responded to the treatment, with 67% of those individuals experiencing complete disease remission [237]. These same Crohn's disease patients given LDN also reported an improvement in their quality of life as measured by a survey, and an overall disease improvement as measured by a significant decrease in the Crohn's disease activity index score compared to control subjects.

A pilot trial was recently conducted that examined the effects of LDN in 40 patients with PP-MS [276]. The primary outcomes of the study were safety and tolerability. The secondary outcomes of the study were the appearance of fatigue (measured by the fatigue severity scale), pain (measured by the visual analog score, VAS), spasticity (measured by the Modified Ashworth Scale), depression (measured by the Beck Depression Inventory), and quality of life (measured by a version of the SF-36). β-endorphin concentration and mRNA expression levels of μ opioid receptor were also measured in PBMCs extracted from patients at baseline, 3 months and 6 months after treatment began, and 1 month after LDN treatment stopped. Two adverse effects (lung carcinoma and renal failure) were reported during the 1 year study, but it was concluded

that these were unrelated to the LDN. This study determined that LDN is safe and well-tolerated. One secondary outcome examined, spasticity, was significantly impacted by LDN. Patients given LDN had a lower incidence of spasticity compared to baseline at 3 and 6 months after treatment began and one month after treatment stopped. Fatigue, depression, and quality of life were not impacted by LDN. Pain, however, increased at 3 and 6 months after LDN treatment began, with 56.4% of patients reporting a worsening in pain as measured by VAS. β-endorphin concentration, which is lower in MS patients [277], increased at 3 and 6 months after LDN treatment began. This increase was maintained for at least one month after treatment was stopped. mRNA levels of μ opioid receptor remained unchanged throughout the study.

7.2.10. Involvement of the OGF-OGFr axis in NTX and OGF treatment for EAE is under investigation.

The growth properties of the two peptides utilized in these experiments, OGF and NTX, are well documented, and it has been proven that OGF and NTX regulate growth through the OGF-OGFr axis [177, 179, 181, 185, 186, 214, 216, 217, 223, 278]. Data included in the present experiments demonstrate that OGF and LDN are successful at preventing the onset and progression of EAE. Conversely, HDN does not affect EAE on a behavioral or histological level. It is interesting and important to note that OGF and LDN have the same effects on cell growth in culture and OGF and LDN have the same overall effects on EAE *in vivo*. However, it is unknown if the beneficial effects of OGF and LDN on EAE are mediated through the OGFr. In MS and EAE, there is a dysregulation of the immune system and a hyperproliferation of immune cells that contribute to inflammatory processes [40, 54]. It can be speculated that the negative growth actions of OGF and LDN are decreasing proliferation of cells that foster the development of EAE, thus inhibiting disease progression. If this were true, it would be

suspected that HDN, which leads to increased cell proliferation in cell growth studies [181, 186, 217, 223, 279], would lead to a more severe form of EAE. However, there was only a very modest increase in disease severity on day 20 as measured by the number of animals with hind limb paralysis. Other than this observation, the only differences noted between vehicle and HDN treatment were a decrease in HDN Day 30 and 60 astrocyte activation and Day 30 neuronal damage.

7.2.11. It is not known which cells are affected by the OGF and NTX treatment in our EAE model.

The mechanism of how LDN and OGF alleviate symptoms of EAE is unknown. Because EAE is a complex disease that involves the CNS and the immune system, cells of either system could be affected by the drugs. It is known that LDN and OGF are able to downregulate cell proliferation [177, 182, 204, 228, 279]. Furthermore, it was demonstrated in these experiments that OGF can decrease the *in vitro* proliferation of splenic-derived lymphocytes. It is possible that LDN and OGF are decreasing the rate of proliferation of pro-inflammatory cells of the immune system, such as $CD8^+$ T cells and NK cells, thereby inhibiting the primary stage of EAE, inflammation. It is also possible that LDN and OGF are inhibiting proliferation of CNS cells that contribute to MS pathogenesis, such as astrocytes and microglia. Decreasing proliferation of astrocytes and microglia would inhibit the production of cytokines that are pro-inflammatory (TNF-α and IL-1) and that stimulate antibody production and activate autoreactive T cells (IL-6) [280, 281]. Additionally, opioid administration causes analgesia and modulates the endocrine system, which could also affect behavioral presentation of EAE. Further studies are needed to elucidate the mechanism of action of LDN and OGF.

7.2.12. Manipulation of the endogenous opioid system could alleviate MS-related pain.

Pain is perceived in humans in response to noxious stimuli. Nociceptors, or free nerve endings connected to the dorsal horn of the spinal cord, are activated in response to pain. Neurotransmitters are subsequently released and feelings of pain are processed in the CNS. Nociception can be inhibited by administration of opioids. Activation of opioid receptors causes hyperpolarization of nociceptors, which inhibit release of neurotransmitters into the CNS. [282]

A significant body of evidence demonstrates differences in the ways men and women perceive pain, likely due to hormonal and genetic differences [283]. Conditions associated with chronic pain, such as headaches, fibromyalgia, and arthritis, occur in nearly twice as many women as men [283]. Women are also more likely to show increased sensitivity to pain and suffer greater pain-induced distress in experimental settings compared to men [283]. While cultural and psychological factors are likely to account for some of the differences observed in the frequency of reporting pain [283], it is likely that physiological differences between men and women also account for differences in pain perception between genders. The analgesic effects of morphine, an opioid specific for the μ opioid receptor, are more potent in females than males [284], which is probably because females have a higher endogenous concentration of μ opioid receptors than men [130].

Nociception increases in MS, and 50-80% of all MS patients report some type of pain [285]. Pain reported from MS patients includes trigeminal neuralgia, peripheral pain, and musculoskeletal pain [286]. A study that examined pain in MS patients showed that more women than men experience MS-associated pain [285]. The patient

population in the study was 2.1 women for every man, but pain was reported in 3 women for every man [285].

Experiments have shown that pain perception is less sensitive in the animal model of MS. In an experiment testing tail withdrawal in response to heat, EAE-positive mice had increased latency to withdrawal their tail compared to healthy controls [286]. A separate study using the TMEV-induced model of EAE showed that female rats experienced decreased pain perception at an earlier date than male counterparts. Female rats with EAE experienced decreased nociception beginning on day 90, while male counterparts did not experience decreased nociception until 120 days post-induction [287]. This study also compared μ, δ, and κ opioid receptor mRNA levels in the spinal cords of animals infected with TMEV versus controls [287]. The rat spinal cords were examined 90, 150, and 180 days post-EAE induction, and all opioid receptor mRNA levels were elevated following TMEV infection [287].

It is interesting to note that feelings of pain are increased in patients with MS but nociceptive response is decreased in animals with EAE. There are three possibilities as to why the EAE mice have decreased pain perception. First, animals with EAE experience severe demyelination that could delay the processing of pain. If this were true, the animals could still feel pain, but there would be a delay in their response to the noxious stimuli. Second, animals with EAE could experience so much demyelination that they are paralyzed and cannot respond to pain. This is unlikely, as the rats in the study described above were still able to detect pain, but had a delayed response in doing so. Third, the decrease in pain perception in animals with EAE could be due to an upregulation in endogenous opioid receptor production. Analgesia is mediated through opioid receptors, which are upregulated in the spinal cords of animals with EAE [287]. If this third option is true, upregulation in opioid receptor expression would be beneficial for

MS patients experiencing pain. In the case of LDN, the 4 – 6 hour opioid receptor blockade causes an increase in the endogenous opioid receptor expression. Therefore, LDN would be beneficial at not only alleviating the symptoms of MS, but it could also decrease the pain associated with the disease.

7.2.13. Endogenous opioid production changes in MS patients during pregnancy.

In previous years, women with MS were discouraged from having children because pregnancy was associated with an increased MS relapse rate [288]. Recent studies, however, have demonstrated that it is safe for women with MS to become pregnant. A European study titled PRIMS (Pregnancy in Multiple Sclerosis) published in 2004 examined the effects of pregnancy on MS progression [289]. 227 pregnant women with RR-MS were included in the study, and their relapse rates 1 year prior to pregnancy, during pregnancy, and 2 years post-partum were included in the data analysis. The study found that relapse rate decreased during pregnancy, especially in the third trimester, but relapse rate increased in the three month immediately following childbirth. The mean annual relapse rate was 0.2 relapses per year during the last trimester of pregnancy, but increased 6 fold to 1.2 during the 3 months after delivery. These findings correlated with a 1998 study of 254 pregnant women with RR-MS that also reported a decrease in relapse rate during the third trimester of pregnancy and an increased relapse rate for 3 months post-partum [290]. Numerous speculations have been made as to why MS relapse rate decreases during gestation, and there are many physiological changes during pregnancy that could account for the alleviation of MS symptoms.

During pregnancy, there is a shift from cell-mediated immunity to humoral immunity [290]. Women with MS and rheumatoid arthritis, both cell-mediated

autoimmune diseases, experience a decrease in disease symptoms during pregnancy, while women with lupus, a disease characterized by increased autoantibody production, experience disease flare-ups during pregnancy [291]. Administration of Th1 cytokines during pregnancy in mice leads to fetal complications [291]. Fetal production of Th2 cytokines increases during pregnancy causing a dramatic shift in the usual Th2/Th1 cytokine ratio, possibly as a method of self-protection [291]. The shift to Th2 cytokine secretion, including the cytokines IL-5, IL-6, and IL-10 that play a role in B cell development, could be responsible for the decrease in MS symptoms during pregnancy.

It is possible that the decrease in MS symptoms during pregnancy is due to fetal production of estriol, an endogenously produced derivative of the hormone estrogen. Estriol production is especially high during the third trimester of pregnancy, which coincides with the time of greatest MS symptom alleviation during pregnancy [292]. A study in an EAE model of MS showed that administration of estriol to animals decreased behavioral and histological symptoms of EAE [292]. Additionally, administration of pregnancy-related doses of estriol to nonpregnant females with MS caused a decrease in MS symptoms and gadolinium-enhanced lesions in the brain [293].

During pregnancy β-endorphin concentration increases [294], but OGF levels remain stable [295, 296]. Therefore, is possible that the increased endogenous production of β-endorphin or other opioid peptides is beneficial for pregnant MS women, but it is unlikely that OGF is contributing to the alleviation of MS symptoms during pregnancy. However, if OGF is used to alleviate symptoms of MS in nonpregnant women, treatment should cease if the woman becomes pregnant. Rats exposed to 10 mg/kg OGF throughout pregnancy had a fourfold increase in the number of stillborn pups and a 25% decrease in litter size and number of live births [221]. Pups that survived were lethargic and had decreased organ and body weight [221]. Human fetal

cells contain both OGF and OGFr, so exogenous OGF has the potential to cause the same detrimental effects in humans that were observed in the rats [297]. While OGF treatment should not be given during the gestation period, OGF given immediately following delivery could potentially decrease the common post-partum MS exacerbations. Studies have not been completed with LDN in pregnant animals or humans.

7.2.14. Depression, a disorder that involves changes in endogenous opioid and opioid receptor production, is common in MS patients.

A study published in 1995 examined μ opioid receptor distribution in the brains of people who died violently, with half of the deaths as a result of suicide [130]. Half of the suicide victims had clinically confirmed depression (6/15) or schizophrenia (1/15), and mental state was unknown in the remainder of the victims [130]. Brains from the accidental and self-induced deaths were matched for age and post-mortem delay until laboratory analysis [130]. Of those who committed suicide, μ opioid receptor concentration was significantly higher in the frontal lobe by 39% compared to controls [130]. There was a 36% higher μ opioid receptor concentration in the caudate of suicide victims compared to controls [130]. These findings suggest that upregulation of μ opioid receptor production is associated with suicide and/or depression. μ opioid receptor activity increases in response to feelings of reward [298]. It is possible that the upregulation of μ opioid receptor production could occur in the brains of suicide victims to compensate for either a decrease in μ opioid receptor sensitivity or a decrease in the levels of endogenous opioid production.

22.8 - 54% of all MS patients experience a major depressive disorder [18]. Factors that have been linked to the cause of depression in MS include disease severity,

cost of medication, stress, fatigue, endocrine dysfunction, and greater neuropathological symptoms in the left anterior temporal/parietal regions of the brain [18]. μ opioid receptor concentration increases with depression. No studies have been done that test μ opioid receptor levels in the CNS of MS patients, but an animal EAE study showed a decrease in the μ, δ, and κ opioid receptor levels in the CNS of animals with EAE compared to healthy controls [287]. If μ opioid receptors lose sensitivity in depressed patients and decrease in number in MS patients, LDN and OGF could prove to be effective therapies at not only treating the histological and impaired motor control in MS but also at alleviating the symptoms of depression in MS patients. LDN could be effective at treating depression in MS patients because LDN stimulates a further increase in opioid receptor production. In the pilot study completed by Gironi and colleagues [276], LDN improved signs of depression in 55.6% of the MS patients in the study, but this was not statistically significant. A larger study is warranted to test the efficacy of LDN in alleviating signs of depression in MS patients, as the Gironi pilot study included only 36 patients. OGF could be effective in treating MS by increasing μ opioid receptor stimulation, and if so, it could also possibly alleviate symptoms of depression in MS patients.

7.2.15. There were responders and non-responders to LDN and OGF treatment in our EAE model.

All MOG+Vehicle and MOG+HDN mice developed EAE before the time of sacrifice (Day 20, 30, or 60), but their maximum disease scores ranged from 1 (limp tail) to 3 (complete hind limb paralysis). Conversely, some MOG+LDN and MOG+OGF mice never developed symptoms of EAE, while other animals given LDN or OGF developed hind limb paralysis. The results observed in the mice given LDN and OGF are puzzling, as one would expect that the same treatment given to genetically identical animals

would produce the same result (i.e. the same disease score). One would expect MOG+LDN and MOG+OGF mice to either all show behavioral symptoms of EAE or all remain free of disease symptoms. Possibilities for the source of variation in the scores of MOG+LDN and MOG+OGF mice include stress and dynamics between the animals. Stressors that affect been shown to affect EAE induction and severity include handling and noises in the environment. Studies completed in rats demonstrated that 3-15 minutes of handling in the newborn stage was enough to make significant behavioral changes to the animals later in life [299]. Adult rats that were handled for 28 days during infancy showed a significantly higher rate of EAE susceptibility compared to those animals not handled as pups [299]. Some mice included in our experiments could have been handled more than others. In an experiment to test how sound affects EAE induction, rats were exposed to sound stressors on postnatal days 15, 18, and 21, and EAE was induced at 8 weeks. Rats exposed to sound stressors developed a more severe form of EAE compared to rats not exposed to sound stressors [300]. It is possible that some cohorts of mice were exposed to more sound stressors during the transport process, or were more sensitive to sound stressors than others. In addition to stressors, dynamics between the mice could alter EAE induction and severity. In all of our experiments, mice were housed 5 per cage. Inter-cage dynamics establish a pattern of dominance and weakness. Dominant animals have higher antibody production levels compared to genetically identical mice that are subordinates [301], and thus would be more likely to develop EAE. Differential group housing (when mice are housed with non-related mice), social instability within a cage, and low social rank within a stable group can increase disease susceptibility [301]. Subordinate and outcast rats have been shown to have decreased immune cell proliferation and decreased response to Con A and PHA [302, 303]. Because animals are randomly placed in cages with a new cohort

1 week prior to EAE induction, the establishment of dominance, the absence of siblings, and the group instability can lead to different immune system responses in the genetically identical animals. Therefore, it would be expected that increased dominance, cage diversity, handling, and exposure to sound stressors would elevate the severity of EAE.

7.2.16. Although both LDN and OGF decrease severity of EAE, OGF was a better long term therapy in our EAE model.

LDN and OGF were both successful at decreasing the disease incidence, disease severity, and histological symptoms of inflammation and neuronal damage compared to vehicle treatment in the *in vivo* EAE experiments (Figure 7.5). Based on these data, valid and convincing arguments could be made for the use of either therapy for treating MS patients. There were, however, differences in incidence, relapse rate, and inflammation that suggest OGF is a more effective therapy than LDN for our EAE model.

LDN was able to successfully decrease the number of animals that presented with symptoms of EAE compared to vehicle-treated controls on Days 20 – 35 and 50, while OGF decreased EAE disease incidence on Days 20 – 40 and 50 – 60. 60 days was the latest time point examined in our studies, and disease incidence in the MOG+OGF group was only 44%. LDN disease incidence was 64% on Day 60. The highest disease incidence in the MOG+OGF group was reported on Day 45, with only 56% of OGF mice displaying a disease score ≥ 1. These data show that OGF is more successful at preventing disease and can do so for a longer period of time.

The rate of remission for both LDN and OGF mice was higher than vehicle-treated controls. Nearly 25% of MOG+LDN mice had a remission, but over 20% of these mice relapsed back to having a disease score ≥ 1 before the time of sacrifice.

Conversely, over 40% of MOG+OGF mice had a remission, and only 15% of these mice relapsed. Over 25% of MOG+OGF mice that displayed a disease score recovered from behavioral symptoms of EAE. These data establish that OGF is more effective than LDN at reversing established EAE, making OGF a more attractive therapy for patients with RR-MS.

Astrocyte activation was used as a marker for inflammation in the spinal cords of animals with EAE. LDN treatment was effective at decreasing astrocyte activation compared to MOG+Vehicle mice on Days 10, 20, and 30. OGF treatment provided a more sustained effect, as inflammation was decreased in the spinal cords of MOG+OGF mice compared to vehicle-treated controls at 10, 20, 30, and 60 days. Therefore, OGF is a more effective long-term treatment for decreasing inflammation.

Taken together, these data show that OGF decreases disease incidence, increases rate of remission, and decreases inflammation more effectively and for a longer period of time compared to LDN treatment. While LDN is undoubtedly beneficial for decreasing behavioral and histological symptoms of EAE, OGF proved to be a slightly better therapy in our EAE model. It is important to note that these results are only those obtained in a chronic EAE model. Therefore, further studies should be done comparing the efficacy of LDN and OGF at alleviating symptoms of EAE in various disease stages and in an assortment of EAE models.

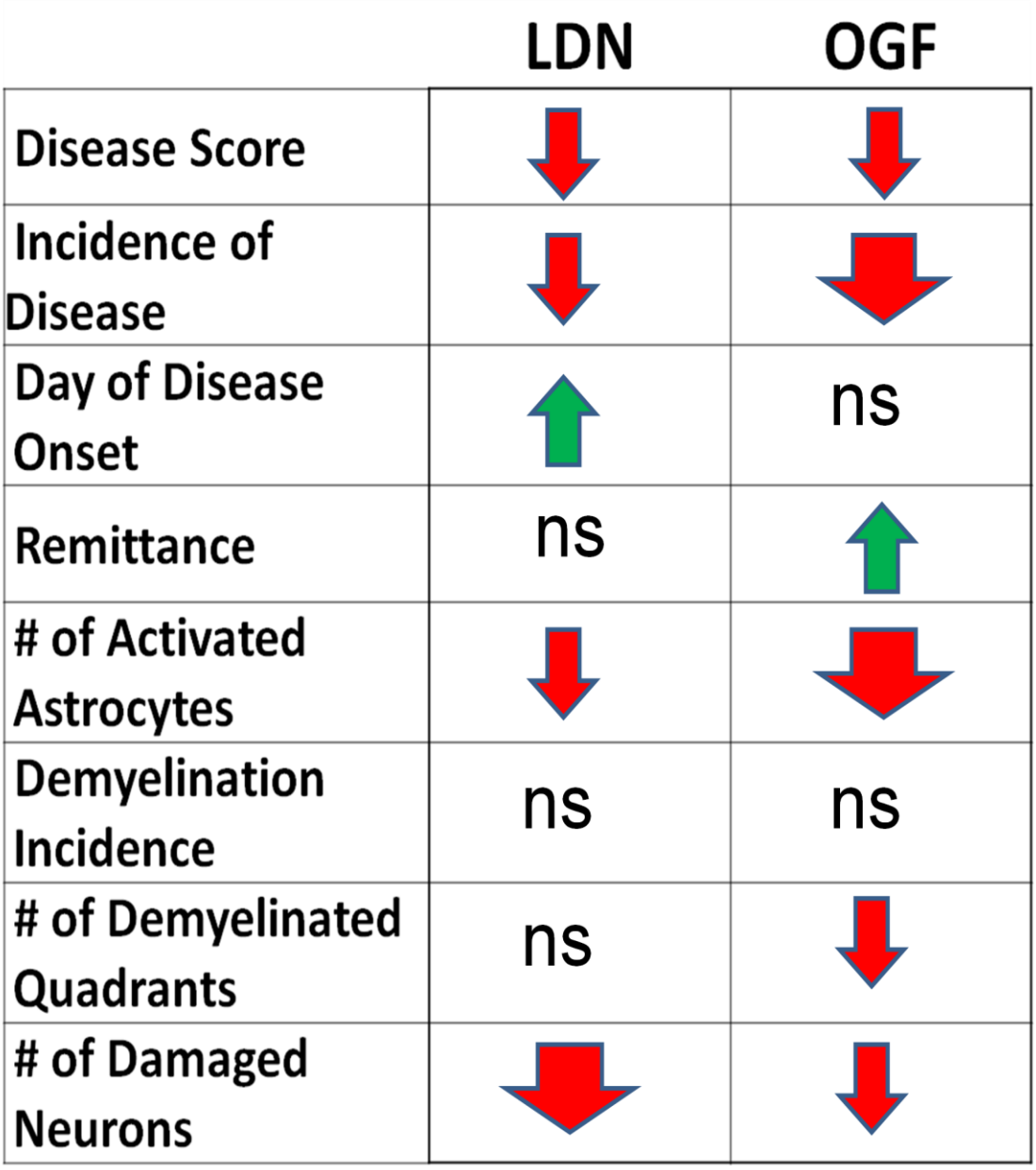

Figure 7.5: Summary of the behavioral and histological effects of LDN and OGF. Arrows indicate significant increases (green arrow up), decreases (red arrow down), or no change (ns) compared to MOG+Vehicle mice.

CHAPTER 8: FUTURE DIRECTIONS

8. Future Directions

The data obtained from these experiments support the use of LDN and OGF for the treatment of EAE and MS. While this report provides considerable evidence that either therapy would be beneficial for MS patients, more studies should be completed that examine other aspects of disease and test therapy efficacy in other model systems. Studies in our laboratory using the C57BL/6 MOG model are currently underway to test the efficacy of preventing EAE by giving LDN or OGF prophylactically (7 days before the first MOG injection). Additional studies have also begun that were designed to test the ability of LDN and OGF at reversing the symptoms of already-established EAE. In addition, experiments should be conducted that test LDN and OGF therapy in relapsing models of EAE.

The remyelination phenomenon observed between days 30 and 60 should be explored. It is possible that either the healthy myelinated white matter of the lumbar spinal cord is new myelin or that the animals sacrificed on Day 60 never experienced demyelination in the first place. Immunohistochemical analysis could be conducted to resolve this matter. In toluidine blue-stained resin sections that are 1 µm thick, demyelination is evident by the absence of myelin around the axon, while new myelin forms a dark and very thin sheath around an unusually small axon [304]. A new 60 day study will have to be completed to test for remyelination, as toluidine blue staining is completed on the spinal cords of animals perfused with 4% glutaraldehyde and embedded in resin [304]. Animals included in these analyses were perfused with 10% neutral buffered formalin and cords were embedded in paraffin wax.

The speed of remyelination has been shown to be dependent on the speed of macrophage recruitment to the site of the CNS lesion [305]. Therefore, if remyelination is occurring, it would be useful to correlate this with the amount of macrophages present

at the lesion sites. Similarly, it would be useful to determine if the amount of macrophage recruitment differed between animals that remain sick throughout the duration of the experiment and those that experienced a remission (returned to a disease score of 0). For example, if EAE positive mice (disease score > or = 1) were both given OGF treatment and one remained EAE positive while the other experienced a remission, the amount of macrophages present in the spinal cord might be indicative of EAE score (with more macrophages expected in the spinal cords of those animals that experience remissions). Immunohistochemistry can easily be conducted in the spinal cords with the CD68 antibody to test for presence of macrophages.

In the included analyses, axonal damage was measured with an SMI-32 antibody directed against nonphosphorylated heavy neurofilaments. According to Bannerman and colleagues, only 2/3 of all damaged motor neurons in the EAE spinal cord stained positive for SMI-32 [273]. Therefore, another antibody that measures axonal damage should be employed to get a complete and representative picture of the amount of damage in the spinal cord as a result of EAE. For our purposes, SMI-32 is an acceptable marker because we are comparing neuronal damage between treatment groups. However, if the total amount of axonal damage is to be measured, more markers must be utilized. An antibody that has been previously demonstrated to accurately measure axonal damage is β-amyloid precursor protein (APP) [306]. A noninvasive marker that could be useful for measuring axonal damage throughout the course of EAE is diffusion tensor imaging. This technique is done on live animals, and EAE studies have shown that the level of radial diffusivity correlates with both EAE disease scores and SMI-32 positivity [307].

Because MS is an autoimmune disease, it would be interesting to do immunohistochemical analysis of T and B cells in the spinal cord to determine if LDN or

OGF therapy decreases the symptoms of EAE by preventing infiltration and/or proliferation of immune cells in the CNS. A recent report showed that T cell infiltration peaked during the onset of the behavioral symptoms of EAE [93]. It is likely that T cells contribute to disability. Current FDA-approved therapies for MS target the immune system, and it would be interesting to know if LDN and OGF also target the immune system. Flow cytometry is another way to measure how LDN and OGF affect MOG-specific lymphocyte proliferation. Flow cytometry experiments were completed in our laboratory that measured the amount of B cells and $CD4^+$ and $CD8^+$ T cells in spleens of mice given EAE and treated for 3, 5, and 8 days with vehicle, HDN, LDN, or OGF (data not shown), but data were inconclusive due to variances within treatment groups. A more specific experiment would be to double label the splenic-derived lymphocytes using the T or B cell markers and a MOG-specific tetramer. Measuring the changes in MOG-specific lymphocyte profiles of the T and B cell subsets would clarify if the HDN, LDN, and OGF affect MOG-specific lymphocyte proliferation that occurs due to the EAE.

As previously stated, the mechanism of action through which LDN and OGF alleviated EAE symptoms in the experiments described here is unknown. Based on the well-established and unique growth properties of NTX and OGF, it can be hypothesized that LDN and OGF work by decreasing proliferation of proinflammatory cells of the immune system. To test this idea, other opioid peptides specific for the μ, δ, and κ opioid receptors could be administered to animals with EAE. Based on our ideas that LDN and OGF work through the OGFr, we would expect that administration of any other opioid agonist would not alleviate symptoms of EAE as OGF has the highest affinity (100x higher than other opioids) for OGFr. Another approach that could be taken to solve this problem would be to use knockout mice that are lacking OGFr. Based on the idea that LDN and OGF work through OGFr, we would predict that LDN and OGF would

be ineffective at treating EAE in OGFr knockout mice. If this was true, the disease course and histological profile in animals given LDN and OGF would be identical to that of vehicle-treated controls. If, however, LDN and OGF improve behavioral and histological symptoms of EAE in OGFr knockout mice, the mechanism of action would be separate from OGFr.

Mixed success has been reported in using two FDA-approved therapies for MS in combination. Using LDN or OGF in conjunction with an established therapy could be an excellent treatment method if LDN and OGF target unique cells not affected by the existing therapy. The majority of current therapies work by suppressing the immune system. If LDN and OGF work through a unique mechanism of action, concomitant administration of LDN or OGF with an existing therapy could enhance the efficacy of the existing therapy.

The experiments described here were conducted to determine if endogenous opioids play a role in the onset and progression of EAE. To begin testing this hypothesis, EAE was induced in mice, and a high or low dose of an opioid receptor antagonist was administered daily to facilitate complete or intermittent opioid receptor blockade, respectively. While continuous opioid receptor blockade with HDN had negligible effects on the progression of EAE, daily intermittent opioid receptor blockade with LDN delayed disease onset and decreased average disease score, disease incidence, disease severity, the number of activated astrocytes, and the amount of neuronal damage compared to MOG+Vehicle mice. These results suggested that the interaction of opioids with opioid receptors was the beneficial component in the LDN treatment. To test this idea, an opioid that can be produced endogenously was administered exogenously. Daily administration of exogenous OGF from the time of the first EAE induction injection increased remission rates and decreased average disease

score, disease incidence, disease severity, the number of activated astrocytes, the severity of demyelination, and the amount of neuronal damage compared to MOG+Vehicle mice. Overall, data demonstrate that both LDN and OGF are effective at minimizing behavioral and histological symptoms of EAE, and both show promise as future treatments for MS. It appears that both treatments are capable of significantly decreasing the first histological sign of EAE (inflammation) compared to MOG+Vehicle before the onset of disease symptoms (Day 10). The absence of the second histological sign of EAE (demyelination) until after the onset of disease symptoms (Day 20) suggests that LDN and OGF are effective at treating EAE by decreasing the synthesis and proliferation of proinflammatory cells. Further studies are necessary to confirm this proposal, but *in vitro* analyses have shown that the OGF-OGFr axis is present and functioning in splenic-derived lymphocytes. EAE is an analogous but imperfect model of MS, so clinical trials are needed to confirm that LDN and OGF are effective at treating MS. A small clinical trial has demonstrated that LDN is safe, tolerable, and can raise the production of an endogenous opioid (β-endorphin), but larger studies are necessary to determine the efficacy of LDN for the treatment of MS. In conclusion, this work provides evidence to support the funding of large scale clinical trials that would test the efficacy of LDN and OGF for the treatment of MS. Additionally, future studies could be designed with LDN and OGF in both the currently employed EAE model and a relapsing EAE model to test various treatment timing sequences, alternative histological markers, and different endpoint sacrifice times to more thoroughly understand how modulation of endogenous opioids affects the onset and progression of EAE.

REFERENCES

1. Forte, M., et al., *Cyclophilin D inactivation protects axons in experimental autoimmune encephalomyelitis, an animal model of multiple sclerosis.* PNAS USA, 2007. **104**(18): p. 7558-7563.
2. Rizvi, S.A. and M.A. Agius, *Current approved options for treating patients with multiple sclerosis.* Neurology, 2004. **63**(12S6): p. S8-14.
3. Lees, J.R. and A.H. Cross, *A little stress is good: IFN-gamma, demyelination, and multiple sclerosis.* J Clin Invest, 2007. **117**(2): p. 297-9.
4. Irvine, K.A. and W.F. Blakemore, *Remyelination protects axons from demyelination-associated axon degeneration.* Brain, 2008. **131**(Pt 6): p. 1464-77.
5. Charcot, J., *Histologie de la sclérose en plaque.* Gazette des Hôpitaux, 1868. **41**: p. 554-566.
6. Terayama, R., et al., *Involvement of neuropsin in the pathogenesis of experimental autoimmune encephalomyelitis.* Glia, 2005. **52**(2): p. 108-18.
7. Fernandez, M., et al., *Thyroid hormone administration enhances remyelination in chronic demyelinating inflammatory disease.* Proc Natl Acad Sci U S A, 2004. **101**(46): p. 16363-8.
8. Ercolini, A.M. and S.D. Miller, *Mechanisms of immunopathology in murine models of central nervous system demyelinating disease.* J Immunol, 2006. **176**(6): p. 3293-8.
9. Alonso, A. and M.A. Hernan, *Temporal trends in the incidence of multiple sclerosis: a systematic review.* Neurology, 2008. **71**(2): p. 129-35.
10. Dyment, D.A., G.C. Ebers, and A.D. Sadovnick, *Genetics of multiple sclerosis.* Lancet Neurol, 2004. **3**(2): p. 104-10.
11. Ramagopalan, S.V. and G.C. Ebers, *Genes for multiple sclerosis.* Lancet, 2008. **371**(9609): p. 283-5.
12. Cantorna, M.T., *Vitamin D and multiple sclerosis: an update.* Nutr Rev, 2008. **66**(10 Suppl 2): p. S135-8.
13. Ramagopalan, S.V., et al., *Expression of the multiple sclerosis-associated MHC class II Allele HLA-DRB1*1501 is regulated by vitamin D.* PLoS Genet, 2009. **5**(2): p. e1000369.
14. Cantorna, M.T., C.E. Hayes, and H.F. DeLuca, *1,25-Dihydroxyvitamin D3 reversibly blocks the progression of relapsing encephalomyelitis, a model of multiple sclerosis.* Proc Natl Acad Sci U S A, 1996. **93**(15): p. 7861-4.
15. Bach, J.F., *The effect of infections on susceptibility to autoimmune and allergic diseases.* N Engl J Med, 2002. **347**(12): p. 911-20.
16. Correale, J. and M. Farez, *Association between parasite infection and immune responses in multiple sclerosis.* Ann Neurol, 2007. **61**(2): p. 97-108.
17. Buttman, M. and P. Rieckmann, *Interferon-beta-1b in multiple sclerosis.* Expert Reviews in Neurotherapeutics, 2007. **7**(3): p. 227-239.
18. Bamer, A.M., et al., *Validation study of prevalence and correlates of depressive symptomatology in multiple sclerosis.* Gen Hosp Psychiatry, 2008. **30**(4): p. 311-7.

19. Renoux, C., et al., *Natural history of multiple sclerosis with childhood onset.* N Engl J Med, 2007. **356**(25): p. 2603-13.
20. Harding, A., *Fine-tuning our defenses.* The Scientist, 2007. **Autoimmunity**: p. 56-61.
21. Eriksson, M., E. Ben-Menachem, and O. Andersen, *Epileptic seizures, cranial neuralgias and paroxysmal symptoms in remitting and progressive multiple sclerosis.* Mult Scler, 2002. **8**(6): p. 495-9.
22. Kraft, G.H., *Improving health care delivery for persons with multiple sclerosis.* Phys Med Rehabil Clin N Am, 1998. **9**(3): p. 703-15, viii-ix.
23. Wekerle, H., *Lessons from multiple sclerosis: models, concepts, observations.* Ann Rheum Dis, 2008. **67 Suppl 3**: p. iii56-60.
24. Charil, A. and M. Filippi, *Inflammatory demyelination and neurodegeneration in early multiple sclerosis.* J Neurol Sci, 2007. **259**(1-2): p. 7-15.
25. Tsunoda, I., et al., *Axonal injury heralds virus-induced demyelination.* Am J Pathol, 2003. **162**(4): p. 1259-69.
26. Tsunoda, I. and R.S. Fujinami, *Inside-Out versus Outside-In models for virus induced demyelination: axonal damage triggering demyelination.* Springer Semin Immunopathol, 2002. **24**(2): p. 105-25.
27. Kabat, E.A., M. Glusman, and V. Knaub, *Quantitative estimation of the albumin and gamma globulin in normal and pathologic cerebrospinal fluid by immunochemical methods.* Am J Med, 1948. **4**(5): p. 653-62.
28. Costantino, C.M., C. Baecher-Allan, and D.A. Hafler, *Multiple sclerosis and regulatory T cells.* J Clin Immunol, 2008. **28**(6): p. 697-706.
29. Luster, A.D., R. Alon, and U.H. von Andrian, *Immune cell migration in inflammation: present and future therapeutic targets.* Nat Immunol, 2005. **6**(12): p. 1182-90.
30. Johnson, K.P., *Natalizumab (Tysabri) treatment for relapsing multiple sclerosis.* Neurologist, 2007. **13**(4): p. 182-7.
31. Morgan, L., et al., *Inflammation and dephosphorylation of the tight junction protein occludin in an experimental model of multiple sclerosis.* Neuroscience, 2007. **147**(3): p. 664-73.
32. Redwine, J.M., M.J. Buchmeier, and C.F. Evans, *In vivo expression of major histocompatibility complex molecules on oligodendrocytes and neurons during viral infection.* Am J Pathol, 2001. **159**(4): p. 1219-24.
33. Rodriguez, M., *Effectors of demyelination and remyelination in the CNS: implications for multiple sclerosis.* Brain Pathol, 2007. **17**(2): p. 219-29.
34. Ingram, G., et al., *Complement in multiple sclerosis: its role in disease and potential as a biomarker.* Clin Exp Immunol, 2009. **155**(2): p. 128-39.
35. Prineas, J.W., et al., *Immunopathology of secondary-progressive multiple sclerosis.* Ann Neurol, 2001. **50**(5): p. 646-57.
36. Oh, S., et al., *B-cells and humoral immunity in multiple sclerosis. Implications for therapy.* Immunol Res, 2008. **40**(3): p. 224-34.
37. Friese, M.A. and L. Fugger, *Autoreactive CD8+ T cells in multiple sclerosis: a new target for therapy?* Brain, 2005. **128**(Pt 8): p. 1747-63.

38. Howe, C.L., J.D. Adelson, and M. Rodriguez, *Absence of perforin expression confers axonal protection despite demyelination.* Neurobiol Dis, 2007. **25**(2): p. 354-9.
39. Haring, J.S. and S. Perlman, *Bystander CD4 T cells do not mediate demyelination in mice infected with a neurotropic coronavirus.* J Neuroimmunol, 2003. **137**(1-2): p. 42-50.
40. Hafler, D.A., *Multiple sclerosis.* J Clin Invest, 2004. **113**(6): p. 788-94.
41. Peterson, L.K. and R.S. Fujinami, *Inflammation, demyelination, neurodegeneration and neuroprotection in the pathogenesis of multiple sclerosis.* J Neuroimmunol, 2007. **184**(1-2): p. 37-44.
42. Wujek, J.R., et al., *Axon loss in the spinal cord determines permanent neurological disability in an animal model of multiple sclerosis.* J Neuropathol Exp Neurol, 2002. **61**(1): p. 23-32.
43. Kutzelnigg, A., et al., *Cortical demyelination and diffuse white matter injury in multiple sclerosis.* Brain, 2005. **128**(Pt 11): p. 2705-12.
44. Trapp, B.D., et al., *Axonal transection in the lesions of multiple sclerosis.* N Engl J Med, 1998. **338**(5): p. 278-85.
45. Bitsch, A., et al., *Acute axonal injury in multiple sclerosis. Correlation with demyelination and inflammation.* Brain, 2000. **123 (Pt 6)**: p. 1174-83.
46. Bitsch, A. and W. Bruck, *Differentiation of multiple sclerosis subtypes: implications for treatment.* CNS Drugs, 2002. **16**(6): p. 405-18.
47. De Jager, P.L. and D.A. Hafler, *New therapeutic approaches for multiple sclerosis.* Annu Rev Med, 2007. **58**: p. 417-32.
48. Tsunoda, I., et al., *Massive apoptosis in lymphoid organs in animal models for primary and secondary progressive multiple sclerosis.* Am J Pathol, 2005. **167**(6): p. 1631-46.
49. Weissert, R., et al., *Action of treosulfan in myelin-oligodendrocyte-glycoprotein-induced experimental autoimmune encephalomyelitis and human lymphocytes.* Journal of Neuroimmunology, 2003. **144**: p. 28-37.
50. Van der Aa, A., et al., *Functional properties of myelin oligodendrocyte glycoprotein-reactive T cells in multiple sclerosis patients and controls.* Journal of Neuroimmunology, 2003. **137**: p. 164-176.
51. Tullman, M.J., et al., *Clinical characteristics of progressive relapsing multiple sclerosis.* Multiple Sclerosis, 2004. **10**(4): p. 451-454.
52. Frohman, E.M., M.K. Racke, and C.S. Raine, *Multiple sclerosis--the plaque and its pathogenesis.* N Engl J Med, 2006. **354**(9): p. 942-55.
53. Miller, D.H. and S.M. Leary, *Primary-progressive multiple sclerosis.* Lancet Neurol, 2007. **6**(10): p. 903-12.
54. Compston, A. and A. Coles, *Multiple sclerosis.* Lancet, 2008. **372**(9648): p. 1502-17.
55. Rovira, A. and A. Leon, *MR in the diagnosis and monitoring of multiple sclerosis: an overview.* Eur J Radiol, 2008. **67**(3): p. 409-14.
56. Fuhr, P. and L. Kappos, *Evoked potentials for evaluation of multiple sclerosis.* Clin Neurophysiol, 2001. **112**(12): p. 2185-9.

57. Leocani, L., S. Medaglini, and G. Comi, *Evoked potentials in monitoring multiple sclerosis.* Neurol Sci, 2000. **21**(4 Suppl 2): p. S889-91.
58. Link, H. and Y.M. Huang, *Oligoclonal bands in multiple sclerosis cerebrospinal fluid: an update on methodology and clinical usefulness.* J Neuroimmunol, 2006. **180**(1-2): p. 17-28.
59. McDonald, W.I., et al., *Recommended diagnostic criteria for multiple sclerosis: guidelines from the International Panel on the diagnosis of multiple sclerosis.* Ann Neurol, 2001. **50**(1): p. 121-7.
60. Munschauer, F.E., 3rd and W.H. Stuart, *Rationale for early treatment with interferon beta-1a in relapsing-remitting multiple sclerosis.* Clin Ther, 1997. **19**(5): p. 868-82.
61. Ransohoff, R.M., *Natalizumab for multiple sclerosis.* N Engl J Med, 2007. **356**(25): p. 2622-9.
62. Pette, M., et al., *Interferon-beta interferes with the proliferation but not with the cytokine secretion of myelin basic protein-specific, T-helper type 1 lymphocytes.* Neurology, 1997. **49**(2): p. 385-92.
63. DeAngelis, T. and F. Lublin, *Neurotherapeutics in multiple sclerosis: novel agents and emerging treatment strategies.* Mt Sinai J Med, 2008. **75**(2): p. 157-67.
64. Freedman, M.S., et al., *Efficacy of disease-modifying therapies in relapsing remitting multiple sclerosis: a systematic comparison.* Eur Neurol, 2008. **60**(1): p. 1-11.
65. Arnason, B.G., *Interferon beta in multiple sclerosis.* Clin Immunol Immunopathol, 1996. **81**(1): p. 1-11.
66. Miyazaki, Y., et al., *Expansion of CD4+CD28- T cells producing high levels of interferon-{gamma} in peripheral blood of patients with multiple sclerosis.* Mult Scler, 2008. **14**(8): p. 1044-55.
67. Stoll, G., S. Jander, and M. Schroeter, *Cytokines in CNS disorders: neurotoxicity versus neuroprotection.* J Neural Transm Suppl, 2000. **59**: p. 81-9.
68. Anderson, A.C., et al., *IL-10 plays an important role in the homeostatic regulation of the autoreactive repertoire in naive mice.* J Immunol, 2004. **173**(2): p. 828-34.
69. Larocque, D., et al., *Gene Therapy for Neurological Disorders*. Vol. Chapter 12, Gene Therapy of Multiple Sclerosis and in CNS Autoimmune Mouse Models. 2006, New York.
70. Giuliani, F., et al., *Additive effect of the combination of glatiramer acetate and minocycline in a model of MS.* J Neuroimmunol, 2005. **158**(1-2): p. 213-21.
71. Ridge, S.C., et al., *Suppression of experimental allergic encephalomyelitis by mitoxantrone.* Clin Immunol Immunopathol, 1985. **35**(1): p. 35-42.
72. Levine, S. and A. Saltzman, *Regional suppression, therapy after onset and prevention of relapses in experimental allergic encephalomyelitis by mitoxantrone.* J Neuroimmunol, 1986. **13**(2): p. 175-81.
73. van de Wyngaert, F.A., et al., *A double-blind clinical trial of mitoxantrone versus methylprednisolone in relapsing, secondary progressive multiple sclerosis.* Acta Neurol Belg, 2001. **101**(4): p. 210-6.

74. Jeffery, D.R. and R. Herndon, *Review of mitoxantrone in the treatment of multiple sclerosis.* Neurology, 2004. **63**(12 Suppl 6): p. S19-24.
75. Noseworthy, J.H. and P. Kirkpatrick, *Natalizumab.* Nat Rev Drug Discov, 2005. **4**(2): p. 101-2.
76. Schiess, N. and P.A. Calabresi, *Natalizumab: bound to rebound?* Neurology, 2009. **72**(5): p. 392-3.
77. Polman, C.H., et al., *A randomized, placebo-controlled trial of natalizumab for relapsing multiple sclerosis.* N Engl J Med, 2006. **354**(9): p. 899-910.
78. Baker, D.E., *Natalizumab: overview of its pharmacology and safety.* Rev Gastroenterol Disord, 2007. **7**(1): p. 38-46.
79. Rudick, R.A., et al., *Natalizumab plus interferon beta-1a for relapsing multiple sclerosis.* N Engl J Med, 2006. **354**(9): p. 911-23.
80. Vollmer, T., et al., *Glatiramer acetate after induction therapy with mitoxantrone in relapsing multiple sclerosis.* Mult Scler, 2008. **14**(5): p. 663-70.
81. Arnold, D.L., et al., *Glatiramer acetate after mitoxantrone induction improves MRI markers of lesion volume and permanent tissue injury in MS.* J Neurol, 2008. **255**(10): p. 1473-8.
82. Goodman, A.D., et al., *GLANCE: results of a phase 2, randomized, double-blind, placebo-controlled study.* Neurology, 2009. **72**(9): p. 806-12.
83. Iezzoni, L.I., L.H. Ngo, and R.P. Kinkel, *Working-age persons with multiple sclerosis and access to disease-modifying medications.* Mult Scler, 2008. **14**(1): p. 112-22.
84. Stosic-Grujicic, S., et al., *Down-regulation of experimental allergic encephalomyelitis in DA rats by tiazofurin.* J Neuroimmunol, 2002. **130**(1-2): p. 66-77.
85. Tsunoda, I., et al., *Contrasting roles for axonal degeneration in an autoimmune versus viral model of multiple sclerosis: When can axonal injury be beneficial?* Am J Pathol, 2007. **170**(1): p. 214-26.
86. Kennedy, M.K., et al., *Analysis of cytokine mRNA expression in the central nervous system of mice with experimental autoimmune encephalomyelitis reveals that IL-10 mRNA expression correlates with recovery.* J Immunol, 1992. **149**(7): p. 2496-505.
87. Koritschoner, R.S. and F. Schweinburg, *Induktion von Paralyse und Ru¨ckenmarksentzu¨ndung durch Immunisierung von Kaninchen mit menschlichem Ru¨ckenmarksgewebe.* Z Immunita¨tsf Exp Therapie, 1925. **42**: p. 217-283.
88. Gold, R., *Combination therapies in multiple sclerosis.* J Neurol, 2008. **255 Suppl 1**: p. 51-60.
89. Bajramovic, J.J., et al., *Oligodendrocyte-specific protein is encephalitogenic in rhesus macaques and induces specific demyelination of the optic nerve.* Eur J Immunol, 2008. **38**(5): p. 1452-64.
90. Tsunoda, I., et al., *Modulation of experimental autoimmune encephalomyelitis by VLA-2 blockade.* Brain Pathol, 2007. **17**(1): p. 45-55.

91. Hampton, D.W., et al., *An experimental model of secondary progressive multiple sclerosis that shows regional variation in gliosis, remyelination, axonal and neuronal loss.* J Neuroimmunol, 2008. **201-202**: p. 200-11.
92. Gold, R., C. Linington, and H. Lassmann, *Understanding pathogenesis and therapy of multiple sclerosis via animal models: 70 years of merits and culprits in experimental autoimmune encephalomyelitis research.* Brain, 2006. **129**(Pt 8): p. 1953-71.
93. Jones, M.V., et al., *Behavioral and pathological outcomes in MOG 35-55 experimental autoimmune encephalomyelitis.* J Neuroimmunol, 2008. **199**(1-2): p. 83-93.
94. Linares, D., et al., *The magnitude and encephalogenic potential of autoimmune response to MOG is enhanced in MOG deficient mice.* J Autoimmun, 2003. **21**(4): p. 339-51.
95. Stills, H.F., Jr., *Adjuvants and antibody production: dispelling the myths associated with Freund's complete and other adjuvants.* Ilar J, 2005. **46**(3): p. 280-93.
96. Amend, B., et al., *Induction of autoimmunity by expansion of autoreactive CD4+CD62Llow cells in vivo.* J Immunol, 2006. **177**(7): p. 4384-90.
97. Zhou, J., et al., *Experimental autoimmune encephalomyelitis in the Wistar rat: dependence of MBP-specific T cell responsiveness on B7 costimulation.* Autoimmunity, 2002. **35**(3): p. 191-9.
98. Munoz, J.J., C.C. Bernard, and I.R. Mackay, *Elicitation of experimental allergic encephalomyelitis (EAE) in mice with the aid of pertussigen.* Cell Immunol, 1984. **83**(1): p. 92-100.
99. Sudweeks, J.D., et al., *Locus controlling Bordetella pertussis-induced histamine sensitization (Bphs), an autoimmune disease-susceptibility gene, maps distal to T-cell receptor beta-chain gene on mouse chromosome 6.* Proc Natl Acad Sci U S A, 1993. **90**(8): p. 3700-4.
100. Zhao, C.B., et al., *A new EAE model of brain demyelination induced by intracerebroventricular pertussis toxin.* Biochem Biophys Res Commun, 2008. **370**(1): p. 16-21.
101. Feldmann, M. and L. Steinman, *Design of effective immunotherapy for human autoimmunity.* Nature, 2005. **435**(7042): p. 612-9.
102. Baker, D., et al., *Control of established experimental allergic encephalomyelitis by inhibition of tumor necrosis factor (TNF) activity within the central nervous system using monoclonal antibodies and TNF receptor-immunoglobulin fusion proteins.* Eur J Immunol, 1994. **24**(9): p. 2040-8.
103. McCoy, M.K. and M.G. Tansey, *TNF signaling inhibition in the CNS: implications for normal brain function and neurodegenerative disease.* J Neuroinflammation, 2008. **5**: p. 45.
104. Ruddle, N.H., et al., *An antibody to lymphotoxin and tumor necrosis factor prevents transfer of experimental allergic encephalomyelitis.* J Exp Med, 1990. **172**(4): p. 1193-200.
105. Crisi, G.M., et al., *Staphylococcal enterotoxin B and tumor-necrosis factor-alpha-induced relapses of experimental allergic encephalomyelitis: protection*

by transforming growth factor-beta and interleukin-10. Eur J Immunol, 1995. **25**(11): p. 3035-40.
106. Sharief, M.K. and R. Hentges, *Association between tumor necrosis factor-alpha and disease progression in patients with multiple sclerosis.* N Engl J Med, 1991. **325**(7): p. 467-72.
107. *TNF neutralization in MS: results of a randomized, placebo-controlled multicenter study. The Lenercept Multiple Sclerosis Study Group and The University of British Columbia MS/MRI Analysis Group.* Neurology, 1999. **53**(3): p. 457-65.
108. Takeuchi, H., et al., *Interferon-gamma induces microglial-activation-induced cell death: a hypothetical mechanism of relapse and remission in multiple sclerosis.* Neurobiol Dis, 2006. **22**(1): p. 33-9.
109. Lin, W., et al., *The integrated stress response prevents demyelination by protecting oligodendrocytes against immune-mediated damage.* J Clin Invest, 2007. **117**(2): p. 448-56.
110. Panitch, H.S., et al., *Exacerbations of multiple sclerosis in patients treated with gamma interferon.* Lancet, 1987. **1**(8538): p. 893-5.
111. Papamichail, M., et al., *Natural killer lymphocytes: biology, development, and function.* Cancer Immunol Immunother, 2004. **53**(3): p. 176-86.
112. Steinman, L. and S.S. Zamvil, *Virtues and pitfalls of EAE for the development of therapies for multiple sclerosis.* Trends Immunol, 2005. **26**(11): p. 565-71.
113. Peterson, P.K., T.W. Molitor, and C.C. Chao, *The opioid-cytokine connection.* J Neuroimmunol, 1998. **83**(1-2): p. 63-9.
114. Hughes, J., et al., *Identification of two related pentapeptides from the brain with potent opiate agonist activity.* Nature, 1975. **258**(5536): p. 577-80.
115. Drolet, G., et al., *Role of endogenous opioid system in the regulation of the stress response.* Prog Neuropsychopharmacol Biol Psychiatry, 2001. **25**(4): p. 729-41.
116. Przewlocki, R. and B. Przewlocka, *Opioids in chronic pain.* Eur J Pharmacol, 2001. **429**(1-3): p. 79-91.
117. Okada, Y., et al., *Endomorphins and related opioid peptides.* Vitam Horm, 2002. **65**: p. 257-79.
118. Cuello, A.C., *Central distribution of opioid peptides.* Br Med Bull, 1983. **39**(1): p. 11-6.
119. Di Giulio, A.M., E.M. Majane, and H.Y. Yang, *On the distribution of [met5]- and [leu5]-enkephalins in the brain of the rat, guinea-pig and calf.* Br J Pharmacol, 1979. **66**(2): p. 297-301.
120. Zagon, I.S., R.E. Rhodes, and P.J. McLaughlin, *Distribution of enkephalin immunoreactivity in germinative cells of developing rat cerebellum.* Science, 1985. **227**(4690): p. 1049-51.
121. Inder, W.J., J.H. Livesey, and R.A. Donald, *Peripheral plasma levels of beta-endorphin in alcoholics and highly trained athletes and the relationship to a measure of central opioid tone.* Horm Metab Res, 1998. **30**(8): p. 523-5.
122. Zagon, I.S., et al., *Opioid receptors and endogenous opioids in diverse human and animal cancers.* J Natl Cancer Inst, 1987. **79**(5): p. 1059-65.

123. Shippenberg, T.S., *The dynorphin/kappa opioid receptor system: a new target for the treatment of addiction and affective disorders?* Neuropsychopharmacology, 2009. **34**(1): p. 247.
124. Porro, C.A., et al., *Central beta-endorphin system involvement in the reaction to acute tonic pain.* Exp Brain Res, 1991. **83**(3): p. 549-54.
125. Koehl, M., et al., *Exercise-induced promotion of hippocampal cell proliferation requires beta-endorphin.* Faseb J, 2008. **22**(7): p. 2253-62.
126. Przewlocki, R., et al., *Gene expression and localization of opioid peptides in immune cells of inflamed tissue: functional role in antinociception.* Neuroscience, 1992. **48**(2): p. 491-500.
127. Gerfen, C.R., J.F. McGinty, and W.S. Young, 3rd, *Dopamine differentially regulates dynorphin, substance P, and enkephalin expression in striatal neurons: in situ hybridization histochemical analysis.* J Neurosci, 1991. **11**(4): p. 1016-31.
128. Finley, M.J., et al., *Opioid and nociceptin receptors regulate cytokine and cytokine receptor expression.* Cell Immunol, 2008. **252**(1-2): p. 146-54.
129. Martini, L. and J.L. Whistler, *The role of mu opioid receptor desensitization and endocytosis in morphine tolerance and dependence.* Curr Opin Neurobiol, 2007. **17**(5): p. 556-64.
130. Gabilondo, A.M., J.J. Meana, and J.A. Garcia-Sevilla, *Increased density of mu-opioid receptors in the postmortem brain of suicide victims.* Brain Res, 1995. **682**(1-2): p. 245-50.
131. Trescot, A.M., et al., *Opioid pharmacology.* Pain Physician, 2008. **11**(2 Suppl): p. S133-53.
132. Wang, Y., E.J. Van Bockstaele, and L.Y. Liu-Chen, *In vivo trafficking of endogenous opioid receptors.* Life Sci, 2008. **83**(21-22): p. 693-9.
133. Knapp, P.E., et al., *Endogenous opioids and oligodendroglial function: possible autocrine/paracrine effects on cell survival and development.* Glia, 2001. **35**(2): p. 156-65.
134. Zagon, I.S., D.M. Gibo, and P.J. McLaughlin, *Adult and developing human cerebella exhibit different profiles of opioid binding sites.* Brain Res, 1990. **523**(1): p. 62-8.
135. Varga, E.V., et al., *Agonist-specific regulation of the delta-opioid receptor.* Life Sci, 2004. **76**(6): p. 599-612.
136. Pereira, F.A., et al., *Association of TGF-beta1 codon 25 (G915C) polymorphism with hepatitis C virus infection.* J Med Virol, 2008. **80**(1): p. 58-64.
137. Zhu, M., et al., *Neuroprotective role of delta-opioid receptors against mitochondrial respiratory chain injury.* Brain Res, 2009. **1252**: p. 183-91.
138. Metcalf, M.D. and A. Coop, *Kappa opioid antagonists: past successes and future prospects.* Aaps J, 2005. **7**(3): p. E704-22.
139. Gonzalez, J.P. and R.N. Brogden, *Naltrexone. A review of its pharmacodynamic and pharmacokinetic properties and therapeutic efficacy in the management of opioid dependence.* Drugs, 1988. **35**(3): p. 192-213.
140. Manfredi, B., et al., *Evidence for an opioid inhibitory effect on T cell proliferation.* J Neuroimmunol, 1993. **44**(1): p. 43-8.

141. Verebey, K., et al., *Naltrexone: disposition, metabolism, and effects after acute and chronic dosing.* Clin Pharmacol Ther, 1976. **20**(3): p. 315-28.
142. Panerai, A.E., et al., *The beta-endorphin inhibition of mitogen-induced splenocytes proliferation is mediated by central and peripheral paracrine/autocrine effects of the opioid.* J Neuroimmunol, 1995. **58**(1): p. 71-6.
143. Brown, N. and J. Panksepp, *Low-dose naltrexone for disease prevention and quality of life.* Med Hypotheses, 2009. **72**(3): p. 333-7.
144. Wybran, J., et al., *Suggestive evidence for receptors for morphine and methionine-enkephalin on normal human blood T lymphocytes.* J Immunol, 1979. **123**(3): p. 1068-70.
145. Chuang, L.F., et al., *Expression of kappa opioid receptors in human and monkey lymphocytes.* Biochem Biophys Res Commun, 1995. **209**(3): p. 1003-10.
146. Chuang, T.K., et al., *Mu opioid receptor gene expression in immune cells.* Biochem Biophys Res Commun, 1995. **216**(3): p. 922-30.
147. Alicea, C., et al., *Inhibition of primary murine macrophage cytokine production in vitro following treatment with the kappa-opioid agonist U50,488H.* J Neuroimmunol, 1996. **64**(1): p. 83-90.
148. Alicea, C., et al., *Characterization of kappa-opioid receptor transcripts expressed by T cells and macrophages.* J Neuroimmunol, 1998. **91**(1-2): p. 55-62.
149. Belkowski, S.M., et al., *Sequence of kappa-opioid receptor cDNA in the R1.1 thymoma cell line.* J Neuroimmunol, 1995. **62**(1): p. 113-7.
150. Sharp, B.M., S. Roy, and J.M. Bidlack, *Evidence for opioid receptors on cells involved in host defense and the immune system.* J Neuroimmunol, 1998. **83**(1-2): p. 45-56.
151. Zurawski, G., et al., *Activation of mouse T-helper cells induces abundant preproenkephalin mRNA synthesis.* Science, 1986. **232**(4751): p. 772-5.
152. Padros, M.R., et al., *Mitogenic activation of the human lymphocytes induce the release of proenkephalin derived peptides.* Life Sci, 1989. **45**(19): p. 1805-11.
153. Rosen, H., R.D. Polakiewicz, and R. Simantov, *Expression of proenkephalin A mRNA and enkephalin-containing peptides in cultured fibroblasts.* Biochem Biophys Res Commun, 1990. **171**(2): p. 722-8.
154. Saravia, F., et al., *Differential posttranslational processing of proenkephalin in rat bone marrow and spleen mononuclear cells: evidence for synenkephalin cleavage.* Endocrinology, 1993. **132**(4): p. 1431-7.
155. Shaqura, M.A., et al., *Characterization of mu opioid receptor binding and G protein coupling in rat hypothalamus, spinal cord, and primary afferent neurons during inflammatory pain.* J Pharmacol Exp Ther, 2004. **308**(2): p. 712-8.
156. Jankovic, B.D. and D. Maric, *Enkephalins modulate in vivo immune reactions through delta- and mu-opioid receptors.* Ann N Y Acad Sci, 1988. **540**: p. 691-3.
157. Bhargava, H.N., et al., *Effects of morphine tolerance and abstinence on cellular immune function.* Brain Res, 1994. **642**(1-2): p. 1-10.

158. Bussiere, J.L., et al., *Differential effects of morphine and naltrexone on the antibody response in various mouse strains.* Immunopharmacol Immunotoxicol, 1992. **14**(3): p. 657-73.
159. Eisenstein, T.K., et al., *Immunosuppressive effects of morphine on immune responses in mice.* Adv Exp Med Biol, 1993. **335**: p. 41-52.
160. Shahabi, N.A. and B.M. Sharp, *Antiproliferative effects of delta opioids on highly purified CD4+ and CD8+ murine T cells.* J Pharmacol Exp Ther, 1995. **273**(3): p. 1105-13.
161. Casellas, A.M., H. Guardiola, and F.L. Renaud, *Inhibition by opioids of phagocytosis in peritoneal macrophages.* Neuropeptides, 1991. **18**(1): p. 35-40.
162. Szabo, I., et al., *Suppression of peritoneal macrophage phagocytosis of Candida albicans by opioids.* J Pharmacol Exp Ther, 1993. **267**(2): p. 703-6.
163. Shavit, Y., et al., *Opioid peptides mediate the suppressive effect of stress on natural killer cell cytotoxicity.* Science, 1984. **223**(4632): p. 188-90.
164. Zalys, R., et al., *In vivo effects of chronic treatment with [MET5]-enkephalin on hematological values and natural killer cell activity in athymic mice.* Life Sci, 2000. **66**(9): p. 829-34.
165. Simpkins, C.O., et al., *The effect of enkephalins and prostaglandins on O-2 release by neutrophils.* J Surg Res, 1986. **41**(6): p. 645-52.
166. Sharp, B.M., et al., *Opioid peptides rapidly stimulate superoxide production by human polymorphonuclear leukocytes and macrophages.* Endocrinology, 1985. **117**(2): p. 793-5.
167. Liu, Y., et al., *Effects of in vivo and in vitro administration of morphine sulfate upon rhesus macaque polymorphonuclear cell phagocytosis and chemotaxis.* J Pharmacol Exp Ther, 1992. **263**(2): p. 533-9.
168. Perez-Castrillon, J.L., et al., *Opioids depress in vitro human monocyte chemotaxis.* Immunopharmacology, 1992. **23**(1): p. 57-61.
169. van Epps, D.E. and L. Saland, *Beta-endorphin and met-enkephalin stimulate human peripheral blood mononuclear cell chemotaxis.* J Immunol, 1984. **132**(6): p. 3046-53.
170. Makman, M.H., T.V. Bilfinger, and G.B. Stefano, *Human granulocytes contain an opiate alkaloid-selective receptor mediating inhibition of cytokine-induced activation and chemotaxis.* J Immunol, 1995. **154**(3): p. 1323-30.
171. Ruff, M.R., et al., *Opiate receptor-mediated chemotaxis of human monocytes.* Neuropeptides, 1985. **5**(4-6): p. 363-6.
172. Grimm, M.C., et al., *Opiates transdeactivate chemokine receptors: delta and mu opiate receptor-mediated heterologous desensitization.* J Exp Med, 1998. **188**(2): p. 317-25.
173. Zagon, I.S., K.A. Rahn, and P.J. McLaughlin, *Opioids and migration, chemotaxis, invasion, and adhesion of human cancer cells.* Neuropeptides, 2007. **41**(6): p. 441-52.
174. Jankovic, B.D. and D. Maric, *Enkephalins and autoimmunity: differential effect of methionine-enkephalin on experimental allergic encephalomyelitis in Wistar and Lewis rats.* J Neurosci Res, 1987. **18**(1): p. 88-94.

175. Jankovic, B.D. and D. Maric, *Methionine-enkephalin inhibits adoptive transfer of experimental allergic encephalomyelitis in the rat.* Int J Neurosci, 1990. **51**(3-4): p. 197-9.
176. Veljic, J., D. Maric, and B.D. Jankovic, *Changes of experimental allergic encephalomyelitis by methionine-enkephalin injected into lateral ventricles of the rat brain.* Int J Neurosci, 1991. **59**(1-3): p. 81-9.
177. Zagon, I.S. and P.J. McLaughlin, *An opioid growth factor regulates the replication of microorganisms.* Life Sci, 1992. **50**(16): p. 1179-87.
178. Bisignani, G.J., et al., *Human renal cell cancer proliferation in tissue culture is tonically inhibited by opioid growth factor.* J Urol, 1999. **162**(6): p. 2186-91.
179. Zagon, I.S., S.D. Hytrek, and P.J. McLaughlin, *Opioid growth factor tonically inhibits human colon cancer cell proliferation in tissue culture.* Am J Physiol, 1996. **271**(3 Pt 2): p. R511-8.
180. Zagon, I.S., et al., *Identification and characterization of opioid growth factor receptor in human pancreatic adenocarcinoma.* Int J Mol Med, 2000. **5**(1): p. 77-84.
181. Zagon, I.S. and P.J. McLaughlin, *Naltrexone modulates tumor response in mice with neuroblastoma.* Science, 1983. **221**(4611): p. 671-3.
182. Zagon, I.S. and P.J. McLaughlin, *Duration of opiate receptor blockade determines tumorigenic response in mice with neuroblastoma: a role for endogenous opioid systems in cancer.* Life Sci, 1984. **35**(4): p. 409-16.
183. Zagon, I.S. and P.J. McLaughlin, *Gene-peptide relationships in the developing rat brain: the response of preproenkephalin mRNA and [Met5]-enkephalin to acute opioid antagonist (naltrexone) exposure.* Brain Res Mol Brain Res, 1995. **33**(1): p. 111-20.
184. McLaughlin, P.J. and I.S. Zagon, *Modulation of human neuroblastoma transplanted into nude mice by endogenous opioid systems.* Life Sci, 1987. **41**(12): p. 1465-72.
185. Zagon, I.S. and P. McLaughlin, *Endogenous opioids and the growth regulation of a neural tumor.* Life Sci, 1988. **43**(16): p. 1313-8.
186. Zagon, I.S., et al., *Naltrexone, an opioid antagonist, facilitates reepithelialization of the cornea in diabetic rat.* Diabetes, 2002. **51**(10): p. 3055-62.
187. Zagon, I.S., et al., *Immunoelectron microscopic localization of the opioid growth factor receptor (OGFr) and OGF in the cornea.* Brain Res, 2003. **967**(1-2): p. 37-47.
188. Zagon, I.S., et al., *beta-Funaltrexamine (beta-FNA) and neural tumor response in mice.* Eur J Pharmacol, 1985. **116**(1-2): p. 165-9.
189. Zagon, I.S. and P.J. McLaughlin, *beta-Funaltrexamine (beta-FNA) and the regulation of body and brain development in rats.* Brain Res Bull, 1986. **17**(1): p. 5-9.
190. Gluzman, Y., *SV40-transformed simian cells support the replication of early SV40 mutants.* Cell, 1981. **23**(1): p. 175-82.
191. Chen, Y., et al., *Molecular cloning and functional expression of a mu-opioid receptor from rat brain.* Mol Pharmacol, 1993. **44**(1): p. 8-12.

192. Kong, H., et al., *Agonists and antagonists bind to different domains of the cloned kappa opioid receptor.* Proc Natl Acad Sci U S A, 1994. **91**(17): p. 8042-6.
193. Minami, M., et al., *Cloning and expression of a cDNA for the rat kappa-opioid receptor.* FEBS Lett, 1993. **329**(3): p. 291-5.
194. Zagon, I.S., M.F. Verderame, and P.J. McLaughlin, *The expression and function of the OGF-OGFr axis - a tonically active negative regulator of growth - in COS cells.* Neuropeptides, 2003. **37**(5): p. 290-7.
195. Zagon, I.S., S.R. Goodman, and P.J. McLaughlin, *Characterization of zeta (zeta): a new opioid receptor involved in growth.* Brain Res, 1989. **482**(2): p. 297-305.
196. Zagon, I.S., et al., *Cloning, sequencing, expression and function of a cDNA encoding a receptor for the opioid growth factor, [Met(5)]enkephalin.* Brain Res, 1999. **849**(1-2): p. 147-54.
197. Zagon, I.S., M.F. Verderame, and P.J. McLaughlin, *The biology of the opioid growth factor receptor (OGFr).* Brain Res Brain Res Rev, 2002. **38**(3): p. 351-76.
198. Zagon, I.S., S.R. Goodman, and P.J. McLaughlin, *Zeta (zeta), the opioid growth factor receptor: identification and characterization of binding subunits.* Brain Res, 1993. **605**(1): p. 50-6.
199. Cheng, F., et al., *The OGF-OGFr axis utilizes the p16INK4a and p21WAF1/CIP1 pathways to restrict normal cell proliferation.* Mol Biol Cell, 2009. **20**(1): p. 319-27.
200. Cheng, F., et al., *The opioid growth factor (OGF)-OGF receptor axis uses the p16 pathway to inhibit head and neck cancer.* Cancer Res, 2007. **67**(21): p. 10511-8.
201. Cheng, F., et al., *The OGF-OGFr axis utilizes the p21 pathway to restrict progression of human pancreatic cancer.* Mol Cancer, 2008. **7**: p. 5.
202. Zagon, I.S. and P.J. McLaughlin, *Opioids and the apoptotic pathway in human cancer cells.* Neuropeptides, 2003. **37**(2): p. 79-88.
203. Zagon, I.S. and P.J. McLaughlin, *Opioids and differentiation in human cancer cells.* Neuropeptides, 2005. **39**(5): p. 495-505.
204. Zagon, I.S., et al., *Opioid growth factor regulates the cell cycle of human neoplasias.* Int J Oncol, 2000. **17**(5): p. 1053-61.
205. Zagon, I.S., T. Isayama, and P.J. McLaughlin, *Preproenkephalin mRNA expression in the developing and adult rat brain.* Brain Res Mol Brain Res, 1994. **21**(1-2): p. 85-98.
206. Zagon, I.S. and P.J. McLaughlin, *Stereospecific modulation of tumorigenicity by opioid antagonists.* Eur J Pharmacol, 1985. **113**(1): p. 115-20.
207. McLaughlin, P.J., *Regulation of DNA synthesis of myocardial and epicardial cells in developing rat heart by [Met5]enkephalin.* Am J Physiol, 1996. **271**(1 Pt 2): p. R122-9.
208. Wu, Y., P.J. McLaughlin, and I.S. Zagon, *Ontogeny of the opioid growth factor, [Met5]-enkephalin, preproenkephalin gene expression, and the zeta opioid*

receptor in the developing and adult aorta of rat. Dev Dyn, 1998. **211**(4): p. 327-37.
209. Zagon, I.S., et al., *Molecular characterization and distribution of the opioid growth factor receptor (OGFr) in mouse.* Brain Res Mol Brain Res, 2000. **84**(1-2): p. 106-14.
210. Zagon, I.S. and P.J. McLaughlin, *Gene expression of OGFr in the developing and adult rat brain and cerebellum.* Brain Res Bull, 2004. **63**(1): p. 57-63.
211. Zagon, I.S., Y. Wu, and P.J. McLaughlin, *The opioid growth factor, [Met5]-enkephalin, and the zeta opioid receptor are present in human and mouse skin and tonically act to inhibit DNA synthesis in the epidermis.* J Invest Dermatol, 1996. **106**(3): p. 490-7.
212. Zagon, I.S., et al., *Conserved expression of the opioid growth factor, [Met5]enkephalin, and the zeta (zeta) opioid receptor in vertebrate cornea.* Brain Res, 1995. **671**(1): p. 105-11.
213. Zagon, I.S., D.M. Gibo, and P.J. McLaughlin, *Ontogeny of zeta (zeta), the opioid growth factor receptor, in the rat brain.* Brain Res, 1992. **596**(1-2): p. 149-56.
214. Zagon, I.S. and P.J. McLaughlin, *Identification of opioid peptides regulating proliferation of neurons and glia in the developing nervous system.* Brain Res, 1991. **542**(2): p. 318-23.
215. Isayama, T., P.J. McLaughlin, and I.S. Zagon, *Endogenous opioids regulate cell proliferation in the retina of developing rat.* Brain Res, 1991. **544**(1): p. 79-85.
216. Zagon, I.S. and P.J. McLaughlin, *Increased brain size and cellular content in infant rats treated with an opiate antagonist.* Science, 1983. **221**(4616): p. 1179-80.
217. Zagon, I.S. and P.J. McLaughlin, *Naltrexone modulates growth in infant rats.* Life Sci, 1983. **33**(24): p. 2449-54.
218. Zagon, I.S. and P.J. McLaughlin, *Opioid antagonist-induced regulation of organ development.* Physiol Behav, 1985. **34**(4): p. 507-11.
219. McLaughlin, P.J., et al., *Chronic exposure to the opioid antagonist naltrexone during pregnancy: maternal and offspring effects.* Physiol Behav, 1997. **62**(3): p. 501-8.
220. McLaughlin, P.J., et al., *Opioid receptor blockade during prenatal life modifies postnatal behavioral development.* Pharmacol Biochem Behav, 1997. **58**(4): p. 1075-82.
221. McLaughlin, P.J., et al., *Chronic exposure to the opioid growth factor, [Met5]-enkephalin, during pregnancy: maternal and preweaning effects.* Pharmacol Biochem Behav, 2002. **71**(1-2): p. 171-81.
222. Zagon, I.S. and P.J. McLaughlin, *Opioid antagonist-induced modulation of cerebral and hippocampal development: histological and morphometric studies.* Brain Res, 1986. **393**(2): p. 233-46.
223. Zagon, I.S. and P.J. McLaughlin, *Endogenous opioid systems regulate cell proliferation in the developing rat brain.* Brain Res, 1987. **412**(1): p. 68-72.
224. Hauser, K.F., P.J. McLaughlin, and I.S. Zagon, *Endogenous opioids regulate dendritic growth and spine formation in developing rat brain.* Brain Res, 1987. **416**(1): p. 157-61.

225. Zagon, I.S., J.P. Smith, and P.J. McLaughlin, *Human pancreatic cancer cell proliferation in tissue culture is tonically inhibited by opioid growth factor.* Int J Oncol, 1999. **14**(3): p. 577-84.
226. McLaughlin, P.J., R.J. Levin, and I.S. Zagon, *Regulation of human head and neck squamous cell carcinoma growth in tissue culture by opioid growth factor.* Int J Oncol, 1999. **14**(5): p. 991-8.
227. McLaughlin, P.J., I.S. Zagon, and J. Skitzki, *Human neuroblastoma cell growth in tissue culture is regulated by opioid growth factor.* Int J Oncol, 1999. **14**(2): p. 373-80.
228. Zagon, I.S. and P.J. McLaughlin, *Opioid growth factor (OGF) inhibits anchorage-independent growth in human cancer cells.* Int J Oncol, 2004. **24**(6): p. 1443-8.
229. McLaughlin, P.J., R.J. Levin, and I.S. Zagon, *The opioid growth factor receptor in human head and neck squamous cell carcinoma.* Int J Mol Med, 2000. **5**(2): p. 191-6.
230. Levin, R.J., et al., *Expression of the opioid growth factor, [Met5]-enkephalin, and the zeta opioid receptor in head and neck squamous cell carcinoma.* Laryngoscope, 1997. **107**(3): p. 335-9.
231. McLaughlin, P.J., R.J. Levin, and I.S. Zagon, *Opioid growth factor (OGF) inhibits the progression of human squamous cell carcinoma of the head and neck transplanted into nude mice.* Cancer Lett, 2003. **199**(2): p. 209-17.
232. Hytrek, S.D., et al., *Inhibition of human colon cancer by intermittent opioid receptor blockade with naltrexone.* Cancer Lett, 1996. **101**(2): p. 159-64.
233. Smith, J.P., et al., *Treatment of advanced pancreatic cancer with opioid growth factor: phase I.* Anticancer Drugs, 2004. **15**(3): p. 203-9.
234. McLaughlin, P.J., et al., *Enhanced growth inhibition of squamous cell carcinoma of the head and neck by combination therapy of paclitaxel and opioid growth factor.* Int J Oncol, 2005. **26**(3): p. 809-16.
235. Jaglowski, J.R., et al., *Opioid growth factor enhances tumor growth inhibition and increases the survival of paclitaxel-treated mice with squamous cell carcinoma of the head and neck.* Cancer Chemother Pharmacol, 2005. **56**(1): p. 97-104.
236. Zagon, I.S., et al., *Combination chemotherapy with gemcitabine and biotherapy with opioid growth factor (OGF) enhances the growth inhibition of pancreatic adenocarcinoma.* Cancer Chemother Pharmacol, 2005. **56**(5): p. 510-20.
237. Smith, J.P., et al., *Low-dose naltrexone therapy improves active Crohn's disease.* Am J Gastroenterol, 2007. **102**(4): p. 820-8.
238. Agrawal, Y.P., *Low dose naltrexone therapy in multiple sclerosis.* Med Hypotheses, 2005. **64**(4): p. 721-4.
239. Forte, M., et al., *Cyclophilin D inactivation protects axons in experimental autoimmune encephalomyelitis, an animal model of multiple sclerosis.* Proc Natl Acad Sci U S A, 2007. **104**(18): p. 7558-63.
240. Marta, C.B., et al., *Pathogenic myelin oligodendrocyte glycoprotein antibodies recognize glycosylated epitopes and perturb oligodendrocyte physiology.* Proc Natl Acad Sci U S A, 2005. **102**(39): p. 13992-7.

241. Hassen, G.W., et al., *A novel calpain inhibitor for the treatment of acute experimental autoimmune encephalomyelitis.* J Neuroimmunol, 2006. **180**(1-2): p. 135-46.
242. Oliver, A.R., G.M. Lyon, and N.H. Ruddle, *Rat and human myelin oligodendrocyte glycoproteins induce experimental autoimmune encephalomyelitis by different mechanisms in C57BL/6 mice.* J Immunol, 2003. **171**(1): p. 462-8.
243. Hurst, W.J., et al., *The stability of opioid growth factor ([Met5]-enkephalin) in solution using HPLC and photodiode array detection.* Journal of Liquid Chromatography and Related Technologies, 2006. **29**(2): p. 151-157.
244. Milicevic, I., et al., *Ribavirin reduces clinical signs and pathological changes of experimental autoimmune encephalomyelitis in Dark Agouti rats.* J Neurosci Res, 2003. **72**(2): p. 268-78.
245. Suen, W.E., et al., *A critical role for lymphotoxin in experimental allergic encephalomyelitis.* J Exp Med, 1997. **186**(8): p. 1233-40.
246. Bannerman, P., et al., *Astrogliosis in EAE spinal cord: derivation from radial glia, and relationships to oligodendroglia.* Glia, 2007. **55**(1): p. 57-64.
247. Giuliani, F., et al., *Effective combination of minocycline and interferon-beta in a model of multiple sclerosis.* J Neuroimmunol, 2005. **165**(1-2): p. 83-91.
248. MacNamara, K.C., et al., *Increased epitope-specific CD8+ T cells prevent murine coronavirus spread to the spinal cord and subsequent demyelination.* J Virol, 2005. **79**(6): p. 3370-81.
249. Sharp, B.M., *Multiple opioid receptors on immune cells modulate intracellular signaling.* Brain Behav Immun, 2006. **20**(1): p. 9-14.
250. Greeneltch, K.M., et al., *The opioid antagonist naltrexone blocks acute endotoxic shock by inhibiting tumor necrosis factor-alpha production.* Brain Behav Immun, 2004. **18**(5): p. 476-84.
251. Crawford, M.P., et al., *High prevalence of autoreactive, neuroantigen-specific CD8+ T cells in multiple sclerosis revealed by novel flow cytometric assay.* Blood, 2004. **103**: p. 4222-4231.
252. Zukin, R.S., et al., *Naltrexone-induced opiate receptor supersensitivity.* Brain Res, 1982. **245**(2): p. 285-92.
253. El Behi, M., et al., *New insights into cell responses involved in experimental autoimmune encephalomyelitis and multiple sclerosis.* Immunol Lett, 2005. **96**(1): p. 11-26.
254. Kamphuis, S., et al., *Role of endogenous pro-enkephalin A-derived peptides in human T cell proliferation and monocyte IL-6 production.* J Neuroimmunol, 1998. **84**(1): p. 53-60.
255. Ballantyne, J.C. and J. Mao, *Opioid therapy for chronic pain.* N Engl J Med, 2003. **349**(20): p. 1943-53.
256. Linner, K.M., H.E. Quist, and B.M. Sharp, *Met-enkephalin-containing peptides encoded by proenkephalin A mRNA expressed in activated murine thymocytes inhibit thymocyte proliferation.* J Immunol, 1995. **154**(10): p. 5049-60.

257. Sacerdote, P., et al., *Antinociceptive and immunosuppressive effects of opiate drugs: a structure-related activity study.* Br J Pharmacol, 1997. **121**(4): p. 834-40.
258. Foris, G., et al., *Concentration-dependent effect of met-enkephalin on human polymorphonuclear leukocytes.* Ann N Y Acad Sci, 1987. **496**: p. 151-7.
259. Oleson, D.R. and D.R. Johnson, *Regulation of human natural cytotoxicity by enkephalins and selective opiate agonists.* Brain Behav Immun, 1988. **2**(3): p. 171-86.
260. Prete, P., E.R. Levin, and A. Pedram, *The in vitro effects of endogenous opiates on natural killer cells, antigen-specific cytolytic T cells, and T-cell subsets.* Exp Neurol, 1986. **92**(2): p. 349-59.
261. Broderson, J.R., *A retrospective review of lesions associated with the use of Freund's adjuvant.* Lab Anim Sci, 1989. **39**(5): p. 400-5.
262. Buhler, L.A., et al., *Matrix metalloproteinase-7 facilitates immune access to the CNS in experimental autoimmune encephalomyelitis.* BMC Neurosci, 2009. **10**: p. 17.
263. Sharp, A.J., et al., *P2x7 deficiency suppresses development of experimental autoimmune encephalomyelitis.* J Neuroinflammation, 2008. **5**: p. 33.
264. Costa, O., et al., *Optimization of an animal model of experimental autoimmune encephalomyelitis achieved with a multiple MOG(35-55)peptide in C57BL6/J strain of mice.* J Autoimmun, 2003. **20**(1): p. 51-61.
265. Zaheer, A., et al., *Reduced severity of experimental autoimmune encephalomyelitis in GMF-deficient mice.* Neurochem Res, 2007. **32**(1): p. 39-47.
266. Petzold, A., et al., *Quantification of neurodegeneration by measurement of brain-specific proteins.* J Neuroimmunol, 2003. **138**(1-2): p. 45-8.
267. Petzold, A., et al., *Markers for different glial cell responses in multiple sclerosis: clinical and pathological correlations.* Brain, 2002. **125**(Pt 7): p. 1462-73.
268. Kozlowski, P., et al., *Characterizing white matter damage in rat spinal cord with quantitative MRI and histology.* J Neurotrauma, 2008. **25**(6): p. 653-76.
269. Lindner, M., et al., *Sequential myelin protein expression during remyelination reveals fast and efficient repair after central nervous system demyelination.* Neuropathol Appl Neurobiol, 2008. **34**(1): p. 105-14.
270. Garay, L., et al., *Effects of progesterone in the spinal cord of a mouse model of multiple sclerosis.* J Steroid Biochem Mol Biol, 2007. **107**(3-5): p. 228-37.
271. Gilgun-Sherki, Y., et al., *Axonal damage is reduced following glatiramer acetate treatment in C57/bl mice with chronic-induced experimental autoimmune encephalomyelitis.* Neurosci Res, 2003. **47**(2): p. 201-7.
272. Kornek, B., et al., *Multiple sclerosis and chronic autoimmune encephalomyelitis: a comparative quantitative study of axonal injury in active, inactive, and remyelinated lesions.* Am J Pathol, 2000. **157**(1): p. 267-76.
273. Bannerman, P.G. and A. Hahn, *Enhanced visualization of axonopathy in EAE using thy1-YFP transgenic mice.* J Neurol Sci, 2007. **260**(1-2): p. 23-32.

274. Pelizzoni, I., et al., *Iron and calcium in the central nervous system: a close relationship in health and sickness.* Biochem Soc Trans, 2008. **36**(Pt 6): p. 1309-12.
275. Lahti, R.A. and R.J. Collins, *Chronic naloxone results in prolonged increases in opiate binding sites in brain.* Eur J Pharmacol, 1978. **51**(2): p. 185-6.
276. Gironi, M., et al., *A pilot trial of low-dose naltrexone in primary progressive multiple sclerosis.* Mult Scler, 2008. **14**(8): p. 1076-83.
277. Gironi, M., et al., *Beta endorphin concentrations in PBMC of patients with different clinical phenotypes of multiple sclerosis.* J Neurol Neurosurg Psychiatry, 2003. **74**(4): p. 495-7.
278. Zagon, I.S. and P.J. McLaughlin, *Opioid antagonists inhibit the growth of metastatic murine neuroblastoma.* Cancer Lett, 1983. **21**(1): p. 89-94.
279. Zagon, I.S. and P.J. McLaughlin, *Naltrexone modulates body and brain development in rats: a role for endogenous opioid systems in growth.* Life Sci, 1984. **35**(20): p. 2057-64.
280. Dong, Y. and E.N. Benveniste, *Immune function of astrocytes.* Glia, 2001. **36**(2): p. 180-90.
281. Benveniste, E.N., *Role of macrophages/microglia in multiple sclerosis and experimental allergic encephalomyelitis.* J Mol Med, 1997. **75**(3): p. 165-73.
282. Vanderah, T.W., *Pathophysiology of pain.* Med Clin North Am, 2007. **91**(1): p. 1-12.
283. Paller, C.J., et al., *Sex-based differences in pain perception and treatment.* Pain Med, 2009. **10**(2): p. 289-99.
284. Sarton, E., et al., *Sex differences in morphine analgesia: an experimental study in healthy volunteers.* Anesthesiology, 2000. **93**(5): p. 1245-54; discussion 6A.
285. Lynch, J.L., et al., *Analysis of nociception, sex and peripheral nerve innervation in the TMEV animal model of multiple sclerosis.* Pain, 2008. **136**(3): p. 293-304.
286. Aicher, S.A., et al., *Hyperalgesia in an animal model of multiple sclerosis.* Pain, 2004. **110**(3): p. 560-70.
287. Lynch, J.L., et al., *Decreased spinal cord opioid receptor mRNA expression and antinociception in a Theiler's murine encephalomyelitis virus model of multiple sclerosis.* Brain Res, 2008. **1191**: p. 180-91.
288. Argyriou, A.A. and N. Makris, *Multiple sclerosis and reproductive risks in women.* Reprod Sci, 2008. **15**(8): p. 755-64.
289. Vukusic, S., et al., *Pregnancy and multiple sclerosis (the PRIMS study): clinical predictors of post-partum relapse.* Brain, 2004. **127**(Pt 6): p. 1353-60.
290. Confavreux, C., et al., *Rate of pregnancy-related relapse in multiple sclerosis. Pregnancy in Multiple Sclerosis Group.* N Engl J Med, 1998. **339**(5): p. 285-91.
291. Wegmann, T.G., et al., *Bidirectional cytokine interactions in the maternal-fetal relationship: is successful pregnancy a TH2 phenomenon?* Immunol Today, 1993. **14**(7): p. 353-6.
292. Kim, S., et al., *Estriol ameliorates autoimmune demyelinating disease: implications for multiple sclerosis.* Neurology, 1999. **52**(6): p. 1230-8.

293. Sicotte, N.L., et al., *Treatment of multiple sclerosis with the pregnancy hormone estriol.* Ann Neurol, 2002. **52**(4): p. 421-8.
294. Akil, H., et al., *Endogenous opioids: biology and function.* Annu Rev Neurosci, 1984. **7**: p. 223-55.
295. Panerai, A.E., et al., *Plasma beta-endorphin, beta-lipotropin, and met-enkephalin concentrations during pregnancy in normal and drug-addicted women and their newborn.* J Clin Endocrinol Metab, 1983. **57**(3): p. 537-43.
296. Newnham, J.P., et al., *Endogenous opioid peptides in pregnancy.* Br J Obstet Gynaecol, 1983. **90**(6): p. 535-8.
297. Zagon, I.S., Y. Wu, and P.J. McLaughlin, *Opioid growth factor and organ development in rat and human embryos.* Brain Res, 1999. **839**(2): p. 313-22.
298. Ward, H.G., et al., *Mu-opioid receptor cellular function in the nucleus accumbens is essential for hedonically driven eating.* Eur J Neurosci, 2006. **23**(6): p. 1605-13.
299. Laban, O., et al., *Experimental allergic encephalomyelitis in adult DA rats subjected to neonatal handling or gentling.* Brain Res, 1995. **676**(1): p. 133-40.
300. Dimitrijevic, M., et al., *Neonatal sound stress and development of experimental allergic encephalomyelitis in Lewis and DA rats.* Int J Neurosci, 1994. **78**(1-2): p. 135-43.
301. Bartolomucci, A., *Social stress, immune functions and disease in rodents.* Front Neuroendocrinol, 2007. **28**(1): p. 28-49.
302. Bohus, B., et al., *Stress and differential alterations in immune system functions: conclusions from social stress studies in animals.* Neth J Med, 1991. **39**(3-4): p. 306-15.
303. Bohus, B., et al., *Immunological responses to social stress: dependence on social environment and coping abilities.* Neuropsychobiology, 1993. **28**(1-2): p. 95-9.
304. Li, W.W., et al., *Minocycline-mediated inhibition of microglia activation impairs oligodendrocyte progenitor cell responses and remyelination in a non-immune model of demyelination.* J Neuroimmunol, 2005. **158**(1-2): p. 58-66.
305. Hinks, G.L. and R.J. Franklin, *Delayed changes in growth factor gene expression during slow remyelination in the CNS of aged rats.* Mol Cell Neurosci, 2000. **16**(5): p. 542-56.
306. Ferguson, B., et al., *Axonal damage in acute multiple sclerosis lesions.* Brain, 1997. **120 (Pt 3)**: p. 393-9.
307. Budde, M.D., et al., *Axonal injury detected by in vivo diffusion tensor imaging correlates with neurological disability in a mouse model of multiple sclerosis.* NMR Biomed, 2008. **21**(6): p. 589-97.

KRISTEN A. RAHN

School: 500 University Drive, H109
Hershey, PA 17033
717-531-3787

Home: 614 Grey Drive
Hummelstown, PA
217-260-3810

EDUCATION

Ph.D.	Sept 2005-present	Pennsylvania State University; Cell and Molecular Biology
B.S.	Sept 2001-May 2005	University of Illinois, Urbana-Champaign; Molecular and Cellular Biology

COCURRICULAR ACTIVITIES

2008-2009	Graduate Student Association Service Chair
2007-2009	Society for Neuroscience, Predoctoral Student Member
2007-2008	American Society for Cell Biology, Predoctoral Student Member
2007-2008	Institutional Review Board Member
2007	Student Assembly Subcommittee Chair

HONORS & ACHIEVEMENTS

2008	Society for Neuroscience Graduate Chapter Travel Award
2008	National Multiple Sclerosis Society Travel Award for WCTRIMS
2007	American Society for Cell Biology Travel Award
2005-2008	Penn State University Funds for Excellence in Graduate Recruiting Award
2003	Student Employee of the Year finalist, University of Illinois

PEER-REVIEWED PUBLICATIONS

Abstracts:

Rahn, K.A., Bonneau, R.H., McLaughlin, P.J., and Zagon, I.S. Low dose naltrexone (LDN) and opioid growth factor (OGF) prevent or delay experimental autoimmune encephalomyelitis (EAE). Abstract for poster presentation, Society for Neuroscience, Washington, D.C., November 2008.

Zagon, I.S., **Rahn, K.A.**, Bonneau, R.H., Turel, A.P., Thomas, G.A., and McLaughlin, P.J. The complete blockade of opioid receptors with naltrexone exacerbates experimental autoimmune encephalomyelitis in a mouse model. Abstract for poster presentation, World Congress on Treatment and Research in Multiple Sclerosis, Montreal, QC, September 2008.

Rahn, K.A., McLaughlin, P.J., Bonneau, R.H., Turel, A.P., Thomas, G.A., and Zagon, I.S. Low-dose naltrexone (LDN) prevents development or delays onset and reduces severity of experimental autoimmune encephalomyelitis in mice. Abstract for poster presentation, World Congress on Treatment and Research in Multiple Sclerosis, Montreal, QC, September 2008.

Rahn, K.A., Bonneau, R.H., Turel, A.P., Thomas, G.A., McLaughlin, P.J.,and Zagon, I.S. Opioid growth factor and low dose naltrexone inhibit immunological responses associated with experimental autoimmune encephalomyelitis. Abstract for poster presentation, World Congress on Treatment and Research in Multiple Sclerosis, Montreal, QC, September 2008.

Rahn, K.A., McLaughlin, P.J., and Zagon, I.S. Opioids and Multiple Sclerosis. Abstract for poster presentation, Penn State University Forum, Hershey, PA, March 2008.

Zagon, I.S., **Rahn, K.A.**, and McLaughlin, P.J. Endogenous opioids and migration, invasion, and adhesion of human cancer cells. Abstract for poster presentation, Society for Neuroscience, San Diego, CA, November 2007.

Papers:

Zagon, I.S., **Rahn, K.A.**, and McLaughlin, P.J. Opioids and migration, chemotaxis, invasion, and adhesion of human cancer cells. Neuropeptides. 2007 Dec;41(6):441-52.

Baum, J.I., Layman, D.K., Freund, G.G., **Rahn, K.A.**, Nakamura, M.T., and Yudell, B.E. A reduced carbohydrate, increased protein diet stabilizes glycemic control and minimizes adipose tissue glucose disposal in rats. J Nutr. 2006 Jul;136(7):1855-61.